Geometric modeling of delta dynamics coupled with biogeochemical processes

A DISSERTATION

SUBMITTED TO THE FACULTY OF THE GRADUATE SCHOOL

OF THE UNIVERSITY OF MINNESOTA

BY

Jorge Lorenzo Trueba

IN PARTIAL FULFILLMENT OF THE REQUIREMENTS

FOR THE DEGREE OF

DOCTOR OF PHILOSOPHY

Vaughan R. Voller and Chris Paola

February 2012

Acknowledgements

I would not have been able to complete this PhD thesis without the aid and support of many people. First, I would like to express my gratitude to my advisors Vaughan Voller and Chris Paola; I have learnt a great deal from them over the past years and I gratefully acknowledge my debt to them. Many thanks to Robert Twilley, Gary Holm, Azure Bevington, Tetsuji Muto, Wonsuck Kim, and John Swenson for their advice and contributions, which made them a backbone of this thesis work. I would also like to thank Robert Twilley, Gary Parker, Bruce Wilson and Miki Honzdo for taking time out from their busy schedules to serve as committee members and provide me with great assistance and suggestions.

Very special thanks to my family and friends for their support and understanding through the duration of my PhD work.

Thanks to everyone at SAFL. In particular I would like to thank Sharon Bartlett and Jeff Marr. They both spent countless hours helping me when I first came to SAFL as an intern.

I would like to conclude by recognizing that these exciting years of cross-disciplinary research would not have been possible without the financial assistance of the National Center of Earth-surface Dynamics.

Dedication

I dedicate this dissertation to my parents Raquel and Jorge, and my brother Jaime.

Abstract

Today, many of the world's deltas are highly populated and experiencing rapid rates of deterioration. We need tools that can explain and predict the long-term evolution of these systems to the formation of baselines for sustainable restoration. Deltas are complex systems in which diverse processes interact across a vast range of time and space scales. However, contrary to what intuition might suggest, we find that simple geometric models can be powerful at explaining the long-term system response to different external forcing. Based on this framework, we construct the first delta building model able to capture long-term interactions between organic sediment dynamics and delta evolution.

Table of Contents

List of tables

List of figures

Chapter 1: Introduction

Hundreds of millions of people live within coastal floodplains at less than 1m above sea-level. The increase in vulnerability to flooding of many of these regions is considered to be one of the major socio-economic hazards of the future decades (Stern 2007, Syvitski et al. 2009). An example close to home is the Mississippi delta, where more than 2000 km^2 of wetland ecosystems have been converted to open waters since the beginning of the 20^{th} century (Reed and Wilson 2004). In addition to the obvious ecological impact, this rapid deterioration of coastal wetlands has also led to an important reduction of storm surge buffer, which was made abundantly clear by the devastation caused by Hurricanes Katrina and Rita in 2005 (Day et al. 2007). In order to form baselines for coastal management and protection and reverse these land loss trend, we need to understand the natural processes of delta growth and wetland dynamics (Paola 2011).

In Fig.1 we present a simple point model with the key processes behind the dynamics of coastal wetlands. Both the river sediment input and the net accumulation of plant matter contribute to maintaining the elevation in pace with the subsidence and sea-level rise rates. The river sediment input has been significantly reduced by human infrastructure (Day et al. 2007, Paola 2011), and several recent and on-going studies aim at quantifying current budgets. The main focus of this thesis work, however, is the plant matter component. Deltaic marshes are among the most productive ecosystems in the world and plant matter remains are a significant fraction of the sediment column (Kosters et al. 1987, Reddy & DeLaune 2008, Tornqvist 2008, van Asselen et al. 2008).

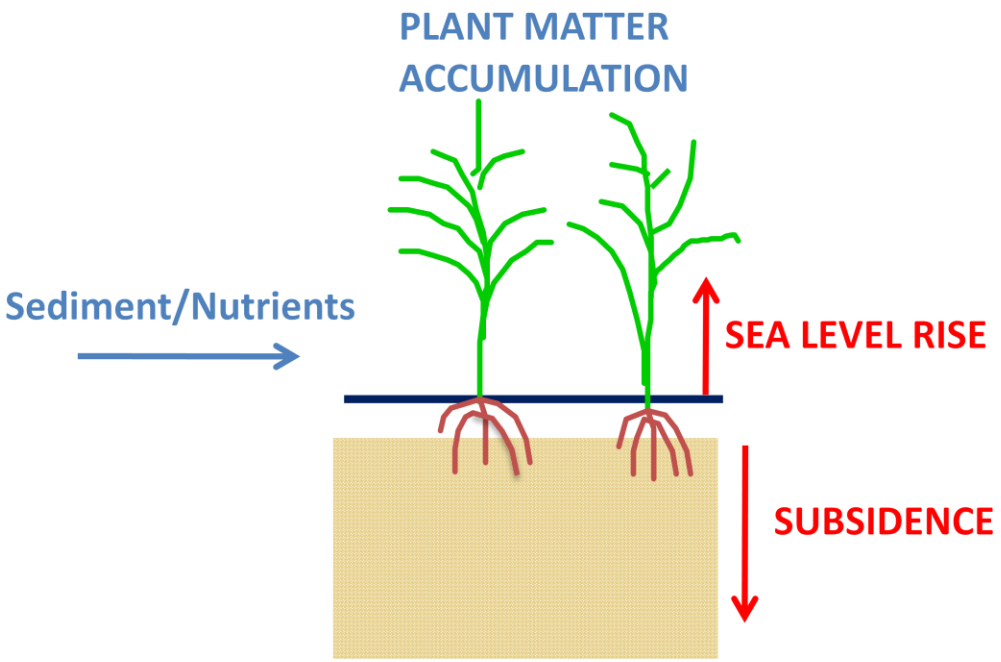

Fig.1-1 Point representation of the coastal wetlands.

Computational models are very powerful tools to quantify the dynamic response of coastal wetlands to subsidence and sea-level rise. The vast range of scales and processes involved invites the use of a wide range of approaches (Fagherazzi & Overeem, 2007, Paola 2011), from simple models to highly detailed simulations. The suitability of the modeling approach depends on the question that we want to address. For instance, one-dimensional longitudinal profile models have proved to be a useful and physically valid approach to model average delta dynamics (Swenson 2000, Paola 2000, Capart et al. 2007, Parker et al. 2008; Paola et al. 2011). If we are interested in capturing lateral processes (e.g., river avulsions) or out-of-plane variations, however, we could use a rule-based cellular delta model (Man Liang, in preparation), or a three-dimensional flow solver coupled with sediment transport such as Delft 3D (Paola et al. 2011). To date, however, none of these approaches account for plant matter accumulation. This leads to a **key objective** of this thesis work: **develop a framework for delta growth that explicitly accounts for plant matter accumulation via plant growth, burial, and microbial processes**.

We start with a one-dimensional longitudinal profile model, which, as discussed above, is sufficient to capture the essential average dynamics. The domain, consisting of a cross-sectional slice through the delta, is defined by three boundaries: the alluvial–basement transition, the shoreline, and the delta toe (fig.2). The fluvial surface is delimited by the alluvial-basement transition and the shoreline, and supports infrastructure, population centers and wetland ecosystems. The foreset is delimited by the shoreline and the delta toe, and typically has a much higher slope than the fluvial surface. When the model is in operation each of the boundaries changes position with time and their location has to be determined as a part of the solution, i.e., it mathematically reduces to a moving boundary problem. Moving boundary problems are inherently non-linear, what can significantly complicate the analysis and produce counterintuitive behaviors. Thus, in **chapters 2, 3** and **5** we explore different analytical and numerical techniques to model appropriately the system depicted in Fig.2. The resulting framework is coupled with an explicit description of plant matter production and decomposition in **chapter 4**.

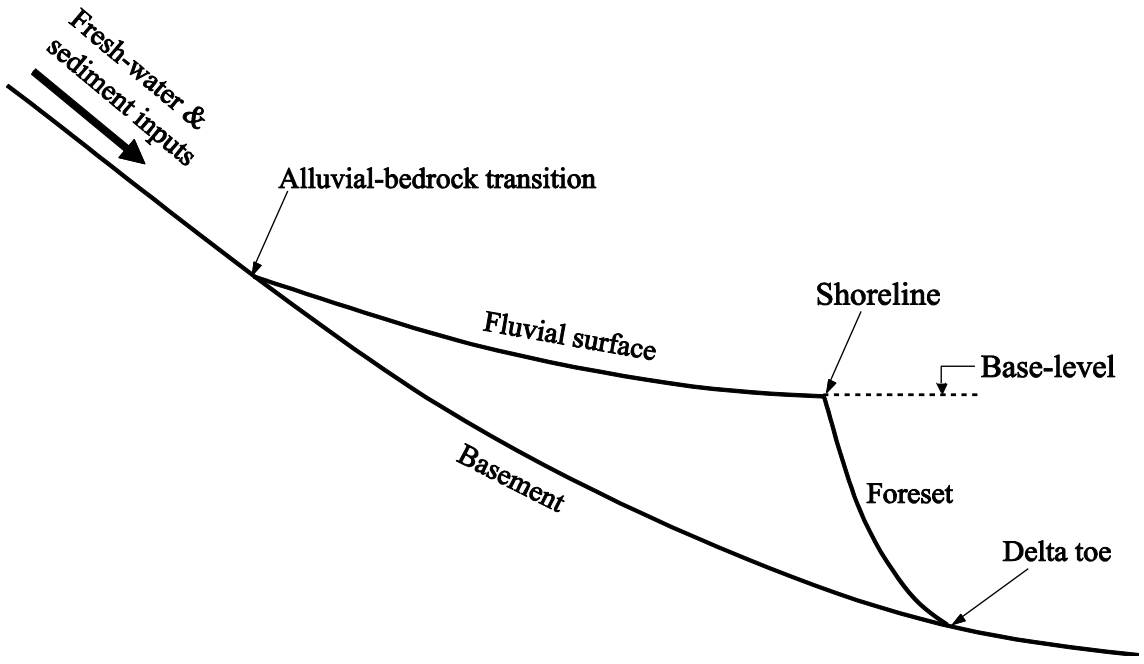

Fig. 1-2 Typical deltaic cross-section

In **chapter 2**, following previous work by Swenson et al. 2000, we assume a linear relationship between the sediment flux and the local slope. Combining this expression with a mass balance equation we obtain a linear diffusion model to describe the morphologic evolution of the fluvial surface. The novel features are the derivation of a close form similarity solution able to track both the alluvial–basement transition and the shoreline, and its validation with flume experiments. An important implication of this solution is that, despite the emphasis on the shoreline in the earth science literature, the alluvial–bedrock transition is typically more sensitive (and potentially a better recorder) to changes in environmental parameters such as sediment size, sediment flux and water discharge.

Follow up work in **chapter 3** expands the similarity solution presented in **chapter 2** to include a power law relationship between the sediment transport rate and the local slope. We identify two limit models: the closed form analytical solution in **chapter 2**, and a simple linear geometric model. Interestingly, for a wide range of parameter values there is essentially no difference between the diffusive models and the linear geometric model. Only in scenarios in which there are important spatial and/or temporal changes of the fluvial surface slope, might we need a higher level of accuracy; we analyze some of these special cases in **chapter 5**.

In **chapter 4** we build on the linear geometric model introduced in **chapter 3** and incorporate, for the first time, a quantitative description for the production and decomposition of organic soils. The key assumption of the model is that both river sediment deposition and plant matter accumulation operate to preserve the geometry of the delta plain. The resulting modeling framework is able to capture the average dynamic response to base-level changes, differential subsidence, and well-known observed patterns of organic sedimentation found in the coal literature. The model also shows that a reduction in fresh water inputs can exacerbate shoreline retreat and wetland loss due to a decrease in plant matter preservation.

In **chapter 5** we explore situation where the linear geometric model presented in **chapter 3** might break down. We develop a quadratic model for the fluvial surface able to capture special and temporal changes in the fluvial slope. The model captures an interesting phenomenon of river incision during base-level rise that to the authors' knowledge has not been reported before.

Chapter 2: A similarity solution for a dual moving boundary problem associated with a coastal-plain depositional system

Published as; J. Lorenzo-Trueba et al. (2009), A similarity solution for a dual moving boundary problem associated with a coastal-plain depositional system, *Journal of Fluid Mechanics*, 628, 427-443.

Assuming that the sediment flux in the Exner equation can be linearly related to the local bed slope, we establish a one-dimensional model for the bed-load transport of sediment in a coastal-plain depositional system, such as a delta and a continental margin. The domain of this model is defined by two moving boundaries: the shoreline and the alluvial–bedrock transition. These boundaries represent fundamental transitions in surface morphology and sediment transport regime, and their trajectories in time and space define the evolution of the shape of the sedimentary prism. Under the assumptions of fixed bedrock slope and sea level the model admits a closed-form similarity solution for the movements of these boundaries. A mapping of the solution space, relevant to field scales, shows two domains controlled by the relative slopes of the bedrock and fluvial surface: one in which changes in environmental parameters are mainly recorded in the upstream boundary and another in which these changes are mainly recorded in the shoreline. We also find good agreement between the analytical solution and laboratory flume experiments for the movements of the alluvial–bedrock transition and the shoreline.

1. Introduction

Coastal areas such as deltas and continental margins are composites of several primary sedimentary environments: at a minimum, a depositional fluvial region and an offshore region (Fig. 1). The latter may include sub-regions (e.g. wave-dominated shelf, mass-flow-dominated slope). The depositional fluvial region typically terminates upstream in a transition to a bedrock fluvial region. The boundaries between these regions, which are often readily visible on topographic maps, represent fundamental qualitative transitions in the processes by which sediment is transported. In fact the shape, large-scale structure and long-term evolution of coastal sedimentary systems are the result of the complex interplay of the different transport regions, and the boundaries separating them are moving boundaries – internal boundaries whose location must be determined as part of the solution to the overall morphological evolution problem (Marr et al. 2000; Swenson et al. 2000; Voller, Swenson & Paola 2004; Kim & Muto 2007; Swenson & Muto 2007). The classical moving boundary problem involves the tracking of the solid–liquid interface during the melting of ice and is known as the Stefan problem (Crank 1984). The first application of moving boundary models to morphodynamics was by Swenson et al. (2000). These authors used an analogy between heat and sediment diffusive transport to develop a generalized Stefan-like model to describe the movement on planetary time scales of the shoreline in a sedimentary continental margin under varying conditions of sediment influx, sea level and tectonic subsidence. In the limit of constant bedrock slope (no subsidence) and sea level, Voller et al. (2004) developed a closed-form similarity solution for the Swenson model which tracks the shoreline movement in a one-dimensional domain driven by a prescribed sediment flux. This solution has common elements with the classic Neumann similarity solution of the Stefan one phase melting problem (Crank 1984). The key differences in the model presented in Voller et al. (2004) from the classic solution are (i) a specified flux at the origin $x = 0$ and (ii) a spatially variable latent heat (ocean depth). The ideas in Voller et al. (2004) have recently been used by Capart, Bellal & Young (2007) and Lai & Capart (2007) to develop analytical solutions for a more extensive solution domain, extending from the alluvial–bedrock transition (the upstream end of a sediment prism developed over the non-erodible

bedrock basement) located at $x = s_1(t) < 0$ through to the shoreline (the sediment–water interface) located at $x = s_2(t) > 0$. These authors essentially developed two similarity solutions; one solves for the movement of the alluvial–bedrock transition, s_1, in the upstream direction when the downstream condition is set at $s_2 \rightarrow \infty$; the other solves for the downstream (progradation) of the shoreline, s_2, when the upstream condition is set at $s_1 \rightarrow \infty$. There is, however, no need to look at the limit settings of the upstream and downstream boundary conditions. It is generally accepted that the geometry of modern river deltas resembles a triangular prism in longitudinal section, superimposed upon a relatively flat basement profile (Posamentier et al. 1992). These domain transitions of the coastal prism are typically marked by changes in surface slope and/or grain size. A general treatment for this problem is to construct a transient model with the initial setting of $s_1 = s_2 = 0$ and allow for the subsequent downstream movement of the shoreline in the positive x-direction and the upstream movement of the alluvial–bedrock transition in the negative x-direction. As noted by Parker & Muto (2003), an interesting feature of this case is that it simultaneously admits two moving boundaries: the shoreline and alluvial–bedrock transition. This feature is found in other systems, notably the liquidus and eutectic fronts in the solidification of binary eutectic alloys (Worster 1986; Voller 1997). In terms of the sediment problem, Parker & Muto (2003) developed a basic numerical scheme to track the evolution of the moving boundaries. In recent attempts to track these boundaries Swenson & Muto (2007) presented a refined numerical treatment based on a Landau front-fixing approach (Crank 1984), and Kim & Muto (2007) employed a geometric mass balance model. To date, however, no closed analytical solution of the two moving boundaries model based on the diffusive transport model in Swenson et al. (2000) has been presented in the literature.

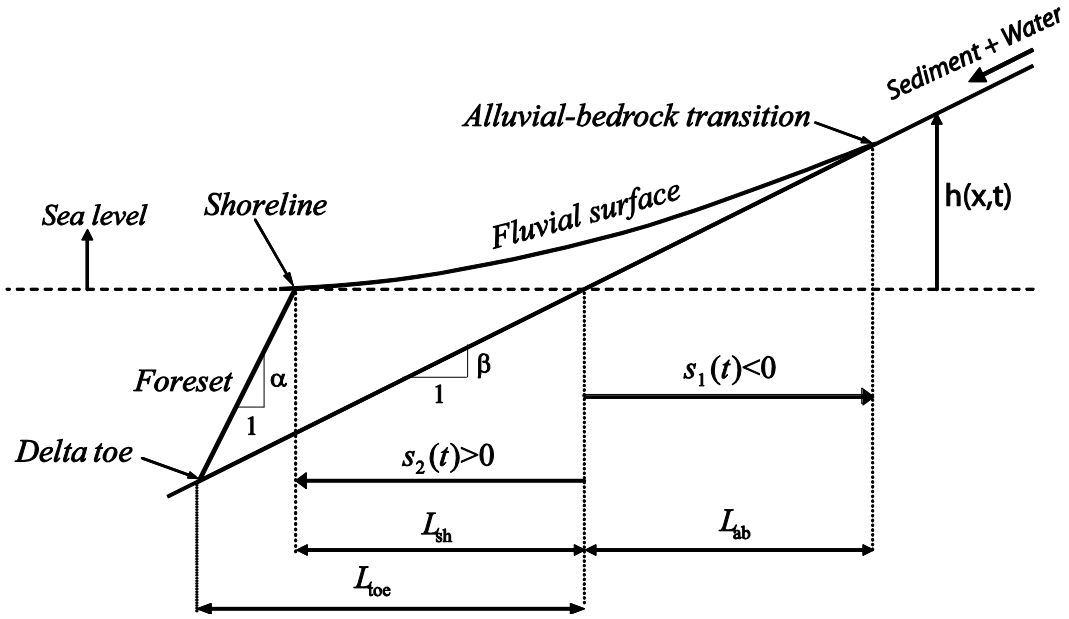

Fig. 2-1 Schematic of sediment basin problem (note the seaward direction is assigned positive).

The objective of this paper is to develop such a solution, examine its implications for response of coastal prisms to imposed changes and compare the solutions with measurements from flume experiments.

2. Governing equations

In the problem at hand, we identify two regions, a sub-aerial fluvial region upstream of the shoreline and a submarine offshore region. As noted above, the depositional fluvial region, which can be referred to as a fluvial plain, is bounded upstream by an alluvial–bedrock transition and downstream by the shoreline. Typically this plain can extend over 10km or even 100 km. At a given instant of time the shoreline boundary may be quite irregular; e.g. at channel and river mouths, deltas will grow radially ahead of the surrounding shoreline. On large time scales, however, due to avulsion (repositioning of channels) events such features can be averaged out.

Hence it is reasonable, to first order, to represent the evolution of the system by the one-dimensional longitudinal section shown in Fig.1.

The mechanism of transport of sediment in each of the domains in Fig. 1 is significantly different. In the sub-aerial fluvial region the sediment is transported through the channel system primarily as bed load; i.e. sediment particles move in a layer along the channel beds via modes such as shear-stress-induced saltation.

The downstream decrease in slope in this region results in a reduction in the bed shear stress, leading to a deposition of sediment in the channel. On non-channelized portions of the fluvial region sediment is deposited by flood events and at larger time scales by channel avulsion. In contrast, in the offshore region sediment transport primarily occurs by slope failure (avalanching) – which may induce gravity currents – in addition to transport as suspended load driven by wind, wave and tide forces (Sommerfield et al. 2007).

Using Fig. 1 as a reference, a suitable governing sediment transport equation is derived by considering the deposition of a sediment prism on to a non-erodible bedrock surface set at constant slope β. At time t =0, with no sediment deposited, the sea level intersects the bedrock surface at x=0. To retain some generality we initially assume that the bedrock surface undergoes a uniform subsidence or uplift – i.e. there is no spatial variation in subsidence/uplift rate. In this way, geometric changes in the domain are defined by the rise or fall of sea level relative to the background subsidence/uplift. At times t >0, the sediment prism starts to grow at x =0 by a steady sediment unit flux q_0 (volumetric sediment bed transport per unit width and time) introduced at the far field upstream boundary and bypassed over the bedrock basement to the sediment prism. Note the unit flux accounts for the bed porosity n; i.e. if q_m is the mass per width and time at a point, the unit flux at that point is $q = q_m/\rho s(1-n)$, where ρs is the density of the sediment. The sediment prism is characterized by its height $h(x,t)$ above the current sea level $z = \ell(t)$. At some time t >0 (Fig. 1), the sediment prism consists of two parts: (i) the sediment, contained between the shoreline $x = s_2(t) > 0$ moving in the positive x-direction (always defined to be seaward), and the alluvial–bedrock transition $x = s_1(t) < 0$ moving in the negative x-direction (landward); (ii) a submarine sediment wedge deposited beyond the

shoreline $x = s_2(t) > 0$. Following the arguments first made by Paola, Heller & Angevine (1992) and elaborated in appendix 1, we assume that the transport of the sediment over the sub-aerial fluvial surface is described by the diffusive flux

$$q = -\nu \frac{\partial h}{\partial x} \tag{2.1}$$

where the diffusivity ν is, in general, a function of the characteristic sediment grain diameter d and the time-averaged water unit discharge q_w over the fluvial surface (Swenson et al. 2000). In appendix 1 we discuss the validity of a linear diffusion model and develop forms for ν applicable to field and experimental scenarios. In the submarine domain, we assume that the time and magnitude scales of slope evolution are small compared to those in the fluvial system. In this way, the slope of the foreset sediment wedge can be assumed to have a constant angle of repose α (Swenson et al. 2000; Voller et al. 2004). These transport behaviors can be incorporated into the Exner sediment balance equation (Paola & Voller 2005) to arrive at the following governing transport equation:

$$\frac{\partial h}{\partial t} = \nu \frac{\partial^2 h}{\partial x^2}, \qquad s_1(t) \le x \le s_2(t) \tag{2.2}$$

The initial conditions are $\ell(0) = h(x,0) = 0$. The appropriate boundary conditions are

$$h\big|_{x=s_1(t)} = -\beta s_1(t) \tag{2.3a}$$

$$h\big|_{x=s_2(t)} = \ell(t) \tag{2.3b}$$

$$\nu \frac{\partial h}{\partial x}\bigg|_{x=s_1(t)} = -\bar{q}_0 \tag{2.3c}$$

$$\nu \frac{\partial h}{\partial x}\bigg|_{x=s_2(t)} = -\frac{\beta s_2 + \ell}{\alpha - \beta}\left(\alpha \frac{ds_2}{dt} + \frac{d\ell}{dt}\right) \tag{2.3d}$$

The first two conditions fix the sediment elevation to coincide with that of the bedrock basement at the alluvial–bedrock transition $x = s_1(t)$ (2.3b) and with the current sea level at the shoreline $x = s_2(t)$ (2.3c). The third condition (2.3d) sets the alluvial–bedrock transition to be the point at which the fluvial sediment flux matches the input flux;

upstream of this transition the sediment is transported over the rock basement without either erosion or deposition. The last condition (2.3d), initially derived by Swenson et al. (2000), is essentially a statement of the mass balance at the shoreline; the flux of sediment arriving at the shoreline is balanced by the requirements of maintaining the geometry of the submarine sediment wedge, compensating for sea-level rise/fall and moving the shoreline forward.

3. The similarity solution

We develop a similarity solution of (2.2) and (2.3) under the condition that the sea level remains fixed at $\ell(t) = 0$. The development of this solution essentially follows the approach previously used by Voller et al. (2004) and Capart and co-workers (Capart et al. 2007; Lai & Capart 2007). A key feature in this case, however, is that the resulting solution allows for the simultaneous existence of two moving boundaries, the shoreline $s_2(t)$ and the alluvial–bedrock transition $s_1(t)$; the previous solutions (e.g. Voller et al. 2004; Capart et al. 2007; Lai & Capart 2007) allow for only a single moving boundary. On setting the movement of the alluvial–bedrock transition (ab) and the shoreline (sh) to be respectively

$$s_1 = -2\lambda_{ab}(\nu t)^{\frac{1}{2}} \tag{3.1a}$$

$$s_2 = -2\lambda_{sh}(\nu t)^{\frac{1}{2}} \tag{3.1b}$$

introducing the similarity variable

$$\xi = \frac{x}{2(\nu t)^{\frac{1}{2}}} \tag{3.2}$$

and scaling the sediment height by

$$\eta = \frac{h}{2(\nu t)^{\frac{1}{2}}} \tag{3.3}$$

(2.2) and (2.3) reduce to the ordinary differential equation

$$\frac{1}{2}\frac{d^2\eta}{d\xi^2}+\xi\frac{d\eta}{d\xi}-\eta=0, \qquad -\lambda_{ab}\le\xi\le\lambda_{sh} \tag{3.4}$$

with

$$\eta\big|_{\xi=-\lambda_{ab}}=\beta\lambda_{ab} \tag{3.5a}$$

$$\eta\big|_{\xi=\lambda_{sh}}=0 \tag{3.5b}$$

$$\left.\frac{d\eta}{d\xi}\right|_{\xi=-\lambda_{ab}}=-\bar{q}_0 \tag{3.5c}$$

$$\left.\frac{d\eta}{d\xi}\right|_{\xi=\lambda_2}=-2\gamma\lambda_2^2 \tag{3.5d}$$

In (3.5d) the compound slope

$$\gamma=\frac{\alpha\beta}{\alpha-\beta} \tag{3.6}$$

is defined as the effective foreset slope; the product of this slope with the shoreline position $s_2(t)$ provides the water depth at the toe of the submarine sediments. The solution of (3.4), satisfying conditions (3.5b) and (3.5c), is

$$\eta(\xi)=\frac{\bar{q}_0}{\nu}\left[\lambda_{sh}\left(\frac{e^{-\xi^2}+\pi^{\frac{1}{2}}\xi\left[erf(\xi)+erf(\lambda_{ab})\right]}{e^{-\lambda_{sh}^2}+\pi^{\frac{1}{2}}\lambda_{sh}\left[erf(\lambda_{sh})+erf(\lambda_{ab})\right]}\right)-\xi\right] \tag{3.7}$$

where $erf(x)=(2/\sqrt{\pi})\int_0^x e^{-t^2}dt$ is the error function. Using (3.7) in the remaining two boundary conditions, (3.5a) and (3.5d), we obtain nonlinear equations in the moving boundary constants λ_{ab} and λ_{sh} in (3.1):

$$\frac{R_{ab}e^{-\lambda_{sh}^2}}{e^{-\lambda_{sh}^2}+\pi^{\frac{1}{2}}\lambda_{sh}\left[erf(\lambda_{ab})+erf(\lambda_{sh})\right]}=2R_{sh}\lambda_{sh}^2 \tag{3.8a}$$

$$\frac{R_{ab}e^{-\lambda_{ab}^2}}{e^{-\lambda_{sh}^2}+\pi^{\frac{1}{2}}\lambda_{sh}\left[erf(\lambda_{ab})+erf(\lambda_{sh})\right]}=\frac{\lambda_{sh}}{\lambda_{sh}}(1-R_{ab}) \tag{3.8b}$$

where the shoreline slope ratio $R_{sh} = \gamma/\beta = \alpha/(\alpha - \beta)$ is the ratio of the effective foreset slope (3.6) to the bedrock slope, and the alluvial–bedrock slope ratio $R_{ab} = \bar{q}_0/(\nu\beta)$ is the ratio of the fluvial to bedrock slopes at the alluvial–bedrock transition. Note that the physical nature of the problem constrains $R_{sh} \geq 1$ and $0 < R_{ab} < 1$. Solving the system (3.8) for λ_{sh} and λ_{ab} provides for simultaneous tracking of the shoreline $s_2(t) = 2\lambda_{sh}(\upsilon t)^{1/2}$ and the alluvial–bedrock transition $s_1(t) = -2\lambda_{ab}(\upsilon t)^{1/2}$ with time.

4. Limit solutions

In the limit $R_{ab} \to 1$, (3.8b) requires that the alluvial–bedrock transition be set at $x \to -\infty$, i.e. $\lambda_{ab} \to \infty$. Substituting this limit into (3.8a) generates the following equation for a finite value of λ_{sh}:

$$2\lambda_{sh}^2 \frac{\alpha}{\alpha - \beta} + \frac{\lambda_{sh}\pi^{\frac{1}{2}}\left[1 + erf\left(\lambda_{sh}\right)\right]}{e^{-\lambda_{sh}^2} + \pi^{\frac{1}{2}}\lambda_{sh}\left[1 + erf\left(\lambda_{sh}\right)\right]} - 1 = 0 \qquad (4.1)$$

This limit solution corresponds to fixing the alluvial–bedrock transition at $x = -\infty$ for all time $t \geq 0$ and tracking the movement of the shoreline into an ocean with a fixed level. A similarity solution specifically for this limit case has been previously developed by Capart et al. (2007), and we note that (4.1) corresponds to the fixed sea-level solution presented in this work: compare (4.1) with (57) in Capart et al. (2007). In the limit $R_{ab} \to 0$ there are two possible solutions. From (3.8) it is easy to see that a trivial solution of zero movement of the shoreline and alluvial–bedrock transition results for the cases in which $R_{ab} \to 0$ via $\bar{q}_0 \to 0$ (with ν and β fixed) or $\beta \to \infty$ (with ν and $\bar{q}_0$ fixed). The first condition corresponds to zero sediment delivery to the system and the second to the case of an infinitely deep ocean that removes all sediment supplied without forming a sediment prism. A non-trivial solution, however, exists when $R_{ab} \to 0$ via $\nu \to \infty$ (with β and $\bar{q}_0$ fixed). This limit does indeed set $\lambda_{ab} \to 0$ and $\lambda_{sh} \to 0$, but on multiplying both sides of (3.8) by ν it is noted that $\lambda_{ab}\nu^{1/2} \to 0$ and $\lambda_{sh}\nu^{1/2} \to \sqrt{\bar{q}_0/(2\gamma)}$. Hence, for this case,

although the alluvial–bedrock transition is fixed at $x = 0$ for all time, the shoreline moves according to

$$s_2 = \sqrt{\frac{2\bar{q}_0 t}{\gamma}} \tag{4.2}$$

The geometry of this problem simply involves a submarine sediment wedge with a horizontal fluvial surface coinciding with sea level and a foreset slope α prograding along the bedrock slope β. In this case, (4.2) can be readily derived from a simple mass balance. Indeed, the result in (4.2) matches the result obtained from the general geometric model of Kim & Muto (2007) under the assumption of a horizontal fluvial surface and no sea-level rise.

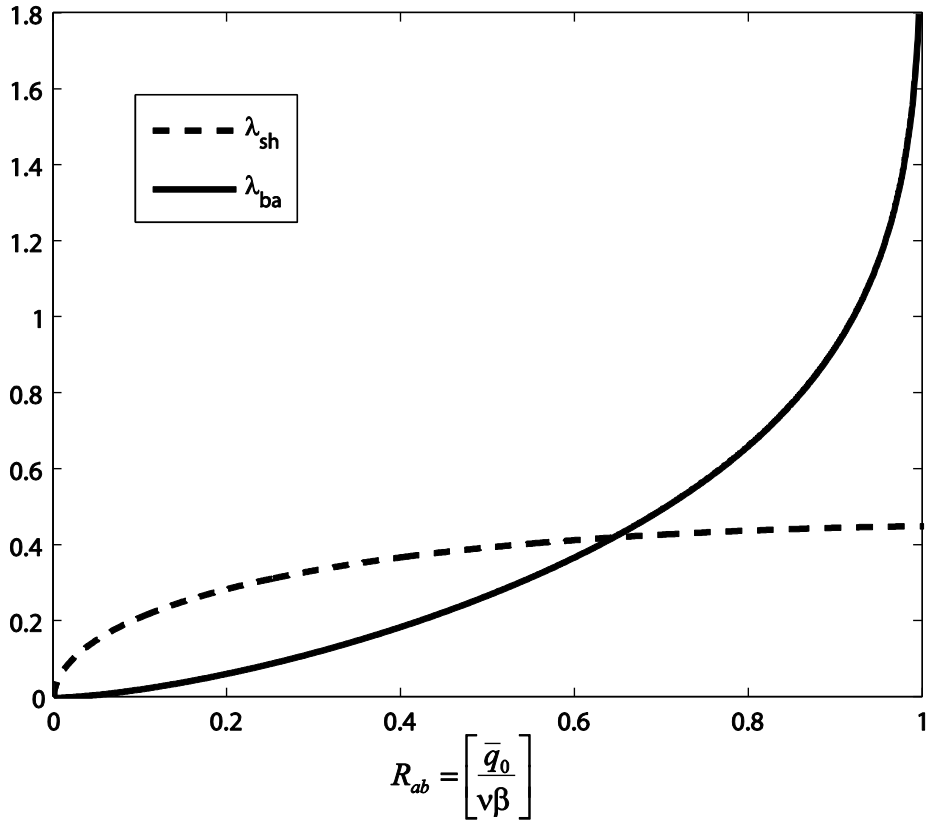

Fig. 2-2 The solution space for the moving boundary parameters in (3.10) in the field-relevant case in which $R_{sh} = \gamma/\beta = 1$.

5. The solution space

For field conditions the foreset slope, α, is typically much greater than the bedrock slope, β, and the shoreline slope ratio $R_{sh} \approx 1$. Hence the physical solution space (λ_{ab}, λ_{sh}) can be characterized by plotting the solutions of (3.8) against $0<R_{ab}<1$ while keeping the shoreline slope ratio fixed at $R_{sh}=1$. This plot is shown in Fig. 2. As a companion to this result the plots of the derivatives $d\lambda_{ab}/dR_{ab}$ and $d\lambda_{sh}/dR_{ab}$ are given in Fig. 3. The latter plot indicates the sensitivity of the moving boundary trajectories to changes in the value of the alluvial–bedrock slope ratio R_{ab}. As R_{ab} increases the movement of the alluvial–bedrock transition becomes increasingly sensitive to changes in R_{ab}, while the shoreline trajectory becomes less sensitive. For $R_{ab}<0.2$ the movement of the shoreline is more sensitive than the movement of the alluvial–bedrock transition. The situation reverses above $R_{ab} \sim 0.2$: the alluvial–bedrock transition is more sensitive to changes in R_{ab} than the shoreline. The results in Fig. 2 and 3 have an important consequence for the interpretation of the stratigraphic record. With an appropriate definition of the diffusivity (e.g. Swenson et al. 2000) the alluvial–bedrock slope ratio can be written as a function of the characteristic sediment type (gravel or sand), the water unit discharge q_w and the sediment unit discharge q_0, all key environmental parameters. Hence, in inferring past environmental changes in field sites at which the alluvial–bedrock slope ratios have $R_{ab}>0.2$, the alluvial–bedrock transition is a more sensitive 'signal recorder' than the shoreline. The reverse is true if $R_{ab}<0.2$. Both cases are possible in the field. We note, for example, that stratigraphic records in the Gulf of Mexico (Anderson & Fillon 2004) indicate alluvial–bedrock slope ratios in the range $0.2<R_{ab}<0.8$, while basins bounded by steep normal faults (e.g. Crowell 2003) would have vanishingly small values of R_{ab}.

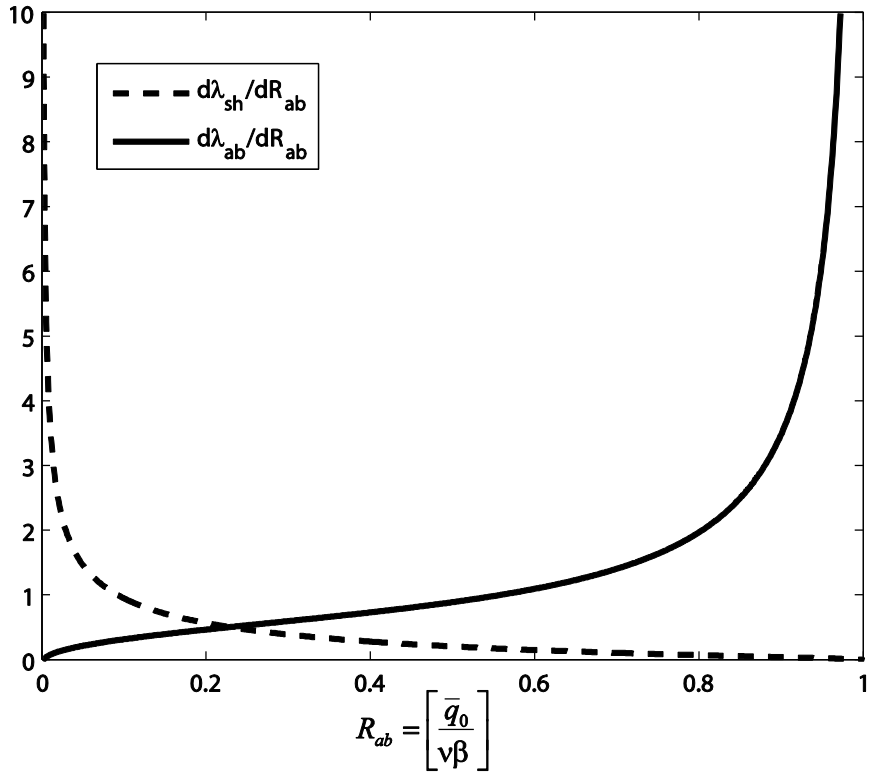

Fig. 2-3 Sensitivity of the moving boundary trajectories to changes in the value of the alluvial–bedrock slope ratio R_{ab}.

6. Comparison with experiment

We turn next to data from the experimental flume set-up at Nagasaki University, Japan, reported in Parker &Muto (2003),Muto & Swenson (2005, 2006), Kim &Muto (2007) and Swenson & Muto (2007), to provide experimental values to compare with the similarity solution given by (3.1) and (3.8). The experiments involved a narrow open-ended flume, 0.02m wide, 4.3m long and 1.3m deep, immersed inside a larger tank (Fig. 4). Both tank and flume contained fresh water. A weir placed at the downstream end of flume, above the tank water level, ensured a constant water depth in the flume. Separate water and sediment (quartz sand with uniform 0.2mm grain diameter and a density ρ =2598 kg/m^3) fluxes were mixed in a funnel and delivered to the upstream end of the flume. The sediment was transported down the flume as bed load with a typical water depth of ~1mm. The inclination of the flume floor (the bedrock slope β), the unit

sediment discharge q_0 (mm^2/s) and unit water discharge q_w (mm^2/s) were varied to provide the nine sets of experimental conditions summarized in table 1. Since the channel width was much greater than the water depth the Reynolds number for the flow in the flume, upstream of the shoreline, could be calculated as $Re = \rho q_w / \mu$. From table 1 this gives Reynolds numbers in the range $189 < Re < 879$; appealing to open channel flow, this suggests that the flow in the experiments was in the laminar or transitional regimes. The flow velocities upstream of the shoreline ranged between 189 and 879 mm/s. There was rapid deceleration when the flow reached and moved downstream of the shoreline, leading to sediment deposit on to the submarine wedge. As noted previously this sediment was redistributed by avalanche processes such that a wedge with a constant angle of repose was maintained. Beyond a few millimetres of the shoreline there was no notable disturbance of the water surface.

	q_w (mm^2/s)	q_0 (mm^2/s)	β
Run1	878.65	42.8	0.1705
Run2	733.1	42.8	0.1705
Run3	579.1	42.8	0.1705
Run4	562.25	42.8	0.2294
Run5	335.45	42.8	0.2294
Run6	232.15	42.8	0.2294
Run7	229.95	13.46	0.1705
Run8	220.45	13.46	0.2294
Run9	188.75	42.8	0.2294

Table 2-1 Experimental set-up conditions.

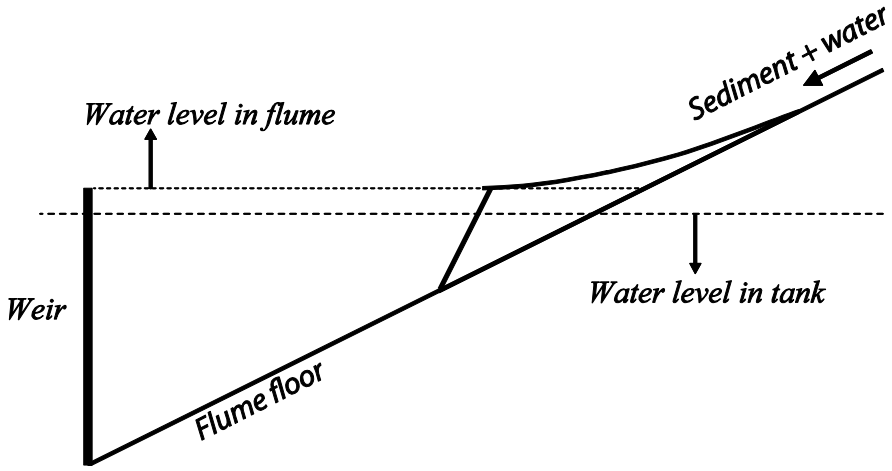

Fig. 2-4 Schematic of experimental flume.

For each experimental condition, high-resolution photographs, taken every 20 s, detailed the evolution of the sediment prism. Digital analysis of these photographs provided a record of the positions, measured from the original shoreline at x =0, of the alluvial–bedrock transition L_{ab}, the shoreline L_{sh} and the intersection of the foreset with the bedrock (the 'toe') L_{toe}. In order to obtain analytical predictions for the trajectories of the shoreline and alluvial–bedrock transition we need to know, for a given system, the input sediment flux q_0, the bedrock slope β, the porosity of the deposit, the shoreline slope ratio $R_{sh} = \alpha/(\alpha - \beta) > 1$ and the alluvial–bedrock slope ratio $0 < R_{ab} = q_0/(v\beta) < 1$. To make a valid

comparison between analytical predictions and experiments these constant parameters have to be determined from measurements taken at a single time, which on subsequent use in the analytical solution recover the experimental measurements through time. The values of q_0 and β are part of the experimental set-up conditions (see table 1). The porosity of the deposited sediment was assumed to be 0.3; this value was chosen by comparing an experimental final time image of the deposit area to the know sediment input. Since the foreset slope is assumed linear, $\alpha = \beta L_{toe}/(L_{toe} - L_{sh})$, the shoreline slope ratio is readily determined as

$$R_{sh} = \frac{L_{toe}}{L_{sh}} \tag{6.1}$$

The estimation of the alluvial–bedrock slope ratio, however, is a little more involved. First it is noted that for a small increment is in the shoreline movement the volume of sediment deposited offshore is given by $\Delta s L_{toe} \beta$. In contrast, on assuming that the curvature of the fluvial surface is large, the volume deposited on the fluvial surface can be approximated as $\Delta s L_{toe} \beta$. In this way, the sediment flux at the shoreline can be expressed as the following fraction of the input sediment flux:

$$\bar{q}_{sh} = \bar{q}_0 \frac{L_{toe}}{L_{toe} + L_{ab}} \tag{6.2}$$

Further, we note that the average fluvial sediment flux on the fluvial surface (defined as the product of diffusivity and average slope) can be written as a weighted average of the input and shoreline fluxes, i.e.

$$\nu \frac{\beta L_{ab}}{L_{sh} + L_{ab}} = \phi \bar{q}_0 + (1 - \phi) \bar{q}_{sh} \tag{6.3}$$

where $0 \leq \varphi \leq 1$. On combining (6.2) with (6.3) and rearranging, we arrive at the following estimate for the alluvial–bedrock slope ratio in terms of the experimental measurement at a fixed point in time:

$$R_{ab} = \frac{\dfrac{L_{ab}}{L_{sh} + L_{ab}}}{\phi + (1-\phi)\dfrac{L_{toe}}{L_{toe} + L_{ab}}} \tag{6.4}$$

To be fully determined we need a choice for the weighting factor φ. The choice of $\varphi = 1$ corresponds to assuming that the fluvial surface is linear, which contradicts the assumption of a diffusive flux that would build a concave surface. The choice of any other constant (e.g. $\varphi = 0.5$) will, in the limit of $L_{ab} \to \infty$, result in non-physical values of $R_{ab} > 1$. Hence, a choice of weighting that varies between 0 and 1 in the physical limits of $0 < L_{ab} < \infty$ is needed. Here, based on assuming the weighting is a function of the fractions of the shoreline and alluvial–bedrock lengths, we use the choice

$$\phi = \frac{L_{ab}}{L_{sh} + L_{ab}} \tag{6.5}$$

Table 2 reports the values of R_{sh} and R_{ab} obtained from the experimental measurements through (6.1), (6.4) and (6.5). These values, reported in terms of the mean μ_R and the standard deviation σ, are obtained by making estimations at each time step in the range $0.1t_{end} < t < t_{end}$ (tend is the total experimental run time); in all cases the sample size exceeded 100. From knowledge of the behavior of the analytical solution it is known that predictions are relatively insensitive to changes in the value of R_{sh} but, especially at values close to 1, sensitive to changes in the alluvial–bedrock ratio R_{ab}. As such, in comparing the analytical predictions with the experimental measurements we use two realizations. While both use the mean value of R_{sh} from table 2, the values for the alluvial–bedrock ratio R_{ab} are set at $\mu_R \pm 2\sigma$. The analytical predictions for the shoreline and alluvial–bedrock transition trajectories obtained with the values in tables 1 and 2 are compared with the experimental measurements in Fig. 5–7. For most of the runs, there is a close match between the analytical predictions and experimental measurements; in particular the upper and lower bound analytical predictions encompass the experimental measurements. In runs 6 and 9, however, there is a clear outward drift of the alluvial–bedrock transition measurements. This discrepancy can be attributed to the fact that these two runs correspond to the largest values of the alluvial–bedrock slope ratio R_{ab}, 0.8729 and 0.9139 (see table 2); from the above analysis we know when this ratio is close to

unity, small changes in its value can have a significant effect on the movement of the alluvial–bedrock transition (see Fig. 3). This is verified on noting that with small increases in the estimated value of R_{ab}, obtained from (6.4), the analytical solution is able to predict alluvial–bedrock transition movement in close agreement with the measurement; e.g. Fig. 8 compares run 9 predictions when the estimated R_{ab} value is increased by 3%.

	Rab		Rsh	
	μR	σ	μR	σ
Run 1	0.6519	0.0109	0.6649	0.0321
Run 2	0.7232	0.0091	0.6621	0.025
Run 3	0.8024	0.0085	0.6689	0.0407
Run 4	0.656	0.0177	0.6765	0.021
Run 5	0.8087	0.0066	0.6528	0.0132
Run 6	0.8729	0.0077	0.6531	0.0126
Run 7	0.8626	0.0079	0.6053	0.0251
Run 8	0.6644	0.0163	0.6404	0.0099
Run 9	0.9139	0.0036	0.6394	0.0174

Table 2-2 The mean and standard deviations of the alluvial–bedrock and shoreline slope ratios obtained from experimental measurements.

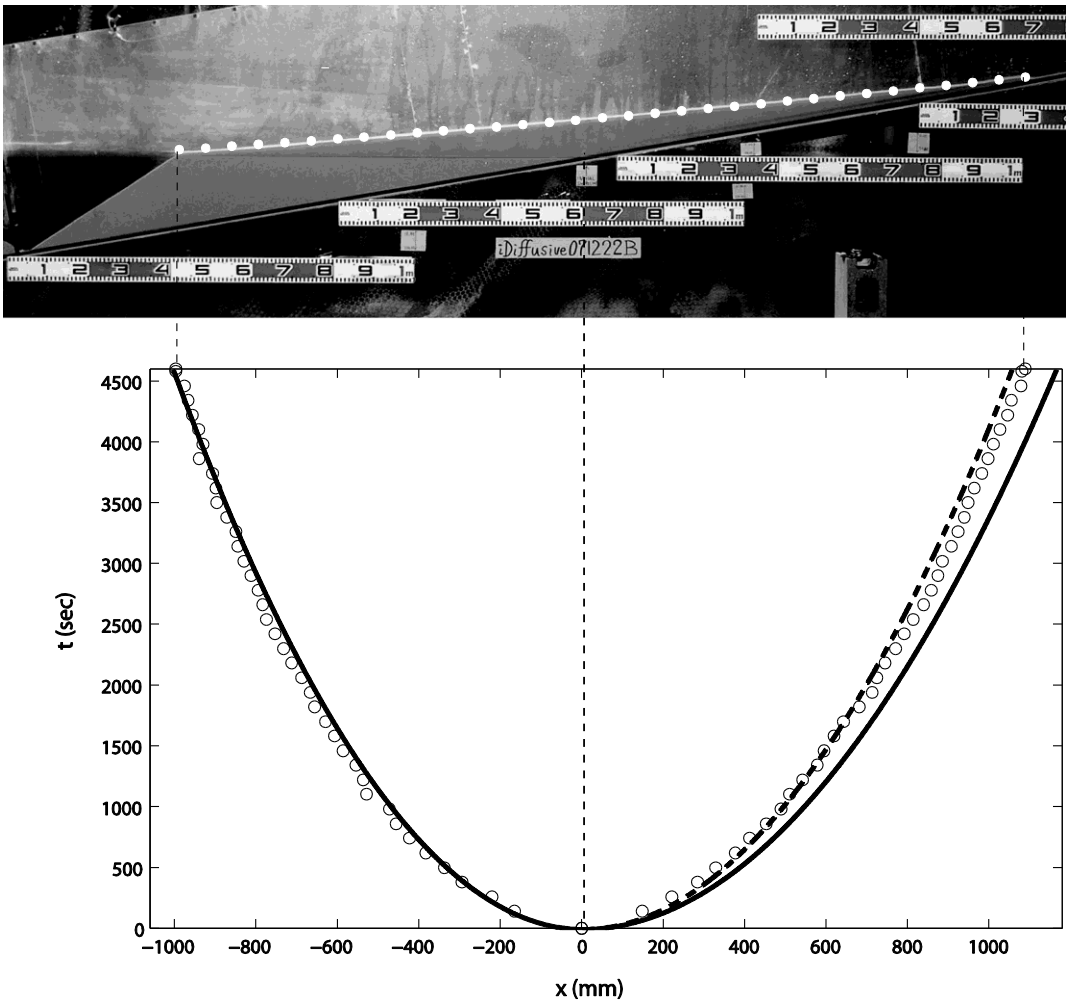

Fig. 2-5 Experimental run 1. Predicted shoreline and alluvial–bedrock movements with time for $R_{ab} = \mu_R + 2\sigma$ (continuous line) and $R_{ab} = \mu_R - 2\sigma$ (dashed line) versus positions extracted from experimental images (open circles). The picture is the experimental image at time $t = t_{end}$. Superimposed on this image is the fluvial surface (white dots) given by the analytical solution when $R_{ab} = \mu_R$.

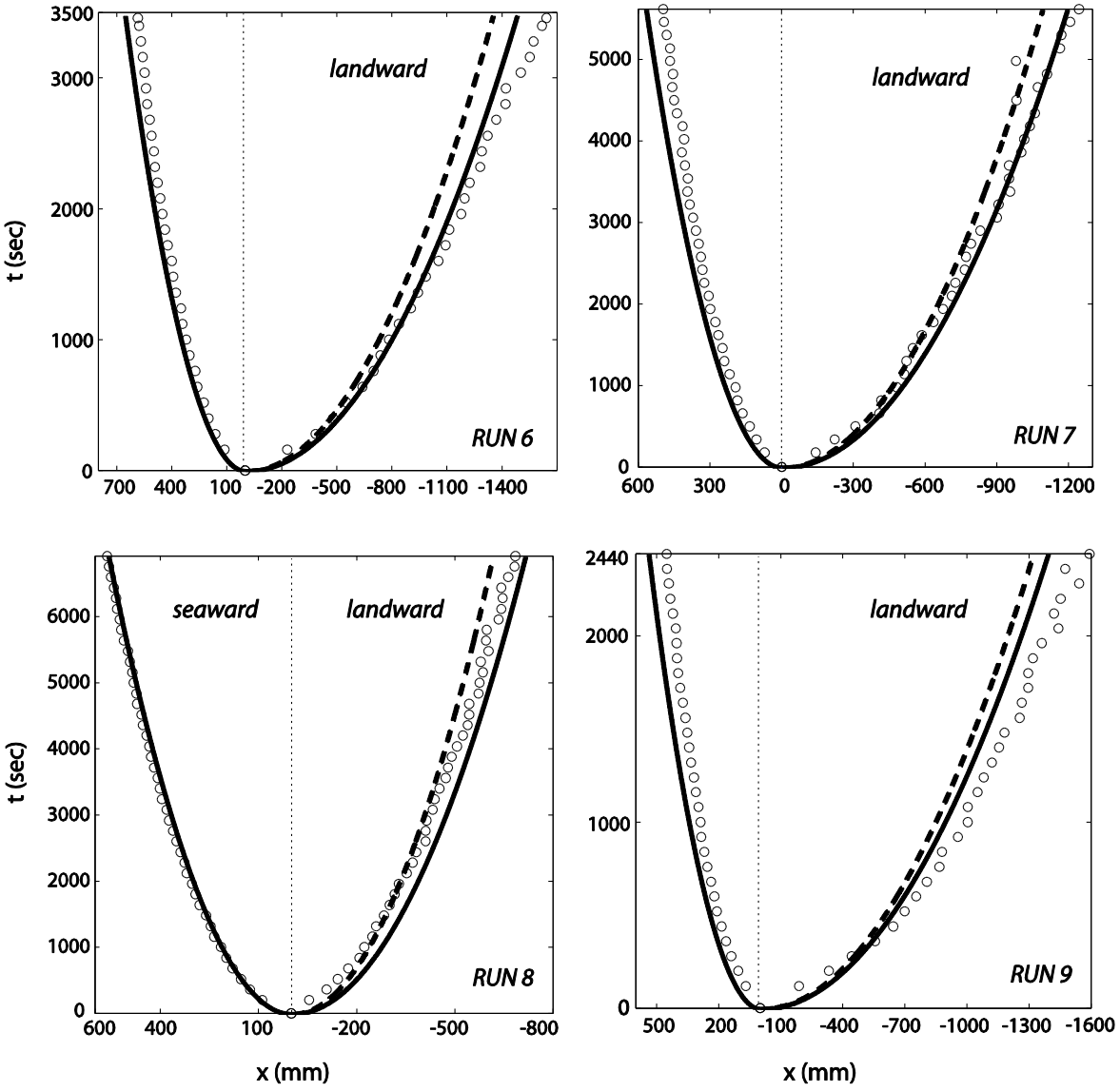

Fig. 2-6 Experimental runs 2–5. Predicted shoreline and alluvial–bedrock movements with time for $R_{ab} = \mu_R + 2\sigma$ (continuous line) and $R_{ab} = \mu_R - 2\sigma$ (dashed line) versus positions extracted from experimental images (open circles).

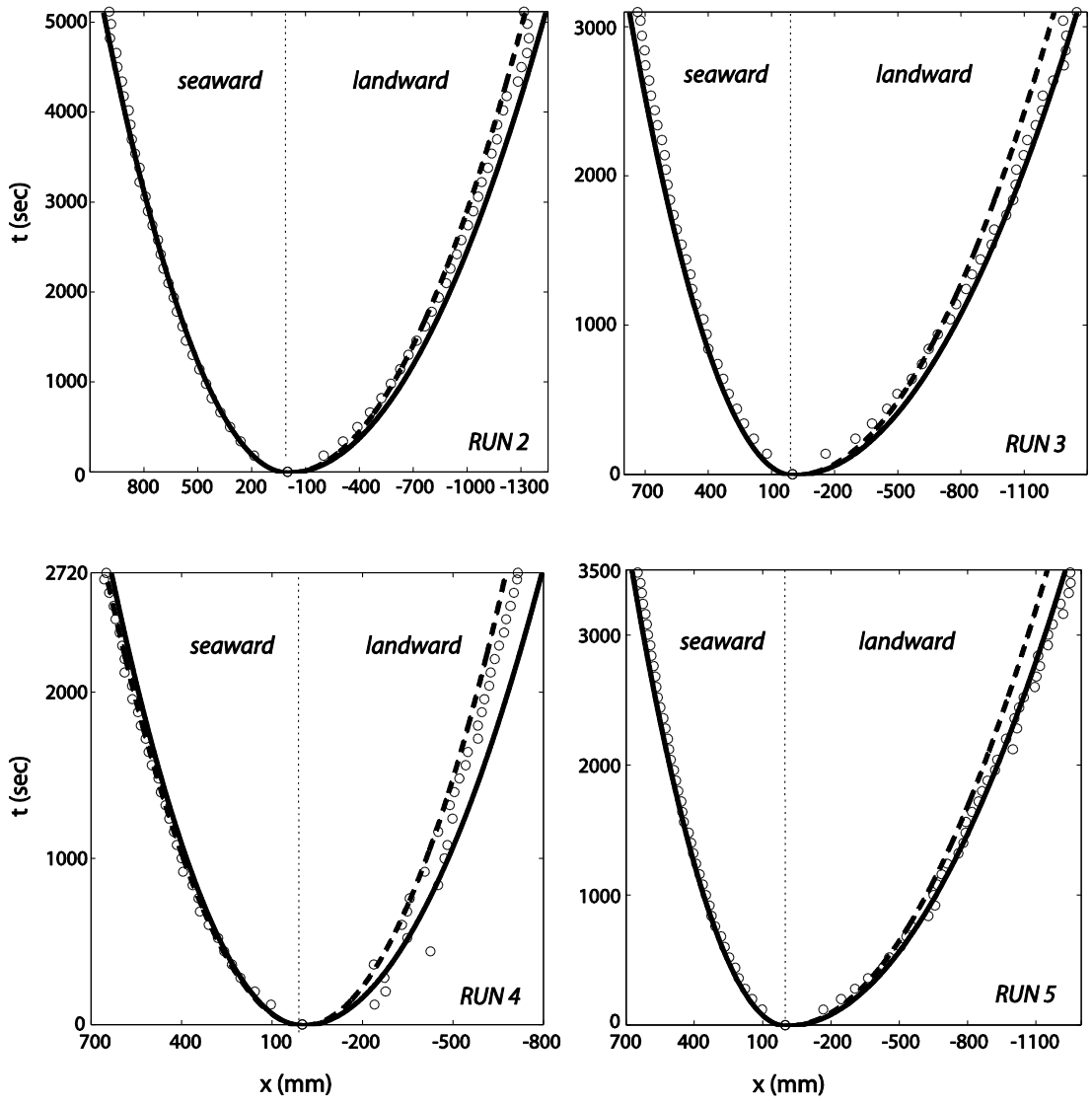

Fig. 2-7 Experimental runs 6–9. Predicted shoreline and alluvial–bedrock movements with time for $R_{ab} = \mu_R + 2\sigma$ (continuous line) and $R_{ab} = \mu_R - 2\sigma$ (dashed line) versus positions extracted from experimental images (open circles).

In addition to the drifts noted above it may be observed that, at some instances, the measured movement of the alluvial–bedrock transition is erratic. This is attributed to the small angle of the sediment wedge at the alluvial–bedrock transition (see photograph in Fig. 5). This feature makes the alluvial–bedrock transition region sensitive to local perturbations in sediment flux, leading to a loss in resolution of the exact position in the digital image.

Another factor that affects the comparisons between the solution and the experiment is the choice of porosity; the dependence of the moving boundaries on the porosity is given by $1/\sqrt{1-n}$. In particular, we note that an increase in porosity from the current value of *n=0.3* to *n=0.4* expands the envelope of the alluvial–bedrock transition and the shoreline in Fig. 5–7 by~7%.

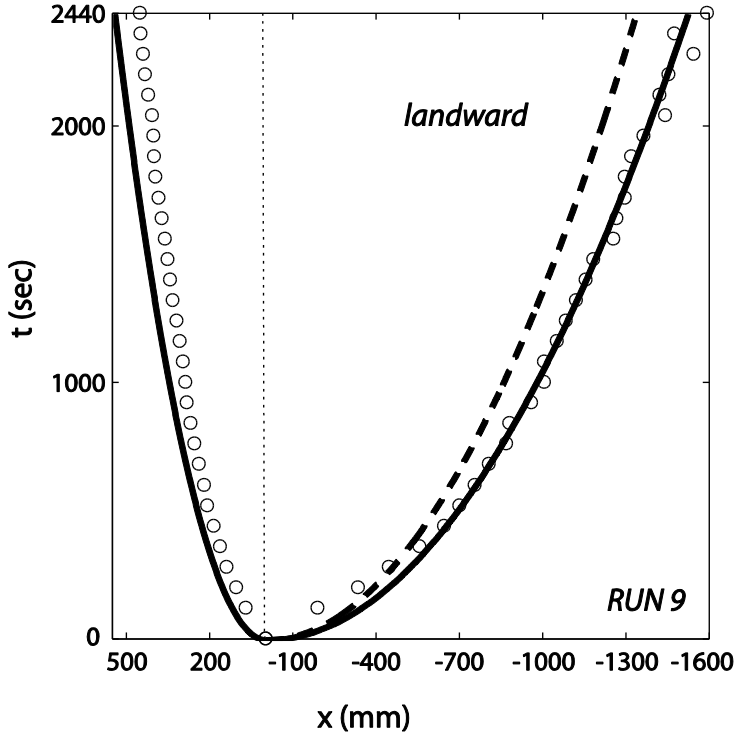

Fig. 2-8 A large change in run 9 alluvial–bedrock transition predictions can be induced by a small increase in alluvial–bedrock slope ratio R_{ab}. Dashed line is the prediction of the alluvial–bedrock transition with original value R_{ab} =0.9139 (table 2); solid line denotes the predictions with a 3% increase (R_{ab}=0.9413); and symbols signify experiments.

7. A comment on sea-level rise

Under the assumption that sea level changes as the square root of time and is bounded from above by rate of the shoreline movement, an accounting of the sea-level variation can be readily incorporated in the closed-form similarity solution presented here. This prescription for sea-level rise, first used by Capart et al. (2007) in their single moving boundary model, does not however lead to any significant physical changes over the

behavior of the solution with a constant sea level. In particular, the common case of shoreline transgression during sea-level rise cannot be attained.

8. Conclusions

The main objective of this paper has been to study the solution to a moving boundary problem arising from the study of the long-term evolution of the coastal sedimentary prism. In keeping with previous work, this problem can be viewed as a generalized version of the well-known Stefan melting problem. The interesting feature here is the appearance of two moving boundaries, the alluvial–bedrock transition and the shoreline. The closed-form similarity solution for this dual moving boundary problem shows that the movement of the alluvial–bedrock transition becomes increasingly sensitive to environmental parameters (sediment type, sediment discharge and water discharge) as the ratio of the alluvial to bedrock slope increases. In particular, the analytical solution indicates that when the alluvial–bedrock slope ratio exceeds 0.2, a condition encountered in the field, determination of these parameters from preserved deposits is better done using the trajectory of the alluvial–bedrock transition than that of the shoreline, despite the emphasis on the latter in the earth science literature.

The relatively simple nature of the problem studied has also allowed the use of experiments in a small laboratory flume to compare physical measurements with the analytical solution. Using estimation of solution parameters obtained from experimental measurements taken at single time, the analytical solution is able to recover the measured movements of the shoreline and alluvial–bedrock transition through time.

Clearly the problem studied here is also amenable to numerical solution, perhaps through using variations of the enthalpy method (Voller et al. 2006) or smooth particle hydrodynamics (SPH; Monaghan, Huppert & Worster 2005). While such solutions may not retain the precision or elegance of the analytical solution presented here, they will allow for the generation of solutions of more general problems, e.g. problem in multiple dimensions with arbitrary imposed changes in sea level.

Chapter 3: Analytical and numerical solution of a generalized Stefan problem exhibiting two moving boundaries.

Published as; J. Lorenzo-Trueba, and V. R. Voller (2010), Analytical and numerical solution of a generalized Stefan problem exhibiting two moving boundaries, *Journal of Mathematical Analysis and Applications*, 366, 538-549.

A model associated with the formation of sedimentary ocean deltas is presented. This model is a generalized one dimensional Stefan problem bounded by two moving boundaries, the shoreline and the alluvial-bedrock transition. The sediment transport is a non-linear diffusive process; the diffusivity modeled as a power law of the fluvial slope. Dimensional analysis shows that the first order behavior of the moving boundaries is determined by the dimensionless parameter $0 \le R_{ab} \le 1$—the ratio of the fluvial slope to bedrock slope at the alluvial-bedrock transition. A similarity form of the governing equations is derived and a solution that tracks the boundaries obtained via the use of a numerical ODE solver; in the cases where the exponent θ in the diffusivity model is zero (linear diffusion) or infinite, closed from solutions are found. For the full range of the diffusivity exponents, $0 \le \theta \to \infty$, the similarity solution shows that when $R_{ab} < 0.4$ there is no distinction in the predicted speeds of the moving boundaries. Further, within the range of physically meaningful values of the diffusivity exponent, i.e., $0 \le \theta \sim 2$, reasonable agreement in predictions extents up to $R_{ab} \sim 0.7$. In addition to the similarity solution a fixed grid enthalpy like solution is also proposed; predictions obtained with this solution closely match those obtained with the similarity solution.

1. Introduction

In a moving boundary problem one or more of the domain boundaries is an *a-priori* unknown function of space and time. The classical example is the one phase Stefan melting problem (Crank 1984) where one of the domain boundaries is the moving solid/liquid front. Generalizations of the Stefan problem have been applied to wide classes of problems. A Stefan like problem of current interest—dating back to the work of Swenson et al. 2000 and Marr et al. 2000—is associated with the formation of sediment ocean deltas and fluvial sediment fans. For such systems, an analogy between sediment and heat transport can be effectively applied to arrive at a generalized Stefan problem that has some interesting features. In particular, the appearance of two moving boundaries; a feature also seen in some solidification (Worster 1986, Voller 1997) and polymer swelling systems (Barry and Caunce 2008).

Both analytical and numerical solutions have been developed for the sediment ocean delta problem. Under the conditions of a constant sediment flux applied at $x = 0$ and a constant bedrock slope, Voller et al. 2004 developed a closed form similarity solution for a one-dimensional version of the sediment delta problem in which the moving boundary of interest is the shoreline (SHL) $x = s_{sh}(t)$. Capart and co-workers (Capart et al. 2007, Lai and Capart 2007, Lai and Capart 2009), and Lorenzo-Trueba et al. 2009 expand on this work by developing analytical and semi-analytical solutions that track two moving boundaries, the seaward movement of the shoreline and the landward movement of the alluvial-bedrock transition (ABT) $x = -s_{ab}(t)$. A feature in the analytical dual moving boundary treatments is the assumption of a linear diffusion law to model the sediment unit flux in terms of a constant diffusivity ν multiplied by the local slope of the sediment deposit, i.e.,

$$q(x) = -\nu \frac{\partial h}{\partial x} \tag{1}$$

where h is the sediment height above a horizontal datum and the units of the flux q are volumetric sediment bed transport per unit width and time; a definition that takes account for porosity in the sediment deposit.

A basic approximate solution to the dual moving boundary sediment delta problem can be obtained by assuming that the surface of the deposited sediment is linear. As detailed in Kim and Muto 2007, this allows for the construction of a geometric relationship that can be used to track both the SHL and ABT. In more sophisticated approximate approaches numerical solutions, employing coordinated transforms have been presented by Parker and Muto 2003, Swenson and Muto 2007. A feature in these works is the consideration of a non-linear model for the unit flux where the constant diffusivity ν in (1) is replaced by a function of the sediment deposit's slope, i.e.,

$$\nu = \nu^* \left| \frac{\partial h}{\partial x} \right|^{\theta} \tag{2}$$

where ν^* is a constant with dimensions of diffusivity and the exponent $\theta \geq 0$ is a constant.

A drawback of the coordinate transform numerical approaches for the sediment delta problem (Parker and Muto 2003, Swenson and Muto 2007) is that there is not an obvious path toward the solution of two dimensional problems. To address this, Voller et al. 2006 develop an "enthalpy" like solution that can operate on a fixed grid in the untransformed space. This solution approach has been successfully verified with the single moving shoreline analytical solution of Voller et al. 2004 and applied to the problems of the growth of two dimensional deltas (Voller et al. 2006). Currently, however, As the method stands, however, is not able to handle the simultaneous tracking of the SHL, $x = s_{sh}(t) > 0$, and the ABT, $x = s_{ab}(t) < 0$.

The objective of this paper is two-fold. In the first place the dual boundary delta growth similarity solution of Lorenzo-Trueba et al. 2009 will be extended to allow for the non-linear diffusion form in (2). In the general case, $\theta > 0$, the resulting similarity ODE requires a numerical solution. In the special limit cases, $\theta = 0$ and $\theta \to \infty$, however,

closed form solutions can be obtained. In the $\theta = 0$ limit, the error function closed form solution presented by Lorenzo-Trueba et al. 2009 results. In the $\theta \to \infty$ limit, the geometrical solution of Kim and Muto 2007 is obtained. Numerical treatment of the similarity equations indicates that the solution in the general case of finite non-zero value of θ is bounded by these two limit solutions.

The second objective of this paper is to further develop the enthalpy solution of Voller et al. 2006 so that it can deal with the dual moving boundary delta growth problem under the assumption of the non-linear diffusion form in (2). This numerical approach is verified by comparing with the closed ($\theta = 0$) and numerical ($\theta > 0$) solutions of the similarity ODE.

2. The Dual Moving Boundary Problem

2.1 Equations

A one-dimensional schematic of the problem of interest, a cross sectional view of a sediment delta building on a non-subsiding constant slope ($-\beta > 0$) bedrock into an ocean with a fixed relative sea-level $z = 0$, is shown in Fig. 1. Initially a constant unit sediment flux $q_0 > 0$ (area/time) is introduced upstream of the initial SHL position $x = 0$. The bedrock slope is sufficient to transport this sediment flux to the ocean where it deposits to form a small sediment wedge. Over time this sediment wedge increases in size, consisting of a submarine component advancing into the deepening ocean and a subaerial fluvial component moving landward, up the bedrock slope, see Fig. 1. When the downstream moving sediment flux on the bedrock encounters the upstream portion of the sediment wedge it begins to deposit. This deposition continues down the length of the fluvial surface. At the SHL the remaining flux is deposited offshore, contributing to the advance of the SHL. The sediment is moved and deposited over the fluvial surface by channel processes. Through the coupling of the momentum balance with fundamental descriptions of the sediment bed-load transport it can be argued, for a wide range of laboratory and field cases (Parker and Muto 2003, Swenson and Muto 2007, Postma et al. 2008), that the sediment flux on the fluvial surface can be modeled by the general non-linear form given in (2). Depending on the assumptions made and situations considered

values of the exponent in this model have been reported in the range $0 \le \theta \sim 2$. To close the model, the mechanism for submarine sediment transport and deposition needs to be defined. In keeping with previous works (Swenson et al. 2000, Marr et al. 2000, Lorenzo Trueba et al. 2009) it is assumed that grain movement by subaqueous avalanches is much more rapid than the movement of sediment by the fluvial processes in the subaerial domain, and as such the offshore transport deposition can be modeled as a "sediment wedge" with a constant angle of repose with slope α.

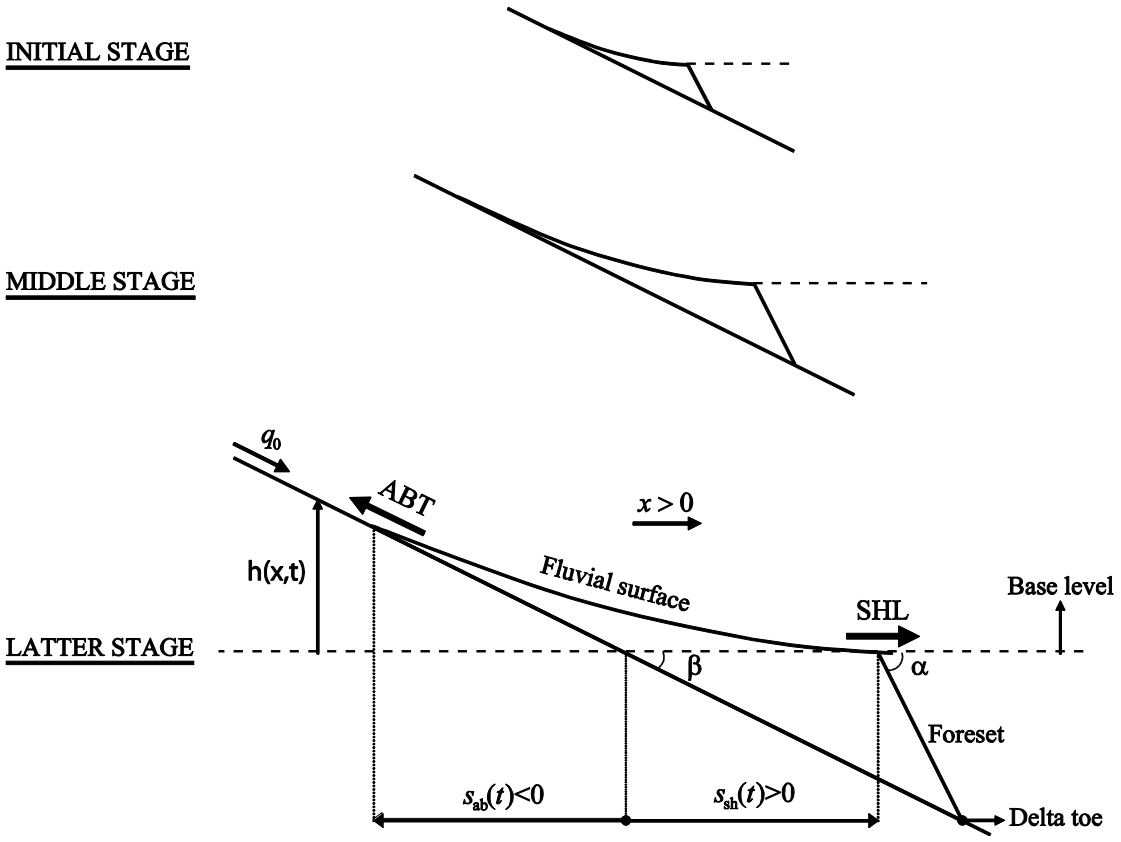

Fig. 3-1 Schematic of dual moving boundary problem; the shoreline (SHL) moves seaward, and the alluvial-bedrock transition (ABT) moves landward.

With the above assumption for the sediment transport, a governing equation is derived by using the unit flux definition (1) in the Exner equation (Paola and Voller 2005) for the mass balance in the sediment wedge, to arrive at the diffusion equation

$$\frac{\partial h}{\partial t} = \frac{\partial}{\partial x}\left(\nu^* \left|\frac{\partial h}{\partial x}\right|^{\theta} \frac{\partial h}{\partial x} \right), \qquad s_{ab}(t) \le x \le s_{sh}(t) \tag{3}$$

The boundary conditions for this dual moving boundary problem are

$$h\big|_{x=s_{ab}(t)} = -\beta s_{ab}(t) \tag{4a}$$

$$h\big|_{x=s_{sh}(t)} = 0 \tag{4b}$$

$$\nu^* \left|\frac{\partial h}{\partial x}\right|^{\theta} \frac{\partial h}{\partial x}\bigg|_{x=s_{ab}(t)} = -q_0 \tag{4c}$$

$$\nu^* \left|\frac{\partial h}{\partial x}\right|^{\theta} \frac{\partial h}{\partial x}\bigg|_{x=s_{sh}(t)} = -\gamma s_{sh} \frac{ds_{sh}}{dt} \tag{4d}$$

where the slope ratio $\gamma = \alpha\beta/(\alpha - \beta)$ is referred to as the effective submarine slope; the product γs_{sh} gives the depth of the ocean at the delta toe. The first condition (4a) fixes the upstream vertex of the sediment wedge to the height of the bed rock at the current position of the ABT. The second condition (4b) sets the SHL at sea level. The extra boundary conditions (4c) and (4d) are required to track the positions of the unknown moving boundaries, the SHL $x = s_{sh}(t)$ and ABT $x = s_{ab}(t)$. The condition (4c) is a statement of the continuity of flux at $x = s_{ab}(t)$ and the condition (4d), analogous to the Stefan condition in heat transfer, expresses the sediment balance at the SHL. The appropriate initial conditions are $s_{sh}(0) = s_{ab}(0) = h(x,0) = 0.$

2.2 Behavior in limit $\theta \to \infty$

At this point it is worthwhile briefly noting the behavior of the problem in (3) and (4) in the limit of a large value for the exponent θ in the non-linear diffusion model (2). First,

based on the purely depositional nature of the system, the following behaviors that hold regardless of the value of θ are noted:

(i) the rate of deposition is finite and positive, $\partial h / \partial t > 0 \;\; \forall x \in [s_{ab}, s_{sh}], \; t \geq 0$,

(ii) the velocity of the SHL ds_{sh} / dt is finite at any SHL position $s_{sh} > 0$,

(iii) the slope of the fluvial surface is bounded by $-\beta \leq \partial h / \partial x < 0, \forall x \in [s_{ab}, s_{sh}], \; t \geq 0$

Together, through (3), (4c), and (4d) these conditions imply that for any value of θ the value of sediment unit flux decreases monotonically between $x = s_{ab}$ and $x = s_{sh}$ and is bounded by

$$q_0 \geq -\nu^* \left| \frac{\partial h}{\partial x} \right|^{\theta} \frac{\partial h}{\partial x} \geq \gamma s_{sh} \frac{ds_{sh}}{dt} \tag{5}$$

This in turn implies, through (iii) above, that the non-linear diffusion term $\nu = \nu^* |\partial h / \partial x|^{\theta}$ is strictly positive and bounded.

Further progress is made from these observations by using the fact that $|\partial h / \partial x| = -\partial h / \partial x$ to expand the left hand side of (3) and arrive at

$$\frac{1}{(\theta + 1)} \frac{\partial h}{\partial t} = \nu^* \left| \frac{\partial h}{\partial x} \right|^{\theta} \frac{\partial^2 h}{\partial x^2}, \qquad s_{ab}(t) \leq x \leq s_{sh}(t) \tag{6}$$

Based on the observations made above, finite positive deposition and bounded non-linear diffusivity, it can be concluded from (6) that in the limit $\theta \to \infty$ the curvature of the fluvial surface $\partial^2 h / \partial x^2 \to 0$, i.e., the fluvial surface becomes linear. As a linear fluvial surface is approached the rate of deposition $\partial h / \partial t$ becomes a function of time alone and hence, with reference to (3), the flux term $\nu^* |\partial h / \partial x|^{\theta} \, \partial h / \partial x$ needs to approach a linear function in space. So in the limit of $\theta \to \infty$ both the fluvial surface and the flux become linear functions in space.

2.3 A dimensionless form

On defining the ratio of the fluvial to bedrock slope at the ABT to be

$$R_{ab} = -\frac{1}{\beta}\frac{\partial h}{\partial x}\bigg|_{x=s_{ab}}, \tag{7}$$

which through (4c) is a constant, appropriate dimensionless variables for the problem at hand can be defined as follows

$$x^d = \frac{x}{\ell}, \quad h^d = \frac{h}{\beta\ell}, \quad s^d = \frac{s}{\ell}, \quad t^d = \frac{tq_0}{\ell^2\beta R_{ab}}, \tag{8}$$

where the superscript *d* indicates a dimensionless variable, and ℓ is a convenient length scale. In this way, dropping the *d* superscript for convenience of notation, the following dimensionless version of the governing equations (3) and (4) results

$$\frac{\partial h}{\partial t} = \frac{\partial}{\partial x}\left(\frac{1}{R_{ab}^{\theta}}\left|\frac{\partial h}{\partial x}\right|^{\theta}\frac{\partial h}{\partial x}\right), \qquad s_{ab}(t) \le x \le s_{sh}(t) \tag{9}$$

with boundary conditions

$$h\big|_{x=s_{ab}(t)} = -s_{ab}(t) \tag{10a}$$

$$h\big|_{x=s_{sh}(t)} = 0 \tag{10b}$$

$$\frac{1}{R_{ab}^{\theta}}\left|\frac{\partial h}{\partial x}\right|^{\theta}\frac{\partial h}{\partial x}\bigg|_{x=s_{ab}(t)} = -R_{ab} \tag{10c}$$

$$\frac{1}{R_{ab}^{\theta}}\left|\frac{\partial h}{\partial x}\right|^{\theta}\frac{\partial h}{\partial x}\bigg|_{x=s_{sh}(t)} = -R_{sh}s_{sh}\frac{ds_{sh}}{dt} \tag{10d}$$

In the above

$$R_{sh} = \frac{\gamma}{\beta} = \frac{\alpha-\beta}{\alpha} \tag{11}$$

is the ratio of the effective submarine slope to the bedrock slope and

$$q^d = -\frac{1}{R_{ab}^{\theta}}\left|\frac{\partial h}{\partial x}\right|^{\theta}\frac{\partial h}{\partial x} \tag{12}$$

is identified as the dimensionless flux, $q^d = qR_{ab}/q_0$.

The dimensionless form (9) and (10) shows that the dual moving boundary problem related to the formation of a ocean sediment delta is fully specified by the value of the exponent in the non-linear diffusion law θ and the dimensionless parameters of the alluvial-bedrock slope ratio, R_{ab}, and the shoreline slope ratio, R_{sh}. For future reference, note that the value of the alluvial-bedrock slope ratio is theoretically bounded by $0 \le R_{ab} \le 1$ and the value of the shoreline slope ratio is restricted to be $R_{sh} \ge 1$.

2.4 Similarity equations

On setting the movement of the ABT and the SHL to be respectively

$$s_{ab} = -2\lambda_{ab}t^{\frac{1}{2}} \tag{13a}$$

$$s_{sh} = 2\lambda_{sh}t^{\frac{1}{2}} \tag{13b}$$

introducing the similarity variable

$$\xi = \frac{x}{2t^{\frac{1}{2}}} \tag{14}$$

and scaling the sediment height by

$$\eta = \frac{h}{2t^{\frac{1}{2}}} \tag{15}$$

equations (9) and (10) reduce to the ordinary differential equation

$$\frac{1}{2}\frac{d}{d\xi}\left(\frac{1}{R_{ab}^{\theta}}\left|\frac{d\eta}{d\xi}\right|^{\theta}\frac{d\eta}{d\xi}\right) + \xi\frac{d\eta}{d\xi} - \eta = 0, \qquad -\lambda_{ab} \le \xi \le \lambda_{sh} \tag{16}$$

with

$$\eta\big|_{\xi=-\lambda_{ab}} = \lambda_{ab} \tag{17a}$$

$$\eta\big|_{\xi=\lambda_{sh}} = 0 \tag{17b}$$

$$\frac{1}{R_{ab}^{\theta}}\left|\frac{\partial\eta}{\partial\xi}\right|^{\theta}\frac{d\eta}{d\xi}\bigg|_{\xi=-\lambda_{ab}} = -R_{ab} \tag{17c}$$

$$\frac{1}{R_{ab}^{\theta}}\left|\frac{\partial\eta}{\partial\xi}\right|^{\theta}\frac{d\eta}{d\xi}\bigg|_{\xi=\lambda_{sh}} = -2R_{sh}\lambda_{sh}^{2} \tag{17d}$$

In application it is worth noting that since $(\partial\eta/\partial\xi)$ is always negative the term $|\partial\eta/\partial\xi|$ can be replaced with the more convenient term $(-\partial\eta/\partial\xi)$.

3. Analytical and numerical solution methods

3.1 Closed form solutions for the similarity equations

Two closed form solutions of the similarity statement of the problem (16) to (17) can be identified. The first at $\theta = 0$, and the second in the limit $\theta \to \infty$. The case $\theta = 0$ has been previously been investigated by Capart and co-workers (Capart et al. 2007, Lai and Capart 2007, Lai and Capart 2009) and Lorenzo-Trueba et al. 2009. A full derivation is given in Lorenzo-Trueba et al. 2009. In brief, in this limit, the solution of (16) satisfying (17b) and (17c) is

$$\eta(\xi) = R_{ab}\left[\lambda_{sh}\left(\frac{e^{-\xi^2} + \pi^{\frac{1}{2}}\left(\xi erf(\xi) + erf(\lambda_{ab})\right)}{e^{-\lambda_{sh}^{\ 2}} + \pi^{\frac{1}{2}}\lambda_{sh}\left(erf(\lambda_{ab}) + erf(\lambda_{sh})\right)}\right) - \xi\right] \tag{18}$$

On substituting this relationship into (17a) and (17d) the following non-linear equations in λ_{ab} and λ_{sh} can be obtained

$$\frac{R_{ab}e^{-\lambda_{sh}^2}}{e^{-\lambda_{sh}^2} + \pi^{\frac{1}{2}}\lambda_{sh}\left(erf(\lambda_{ab}) + erf(\lambda_{sh})\right)} - 1 = 2\lambda_2^2 R_{sh} \tag{19a}$$

$$\frac{R_{ab}e^{-\lambda_{ab}^2}}{e^{-\lambda_{sh}^2} + \pi^{\frac{1}{2}}\lambda_{sh}\left(erf(\lambda_{ab}) + erf(\lambda_{sh})\right)} = \frac{\lambda_{ab}}{\lambda_{sh}}\left(1 - R_{ab}\right) \tag{19b}$$

To arrive at the second closed solution in the limit $\theta \to \infty$, we first note that, by discussion above, in this limit the fluvial surface and the sediment flux approach linear functions of space, i.e.,

$$\lim_{\theta\to\infty} \eta = R_{ab}\left(\lambda_{sh} - \xi\right) \tag{20}$$

$$\lim_{\theta\to\infty} \frac{1}{R_{ab}^{\theta}} \left|\frac{d\eta}{d\xi}\right|^{\theta} \frac{d\eta}{d\xi} = -R_{ab} - \frac{\xi + \lambda_{ab}}{\lambda_{sh} + \lambda_{ab}} (2\lambda_{sh}^2 R_{sh} - R_{ab}) \tag{21}$$

The profile in (20) automatically satisfies the fixed elevation condition at the SHL (17b) and by construction the sediment flux in (21) satisfies the flux conditions in both (17c) and (17d). In order to satisfy the remaining elevation condition (17a) the moving boundary parameters need to be constrained by the relationship

$$\lambda_{ab} = \left[\frac{R_{ab}}{1 - R_{ab}}\right] \lambda_{sh} \tag{22}$$

In this way, the limit values on the left hand sides of (20) and (21) satisfy the boundary conditions but to complete the solution they must also satisfy the governing equation (16). On substitution of the left hand sides of (20) and (21) into (16) it is seen, after some manipulation using (22), that the governing equation is satisfied if the condition

$$\lambda_{sh} = \sqrt{\frac{\frac{1}{2} R_{ab}\left(1 - R_{ab}\right)}{R_{sh}\left(1 - R_{ab}\right) + R_{ab}}} \tag{23}$$

is met. Equations (22) and (23) match the solution generated by Kim and Muto 2007 from geometric arguments alone. Hence, the purely geometric solution of Kim and Muto 2007 is in fact the $\theta \to \infty$ limit solution of the diffusion model given in (3) and (4).

3.2 Numerical Solution of the similarity equations

For the general case of a finite non-zero value of θ, the similarity equations (16) and (17) can also be solved numerically. This involves an iterative approach with the following steps.

(i) For the chosen values of θ, R_{ab}, and R_{sh}, initial estimates of λ_{ab} and λ_{sh} are obtained from an approximate. The geometric solution (22) and (23) can be used to get an initial guess.

(ii) Then Equation (16) along with the initial conditions (17b) and (17c) is solved using the bvp4c routine in Matlab (Kierzenka and Shampine 2001).

(iii) The boundary conditions (17a) and (17d) are then used to update the guesses for λ_{ab} and λ_{sh}; an under-relaxation of 0.25 is used.

(iv) Steps (ii) and (iii) are repeated until convergence; declared when the change in the sum of λ_{ab} and λ_{sh} between iterations falls below 10^{-5}.

This basic approach works well for values of $R_{ab} \leq 0.9$. To achieve convergence at larger values of θ and values of R_{ab} that approach unity care needs to be taken in running the solver e.g., choosing the initial guess.

3.3 A Fixed Grid Numerical Solution

In addition to the numerical solution of the similarity equations a numerical solution of the problem in the physical space can also be developed. Such a solution is seen as having the advantage of being able to operate in cases where similarity does not hold. The solution used here is an adaptation of the fixed grid "enthalpy" like solution proposed by Voller et al. 2006 for modeling linear diffusion sediment transport problems with a single moving boundary.

As a proxy for the enthalpy of heat transfer solutions we define total sediment in the system as

$$H = \begin{cases} h + L(x), & h > 0 \\ 0, & h = 0 \end{cases} \qquad (24)$$

where, taking account of the dimensionless variable definitions in (8), L is the dimensionless depth of the ocean at the delta toe when the SHL is at x, i.e.,

$$L = \begin{cases} 0 & x < 0 \\ x \cdot R_{sh} & x \geq 0 \end{cases} \tag{25}$$

With this definition we can write down a single Exner sediment balance equation for the full solution space as

$$\frac{\partial H}{\partial t} = \frac{\partial}{\partial x}\left(q^d\right) \qquad -\infty \leq x \leq \infty \tag{26}$$

where

$$q^d = \min\left(-\frac{1}{R_{ab}^{\theta}} \left|\frac{\partial h}{\partial x}\right|^{\theta} \frac{\partial h}{\partial x}, R_{ab} \right) \tag{27}$$

and, inverting (24),

$$h = \max\left(H - L, 0\right) \tag{28}$$

The boundary conditions for (26) are

$$\lim_{x \to -\infty} q^d = R_{ab} \quad \text{and} \quad \lim_{x \to \infty} h = 0 \tag{29}$$

and the initial conditions are

$$H = h = \begin{cases} x, & x < 0 \\ 0, & x \geq 0 \end{cases} \tag{30}$$

The one dimensional discretization illustrated in Fig.2 is used to develop a numerical solution of Eq. (24) to (28). Note that (i) this discretization is based on a uniform grid size Δx, (ii) that the origin point $x = 0$ is located at the interface between two nodes, (iii) the first landward node is indexed $i = 0$, (iv) as we move seaward the node index increases $\left(i = 1, 2, 3...\right)$ and (v) as we move landward the node index decreases $\left(i = 0, -1, -2...\right)$. In this way the location of any node is given by $x = (i - 0.5) \cdot \Delta x$.

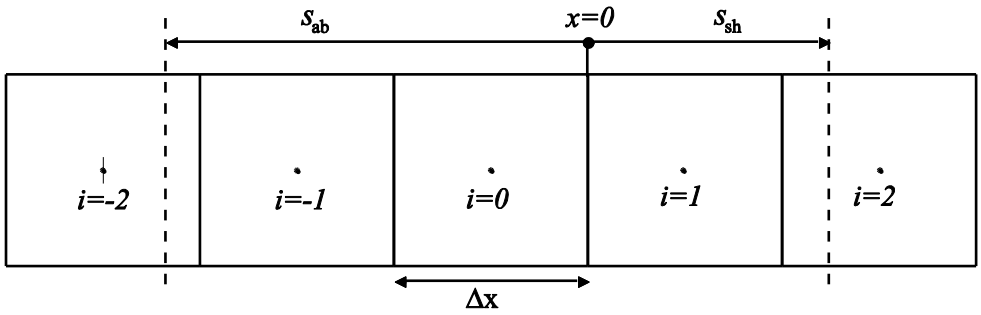

Fig. 3-2 The discrete domain. In general the shoreline and the alluvial-bedrock transition positions, s_{sh} and s_{ab} respectively, are in between two nodes of our discrete domain.

On the domain in Fig.2 the explicit time integration finite difference form of (24) is

$$H_i^{new} = H_i + \frac{\Delta t}{\Delta x} \cdot \left(q^d_{i+\frac{1}{2}} - q^d_{i-\frac{1}{2}} \right) \tag{31}$$

Where the superscript *new* refers to values at the new time step, subscript $i+1/2$ refers to the interface between nodes i and $i+1$, and the flux from node i to node $i+1$ is approximated as

$$q^d_{i+\frac{1}{2}} = \min\left(\frac{1}{R_{ab}^{\theta}} \left| \frac{h_{i+1} - h_i}{\Delta x} \right|^{\theta} \left(\frac{h_i - h_{i+1}}{\Delta x} \right), R_{ab} \right) \tag{32}$$

Note since the slope $\left|\partial h / \partial t\right|$ is bounded above by R_{ab} the maximum value for the non-linear diffusivity in the system

$$\nu = \frac{1}{R_{ab}^{\theta}} \left| \frac{h_{i+1} - h_i}{\Delta x} \right|^{\theta} \tag{33}$$

cannot exceed unity. Therefore positive coefficient and hence a reasonable guarantee of stability will be established if the time and space steps are chosen such that $\Delta t / \Delta x^2 < 0.5$. In addition to stability considerations it is also noted that to retain accuracy the switching of the interface flux $q^d_{i+\frac{1}{2}}$, from the input value R_{ab} to one controlled by the fluvial surface (see (32)), needs to take place at a frequency larger than the simulation time step.

In meeting these stability and accuracy conditions the simulations in the current work use a space step $\Delta x = 1$ and a time step in the range $0.01 \le \Delta t \le 0.05$.

At each time step solution of (31) will explicitly provide new values for the nodal values of the total sediment H^{new}. From this field new time step values for the sediment heights h_i^{new} are calculated from the discrete form of (28). This provides sufficient information to recalculate the fluxes in (32) and propagate the solution of (31) forward in time.

Although not required as part of the solution process, at each time step the location of the SHL and ABT can be estimated with the following steps. For the SHL $(i > 0)$ the current total sediment field H_i is searched, and the unique node i where $0 < H_i < L_i$ is located. The SHL position is then determined by interpolation through the control volume around node i, i.e.,

$$s_{sh} = (i-1)\Delta x + \frac{H_i}{L_i}\Delta x \tag{34}$$

For the ABT a search is made through the nodes in the order $i = 0, -1, -2...$ until the first node where the upstream flux $q_{i-1/2}^d$ is, by (32), calculated as R_{ab}. The ABT position is then determined by interpolation between nodes i and i-1

$$s_{ab} = \frac{h_i - R_{ab}(0.5 - i)\Delta x}{1 - R_{ab}} \tag{35}$$

4. Results

4.1 Similarity solution

The solution of the similarity solution is fully determined by the specification of the alluvial-bedrock slope ratio, R_{ab}, and the shoreline slope ratio, R_{sh}. Our interest is to explore the consequence of the various solutions methods presented under conditions that

match those in the field. In this setting the foreset slope, α, is typically much greater than the bedrock slope, β hence through (11) it is reasonable to always assume a value $R_{sh} = 1$. In contrast the value of R_{ab} could vary across the full theoretical range $0 \le R_{ab} \le 1$; typically observed field values are in the range $0.2 \le R_{ab} \le 0.8$ (see discussion in Lorenzo et al. 2009). In this way the results from the similarity solution are best presented by fixing $R_{sh} = 1$ and plotting the values of the moving boundary parameters λ_{ab} and λ_{sh} against $0 \le R_{ab} \le 1$. Fig.3 shows these plots for the cases where $\theta = 0, 2, 10, \infty$. Predictions for the finite values of θ are obtained from the ODE solution of (16) and (17). Note, however, the $\theta = 0$ solution obtained in this manner is indistinguishable from the values obtained from the closed form analytical solution (19). The $\theta \to \infty$ solution is obtained from the geometric solution in (22) and (23).

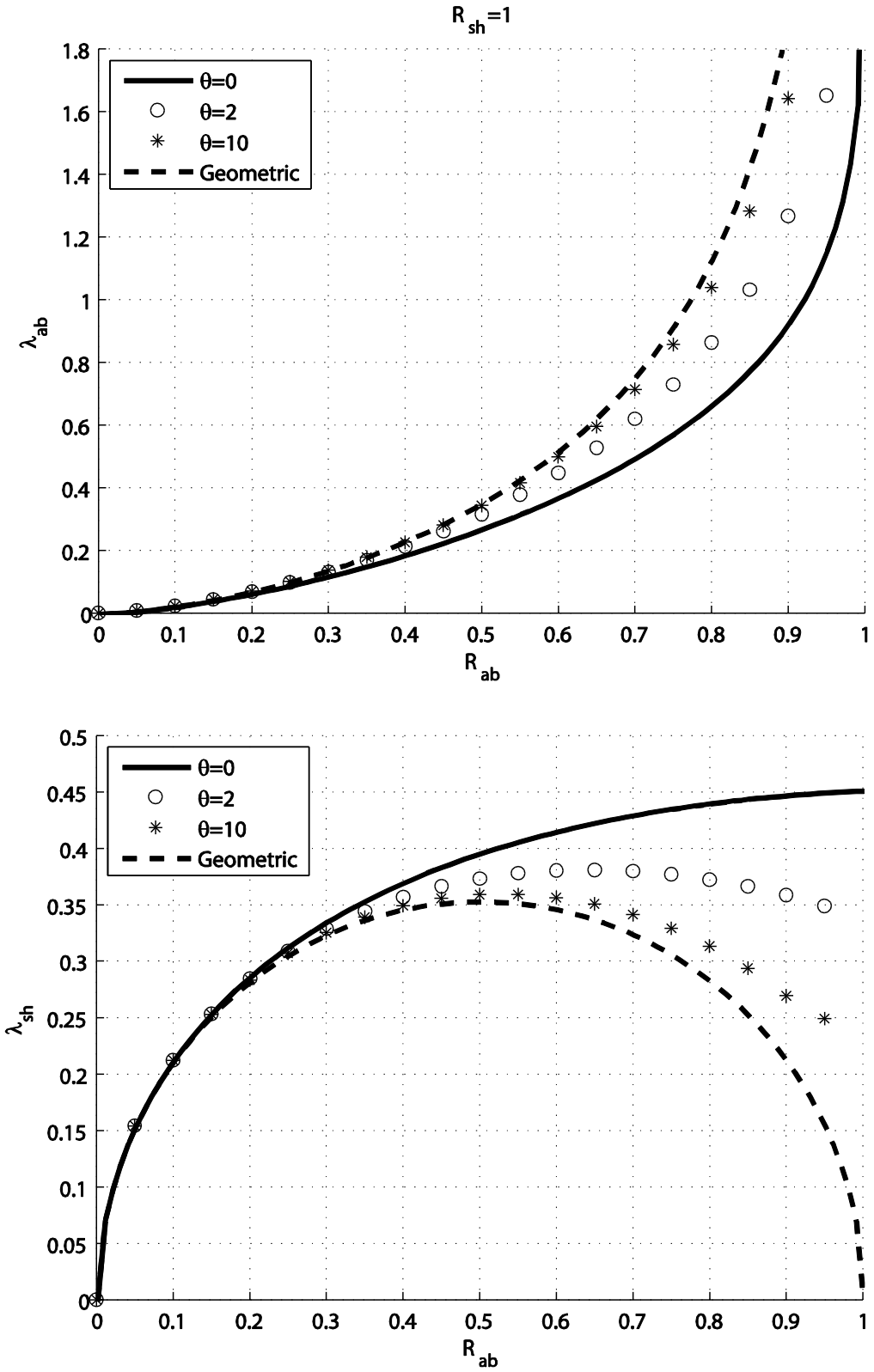

Fig. 3-3 The solution space for the moving boundary parameters λ_{ab} (ABT) and λ_{sh} (SHL).

Some key observation on the predicted behaviours are made

(i) All the solutions are bounded by geometric, $\theta \to \infty$, and linear diffusion, $\theta = 0$ models.

(ii) In the range $0 < R_{ab} < 0.4$ the predicted values of lam λ_{ab} and λ_{sh} are not affected by the value of diffusive exponent θ.

(iii) There is a convergence tendency in the similarity solution predictions to the geometric solution as the value θ increases.

(iv) The value of λ_{sh} that controls the shoreline advance is only monotonic for the linear diffusion case, $\theta = 0$. For all other values there is a decrease in this value at high values of R_{ab}. In the geometric model, $\theta \to \infty$, this value goes to zero as R_{ab} approaches 1 indicating an immobile SHL.

(v) There is a marked sensitivity in the predictions for ABT parameter λ_{ab} as larger values of R_{ab} are approached. The geological consequences of this feature is extensively discussed in the linear diffusion analysis recently precedent by Lorenzo-Trueba et al. 2009.

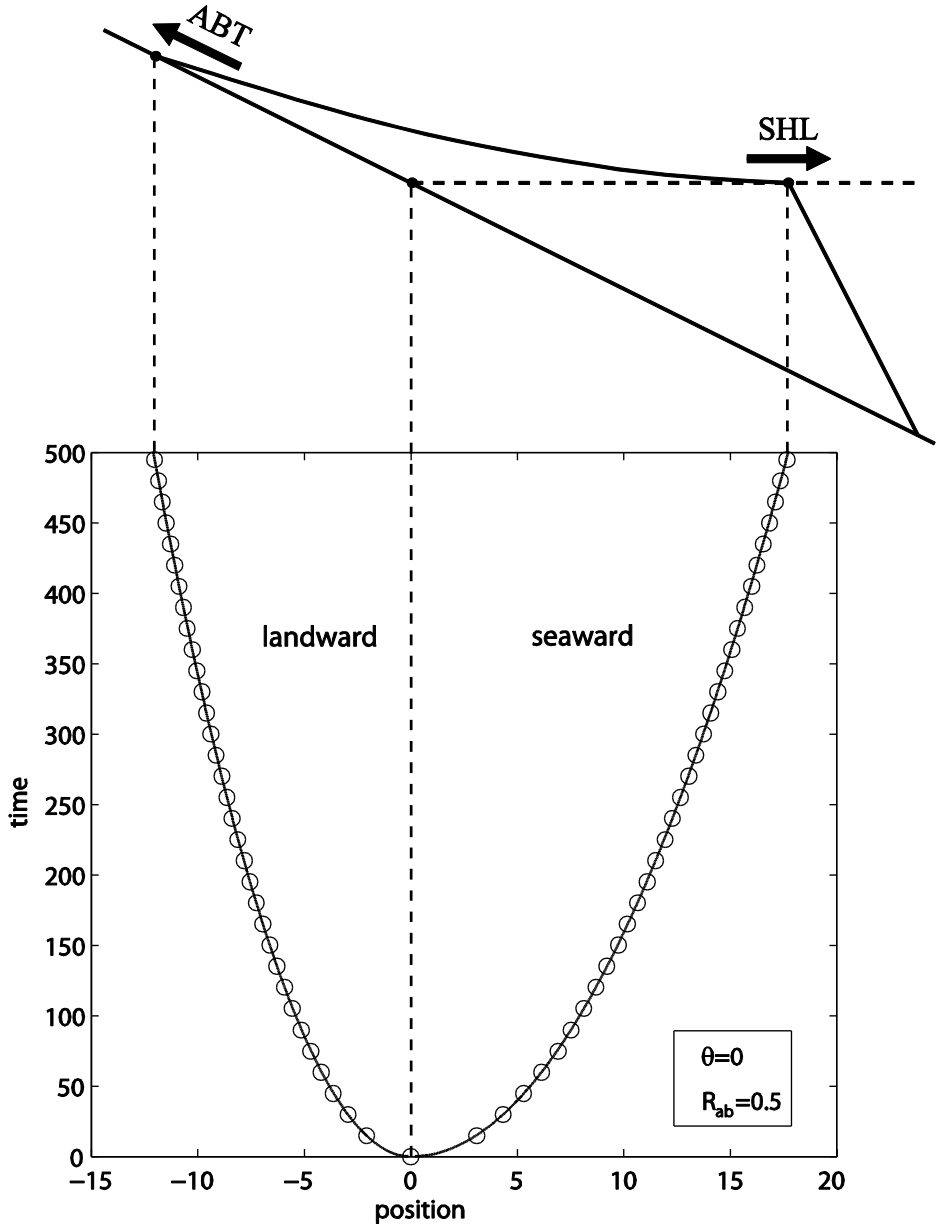

Fig. 3-4 Comparison between enthalpy solution (open circles) and similarity solution (continuous line) .The sketch on top represents the longitudinal profile at the latest time in the graph.

4.2 Enthalpy solution

The enthalpy method provides an accurate approximation of the similarity solution. For a range of θ and R_{ab} values, Figs 4 and 5 show plots of the movement of the SHL and ABT with time. In all cases a close match between the similarity and the enthalpy predictions is observed.

A further test of the robustness of the enthalpy solution is revealed by investigating its performance when θ approaches a large value. Fig. 6 shows predictions of the SHL and ABT movements when $\theta = 200$. As predicted by the theory this enthalpy solution closely matches the geometric model predictions from (22) and (23).

5. Discussion

As noted in the introduction of this paper, depending on the situation considered and the semi-empirical sediment transport laws used experiments (Postma et al. 2008, Lorenzo-Trueba 2009) and theoretical models (Parker and Muto 2003, Swenson and Muto 2007, Postma et al. 2008, Lorenzo-Trueba 2009) report the diffusive exponent to be in the range $0 \le \theta \sim 2$. Currently there is no consensus on a single correct value for use in modelling "real world systems" (Postma et al. 2008). Experiments underscore this point. Lorenzo-Trueba et al. 2009 recover accurate comparisons with experimental delta growth models using an analytical solution based on a linear diffusion law $\theta = 0$. In contrast, reported comparison between numerical models and delta building experiments (Parker and Muto 2003, Swenson and Muto 2007) show a best fit when $0.95 \le \theta \le 1.25$. Finally in analyses of a delta depositing system in a fixed domain (no ABT or SHL moving boundaries) Postma et al. 2008, in fitting to a transient non-linear diffusion model, obtain values of $\theta \sim 2$. In this respect a striking feature of the results in Fig.3 is that while $R_{ab} < 0.7$, deviations between the $\theta = 0$ and $\theta = 2$ predictions of the moving boundary parameters λ_{ab} and λ_{sh} are below 10%. Taking into account the field and experimental difficulties in accurately measuring R_{ab} and other ambiguities in the system such as porosity (Lorenzo-Trueba et al. 2009) these deviations may not be significant. Hence, it is reasonable to suggest that for values $R_{ab} \le 0.7$ the modeling detail of choosing the "correct" value of

the exponent for θ in (2) will make no qualitative difference to the boundary movement predictions and have only a marginal influence on quantitative values. It is not until we move beyond $R_{ab} = 0.7$ —approaching the upper limit for field observations—that care may be required in identifying the appropriate value for the exponent θ.

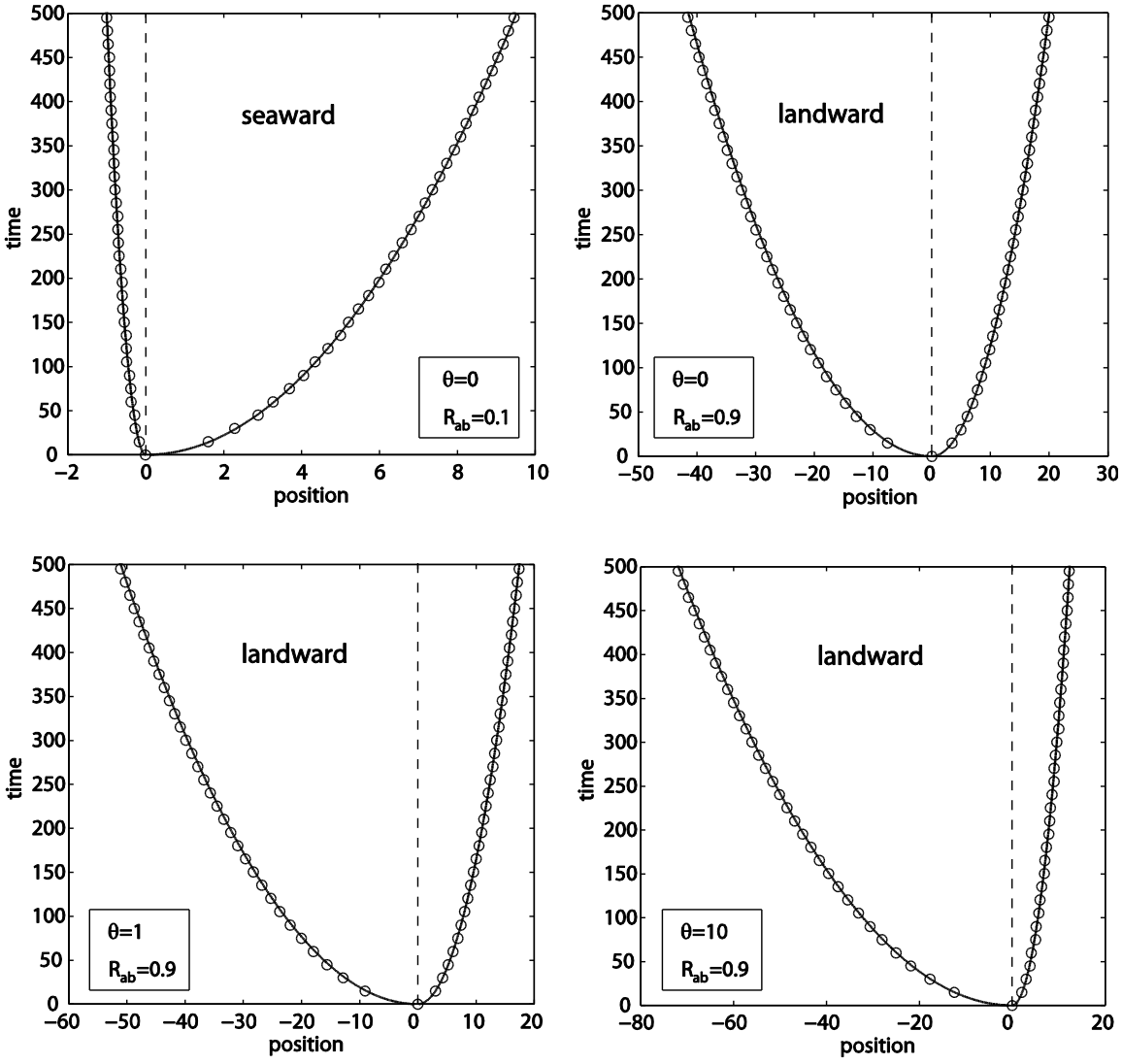

Fig. 3-5 Further comparisons between enthalpy (open circles) solution and similarity solution (continuous line).

Experimental systems of delta building processes (e.g., see Fig.2-5 in Lorenzo-Trueba 2009) often exhibit what on first inspection appears to be a linear profile. This suggests that the simple geometric model $(\theta \to \infty)$ should be a sound approach. The results in Fig.3 confirm that this is more than reasonable provided that $R_{ab} \le 0.4$. As we move beyond this value, however, there is a dramatic departure between the geometric prediction for λ_{ab} and λ_{sh}, and those obtained with "physically reasonable" values for the diffusivity exponent $0 \le \theta \sim 2$. Hence, in terms of retaining quantitative predictions use of the geometric model may only begin to err when higher values R_{ab} are encountered. Nevertheless, due to the almost exact agreement between all models at values of $R_{ab} \le 0.4$ and its profound simplicity, in qualitative studies of delta building processes use of the geometric model could be recommended.

Finally we note that the excellent comparison of the enthalpy and analytical solutions across the full range of θ and R_{ab} values is very encouraging. As noted above the enthalpy method has the most utility in developing solutions in more than one-dimension.

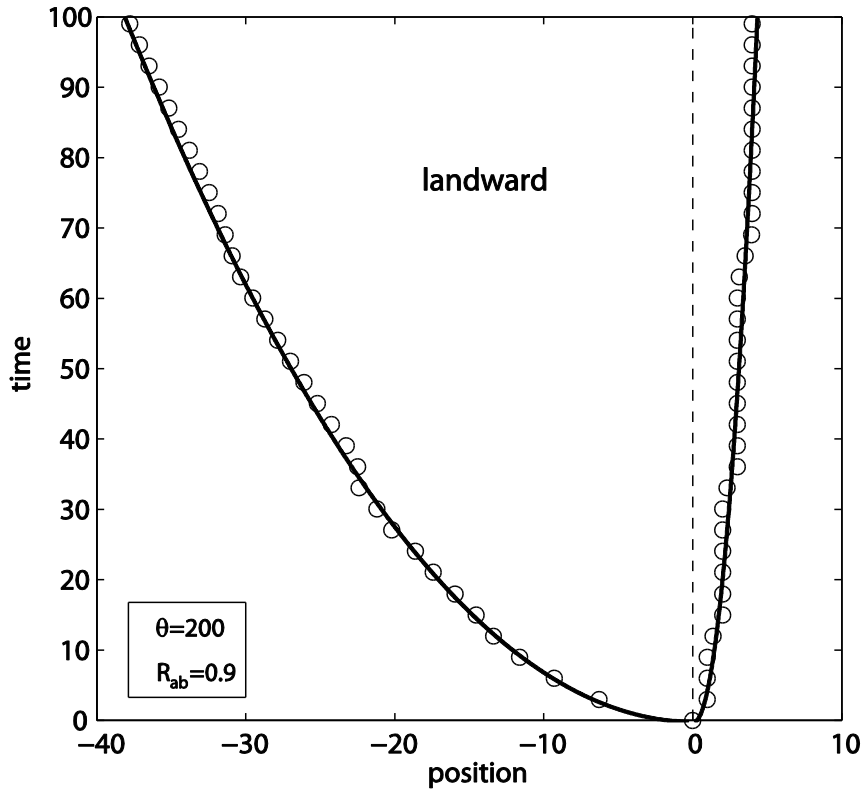

Fig. 3-6 Comparison between enthalpy solution with $\theta = 200$ (open circles) and geometric solution $\theta \to \infty$ (continuous line) for $R_{ab} = 0.9$.

6. Conclusions

This paper has presented a generalized Stefan problem related to the formation of a sediment ocean delta. Ingredients in this problem are a non-linear diffusivity related to the fluvial slope through the power law $\nu = \nu^* \left|\partial h/\partial x\right|^\theta$ and the appearance of two moving boundaries, the shoreline (SHL) and the alluvial-bedrock transition (ABT).

In terms of analysis, the key contribution has been to develop a similarity form and solution for the delta problem. In the limit of a linear diffusion $\theta = 0$ this solution recovers a recently derived closed form analytical solution. At the other extreme, as

$\theta \to \infty$, a closed form solution that matches the solution derived from geometric arguments is obtained.

In addition to the similarity solutions a fixed grid enthalpy like numerical solution of the delta problem has been proposed. Predictions from this solution have been shown to closely match those of the similarity solution. The utility of the enthalpy solution is that it can be applied to situations where similarity will not hold (e.g., more general non-linear diffusive terms) and to multi-dimensional cases.

The results in this paper also have some important geological consequence. First in interpreting field stratigraphy of ocean delta deposits, there may be no need to be concerned about choosing the most appropriate value of the diffusive exponent from the physical meaningful range $0 \le \theta \sim 2$. Provided the alluvial bedrock ratio $R_{ab} < 0.7$—near the upper end of observations—the differences in SHL and ABL predicted are well within the ambiguities in the system. Further, since in the range $R_{ab} < 0.4$ there is essentially no difference between the diffusion models and the geometric model, in developing qualitative models of the formation of sediment ocean deltas, due to its relative simplicity, the geometric model should be favored.

Further work will look toward developing the enthalpy approach to situations outside of the scope of the similarity solution and toward building a description of delta growth that takes into consideration additional features such as sea-level rise and bio-geochemical processes. A model with this capability will be invaluable in developing our understanding for costal restorations associated with the Gulf of Mexico.

Chapter 4: Exploring the role of organic matter accumulation on delta evolution

J. Lorenzo-Trueba et al. (submitted), Exploring the role of organic matter accumulation on delta evolution, *Journal of Geophysical Research (JGR)*, Joint Special Section of *JGR Biogeosciences* and *JGR Earth Surface*.

We explore the role of plant matter accumulation in the sediment column in determining average delta dynamics under base-level rise, and simple subsidence profiles. Making the assumption that delta building processes operate to preserve the geometry of the delta plain, we model organic matter accumulation in terms of the net rate of plant production and the rate of accommodation (space created for sediment deposition). A spatial integration of the organic matter accumulation, added to the known river sediment input, leads to a model of delta dynamics that estimates the fraction of organic sediments preserved in the delta. The model predicts that the maximum organic fraction occurs when the net production rate matches the accommodation rate, a result consistent with field observations. Further, when the model is extended to account for differences in plant matter accumulation between fresh and saline environments (i.e., methanogenesis versus sulfate reduction) we show that an abrupt shift in the location of the fresh-salt boundary can amplify the speed of shoreline retreat.

1. Introduction

Current modeling efforts based on a sediment mass balance as expressed by the Exner equation have proved to be a useful approach for (1) modeling the average dynamics during delta formation (Swenson 2000, Capart et al. 2007, Parker et al. 2008a & b, Lorenzo-Trueba et al. 2009, Lorenzo-Trueba and Voller 2010), and (2) understanding how physical processes of delta growth contribute to delta restoration (Kim et al. 2009, Paola et al. 2011). Such models involve a balance among sediment supply, sea-level rise, and subsidence. To date, however, these models do not include the accumulation of organic matter in the delta plain. Coastal wetlands are among the most productive systems in the world (Reddy & DeLaune 2008), and organic-rich sediment derived from plants typically represents a significant fraction of the sediment column (Kosters et al. 1987, Reddy & DeLaune 2008, Tornqvist 2008). Moreover, plant matter accumulation has been recently identified as a potential control of marsh (Long 2006, Kirwan and Murray 2007) and delta evolution (Meckel 2007, Tornqvist 2008, Van Asselen 2009, Van Asselen 2010). We use more specialized terminology among sedimentologists, and plant matter accumulation is referred to henceforth as organic sedimentation. Thus, our objective here is to extend previous delta-growth geometric models (Kim and Muto 2009, Lorenzo-Trueba and Voller 2010) to include organic sedimentation in the system. The resulting model will be used to predict volume fraction of organics preserved in a delta plain as a function of accommodation rate, and to explore the role of the fresh-salt groundwater boundary in determining shoreline dynamics.

2. Net organic production

Before we move forward with the model development it is required to establish a basic accounting of the organic sedimentation. In this respect it is noted that the generation of organic-rich sediments results from the excess of local plant productivity over microbial decomposition (Moore 1989, Richardson 2001, Reddy & DeLaune 2008). Such excess—referred to henceforth as net organic production and denoted by P—is primarily controlled by the decomposition rate rather than productivity (Moore 1989), i.e., net production increases where physical conditions serve to reduce microbial activity.

Decomposition is generally separated into aerobic and anaerobic components (Richardson 2001, Reddy & DeLaune 2008). Under aerobic conditions, due to enhanced microbial growth (Portnoy 1999, Gambolati et al. 2006), the decomposition is of the same order as production, and as such the net organic production is very small. In contrast, under anaerobic conditions, like those often found in deltaic wetlands, net organic production is significant (Kosters et al. 1987, Richardson 2001, Reddy & DeLaune 2008). In such anaerobic environments, among other factors, the net production of organics is controlled by the presence of sulfate. In saline environments sulfate reduction is the major form of anaerobic decomposition (Howarth and Hobbie 1982, Senior et al. 1982, Howarth 1984, Capone & Kiene 1988). In fresh water environments, however, the amount of sulfate is limited and methanogenesis is the predominant decomposition mechanism (Capone & Kiene 1988). Hence, since sulfate reduction is energetically superior to methanogenesis (Capone and Kiene 1988, Portnoy & Giblin 1997, Ibañez et al.2010), we expect a larger net organic production rate in fresh systems compared to saline, a situation often observed in field studies (Portnoy and Giblin 1997, Portnoy 1999, Ibañez et al.2010). Furthermore, this imbalance between the near-shore saline and the inland fresh regions has been observed in stratigraphic studies of different deltaic environments (Kosters et al. 1987, Kosters and Suter 1993, Staub & Esterle 1994).

3. Model description

The task now is to quantify and incorporate organic sedimentation into a delta growth model. In Fig.1 we present a sketch of a cross-section of a river delta. The system is fed by fresh water and sediment from the river system, and evolves on top of the basement under conditions of sea-level rise and subsidence. The key geometric feature in this system is the deposited sediment prism. This shape is bounded below by the basement, and from above by the subaerial delta plain and the subaqueous foreset. The delta plain is delimited by the shoreline and the alluvial-basement transition, and the foreset by the shoreline and the delta toe. The movements of these three geomorphic boundaries (alluvial-basement transition, shoreline and delta toe) define the delta dynamics.

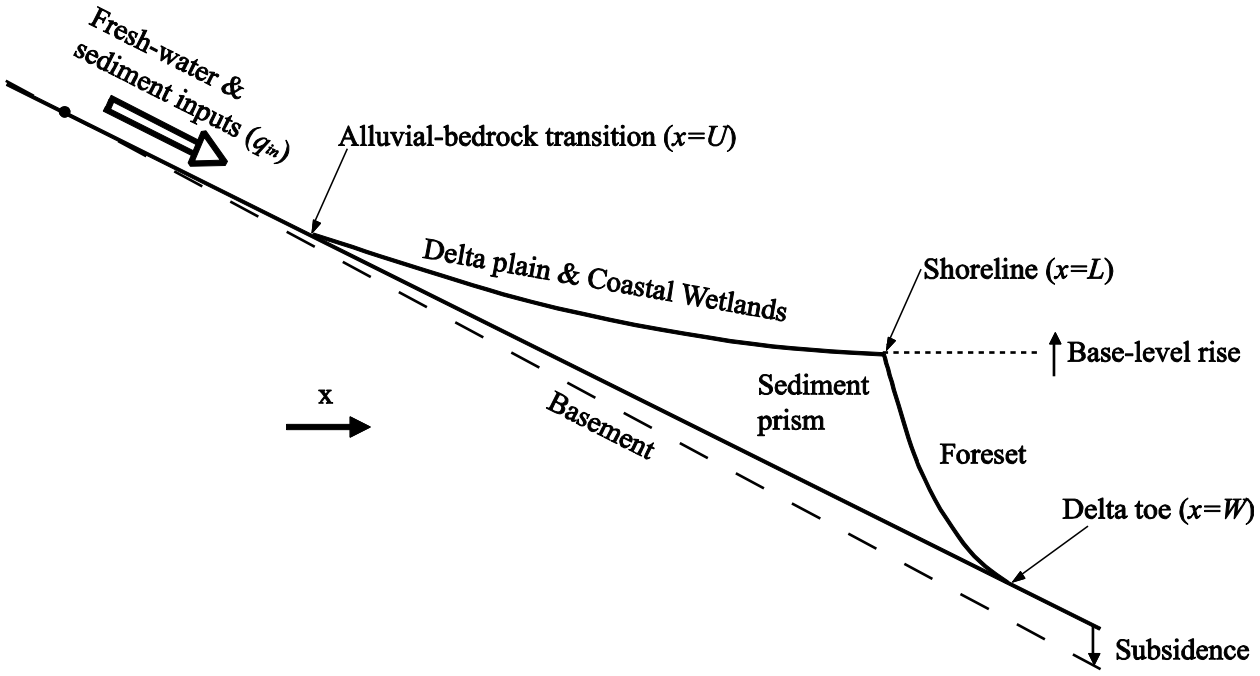

Fig. 4-1 Typical delta profile.

Within the system shown in Fig.1, the sediment volume per unit width in the prism V is determined by the external bulk sediment inputs from the river system q_{in}, and the rate of accumulation of organic sediments within the delta plain. If we define $\chi(x,t)$ to be the thickness of organic as opposed to inorganic sediments at each location, the volume of sediments in the prism, at a time t, is then given by

$$V = \int_0^t q_{in}\,dt + \int_U^W \chi\,dx \qquad (1)$$

where the second term on the right is an integration over the sediment prism in Fig.1 with $x = U$ the location of the alluvial-basement transition and $x = W$ the location of the delta toe.

Assuming q_{in} is constant in time, and that there is negligible accumulation of organic matter in the subaqueous region, between the shoreline located at $x = L$ and the delta toe

located at $x = W$, it follows from (1) that the rate of change of the prism sediment volume $\dot{V} = dV/dt$ can be written as

$$\dot{V} = q_{in} + \int_{U}^{L} \nu_{org} dx \qquad (2)$$

Here we recognize that the sediment column has zero height at the alluvial-basement transition and toe, and have defined $\nu_{org}(x) = \partial\chi/\partial t$ as the rate of organic sedimentation at any location in the delta plain.

To advance from equation (2) we simplify the geometry in Fig. 1. First we note that many previous and successful models of delta growth assume a linear foreset with constant slope ψ and a linear basement with constant slope β (Swenson et al. 2000, Lorenzo-Trueba et al. 2009, Lorenzo-Trueba and Voller 2010, Paola et al. 2011). Kim and Muto 2007 have extended this simplification by assuming a linear profile, with slope γ, for the delta plain as well. In an exact mathematical analysis, based on a diffusion treatment for sediment transport, Lorenzo-Trueba and Voller 2010 explicitly verify the accuracy of this approach when the slope ratio $\gamma/\beta \leq 0.7$; a condition often seen in costal wetland systems of interest here. As such, we adopt this linear shape preserving assumption in the current work which allows us to simplify the geometry to that shown in Fig.2.

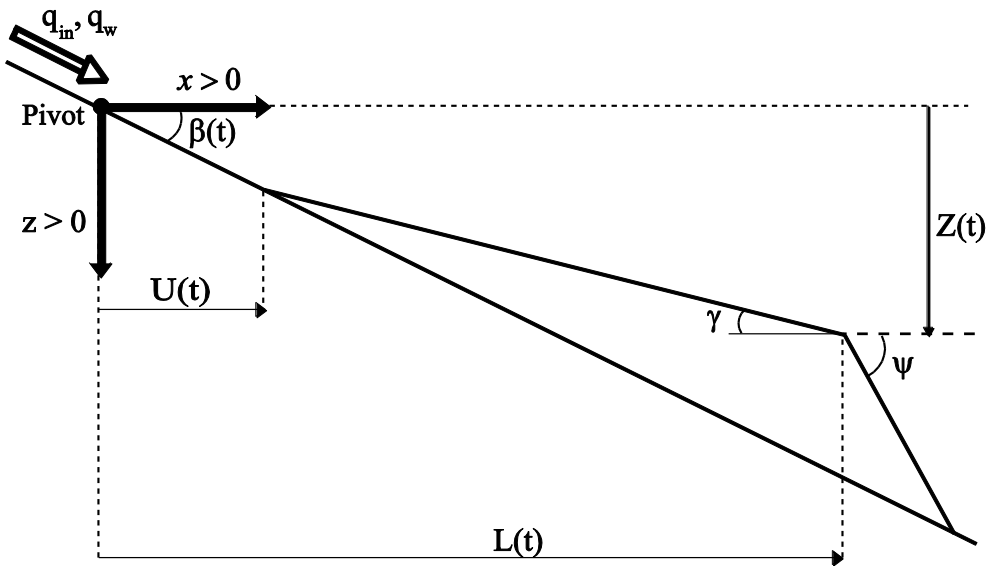

Fig. 4-2 Sketch including the state variables.

We consider two scenarios for the creation of accommodation (i.e., space for sediment deposition): base-level rise and differential subsidence. In the base-level rise case we assume the subsidence, the sum of deep crustal processes and compaction, to be spatially uniform. In contrast, in the differential subsidence scenario the subsidence rate linearly increases seawards from the pivot location (see Fig.1). Thus, the main ingredients in a model for the delta dynamics are (1) the interplay between the rate of change of the sediment per unit width in the prism $\dot{V}$, and (2) either the combination of sea-level and subsidence expressed as a base-level rise $\dot{Z}$, or the pivot subsidence rate $\dot{\beta}$. The base-level Z and basement slope β are defined as

$$Z = Z_0 - \dot{Z}t \tag{3a}$$

$$\beta = \beta_0 + \dot{\beta}t \tag{3b}$$

where Z_0 and β_0 are the base-level and basement slope at $t = 0$. The origin is chosen to be at the pivot location, with x positive in the seaward direction and z positive upwards (Fig. 2). For completeness, in Fig.3, we also show the realization of the concept of the

shape preservation under a situation in which, at a point in time, the sediment supply and accumulation cannot sustain a shoreline advance resulting in an abandonment of the foreset and a shoreline retreat.

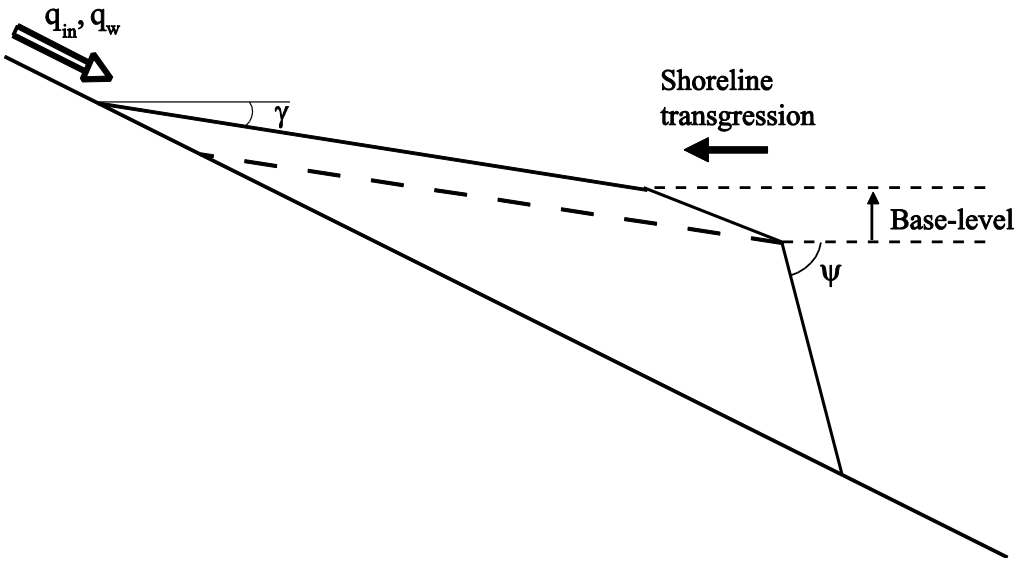

Fig. 4-3 Deltaic system undergoing shoreline retreat.

Taking account of our shape preserving assumption we can constrain the rate of organic sedimentation in (2) by

$$v_{org} = \min(A, P) \tag{4}$$

where P is the net rate of organic production — fully discussed in the previous section—and A the rate of accommodation created by base-level rise (i.e., $A = \dot{Z}$) or differential subsidence (i.e., $A = \dot{\beta} x$). The model in (4) says that, in situations where the net productivity outstrips the rate of accommodation, i.e., $P > A$, the organic excess—to preserve shape—is either rapidly decomposed via aerobic respiration (i.e., oxidation) or eroded away. On the other hand, if the net productivity cannot keep up with accommodation, $P < A$, it is assumed that the shape is preserved by filling in the shortfall with the available mostly inorganic sediment supply.

As discussed in section 2, the net organic production rate P can vary along the delta plain, but in the first instance, we will assume a constant value (an assumption that will be relaxed later). In this way, for the base-level rise case we can use (4) to evaluate the integral on the right hand side of (2) and arrive at

$$\dot{V} = q_{in} + (L - U) \cdot \min(\dot{Z}, P) \tag{5a}$$

and the differential subsidence case becomes

$$\dot{V} = q_{in} + \int_{U}^{L} \min(\dot{\beta} x, P) dx \tag{5b}$$

with initial conditions $V = 0, L = 1$, and $U = 1$. For given values of P, q_{in} and A,the coupling of the solution of (5) to the geometric features in Fig. 2 and 3 will fully realize a model of the delta growth dynamics.

A more general solution approach is achieved by casting (5) into a dimensionless form. Towards this end, using the characteristic basin length $\ell = Z_0 / \beta_0$, and defining a time scale $\tau = \ell^2 \beta_0 / q_{in}$, we identify the following dimensionless variables

$$s_{sh}^d = \frac{s_{sh}}{\ell}, \quad s_{ab}^d = \frac{s_{ab}}{\ell}, \quad Z^d = \frac{Z}{Z_0}, \quad V^d = \frac{V}{\ell^2 \beta_0} \tag{6a}$$

And the following dimensionless groups that control the behavior of the system

$$\psi^d = \frac{\psi}{\beta_0}, \quad \gamma^d = \frac{\gamma}{\beta_0}, \quad \nu_{org}^d = \frac{\nu_{org}\, \ell}{q_{in}}, \quad \dot{Z}^d = \frac{\dot{Z}\, \ell}{q_{in}}, \quad \dot{\beta}^d = \frac{\dot{\beta}\, \ell^2}{q_{in}}, \quad P^d = \frac{P\, \ell}{q_{in}} \tag{6b}$$

4. Parameter values

We are interested in modelling ocean deltas, such as the Mississippi delta, that have a typical length scale $\ell \sim 10\text{-}100\, km$, basement slopes $\beta \sim 10^{-3} - 10^{-4}$ (Kosters et al. 1987, Blum 2008, Kim et al. 2009), a foreset slope $\psi \sim 10^{-2}$ (Swenson 2000), delta plain slope $\gamma \sim 10^{-5}$ (Blum 2008), and a rate of sediment input $\sim 100\, \mathrm{Mton/year}$(Kim et al.

2008). Assuming a bulk density of $2\,\mathrm{ton/m^3}$, the sediment input can be written as $q_{in} \sim 1000\,\mathrm{m^2/year}$, which leads to an approximate time scale of $\tau \sim 1000\,\mathrm{years}$. With these numbers we note the small ratio of $\gamma^d = \gamma/\beta \sim 0.1-0.01$, which validates the linear shape preservation assumption. We also note that the foreset slope ratio is very large ($\psi^d >> 1$), implying that the sediment stored below the foreset is relatively very small and can be dropped without error from any volume balance calculation. As a reference for the following calculations, it is noted that the present base-level rise rate for the Mississippi has been estimated to be $\dot{Z} \sim 7\,\mathrm{mm/year}$ (Kim et al. 2009). Also, data from Holocene peat-forming environments (Diessel et al. 2000) have suggested organic sedimentation to be from less than 0.1 mm/year to more than 5mm/year. This leads to a dimensionless base-level rise $\dot{Z}^d \sim 0.7$, and on assuming that organic sedimentation is on the same order as net-sediment production a dimensionless production $P^d \sim 0.01\text{-}0.5$.

With the definitions in (6), and dropping the *d* superscript for convenience of notation, the dimensionless governing equations under base-level rise and differential subsidence becomes

$$\dot{V} = 1 + (L - U)\cdot \min(\dot{Z}, P) \tag{7a}$$

$$\dot{V} = 1 + \int_U^L \min(\dot{\beta} x, P)\,dx \tag{7b}$$

with initial conditions $V = 0$, $L = 1$, and $U = 1$. And dimensionless base-level and basement slopes

$$Z = 1 - \dot{Z}t \tag{8a}$$

$$\beta = 1 + \dot{\beta}t \tag{8b}$$

5. Model Solution

At a given time $t > 0$, if the right hand side of (7) and the current volume of the delta deposit V^{old} are known, the value of the volume V at a small increment of time Δt beyond time t can be calculated with a simple Euler scheme

$$V = V^{old} + \Delta t \dot{V} \tag{9}$$

where $\dot{V}$ is given by (7). The integral on the right hand side of (7b) is estimated numerically using a simple trapezoidal rule

$$\int_U^L \min(\dot{\beta} x, P) dx \approx \frac{L-U}{2N} \sum_{k=1}^{N} (\min(\dot{\beta} x_{k+1}, P) + \min(\dot{\beta} x_k, P)) \tag{10}$$

where $N+1$ is the number of equally spaced grid points.

In order to define the delta profile evolution and to generate the information to complete subsequent time steps calculations we need a means of extracting the positions of the alluvial-basement transition $U(t)$ and the shoreline $L(t)$ from this updated value of the total volume, V. In Tables 1 and 2 we include a list of the relevant calculation steps to achieve this; all the expressions are derived from direct geometric arguments.

The calculation requires three input parameters: the slope ratio γ, the net production rate P, and either the base-level rise rate $\dot{Z}$ or the pivot subsidence rate $\dot{\beta}$. In operation, following the update of the volume V from (9) we first calculate the shoreline change increment within a time step ΔL and then the shoreline and alluvial-basement transition positions L and U. If the shoreline moves seawards (i.e., $\Delta L \geq 0$), we follow the calculations on the left column in Tables 1 and 2. At some point in the calculation, however, the sediment supply and net production cannot sustain a shoreline advance causing a shoreline retreat indicated by an estimate value $\Delta L < 0$. In this case we switch to the expressions in the right column in Tables 1 and 2. In connecting to previous models, we note that if the net organic production rate is zeroed out, i.e., $P = 0$, the model presented in Table 1 recovers the previous model developed by Kim and Muto 2007.

Shoreline Increment	WHILE $\Delta L = \sqrt{2V(1-\gamma)} + Z - L^{old} \geq 0$	ELSE UNTIL $\Delta L = \frac{\Delta t}{\gamma}\left(\frac{\dot{V}}{L-U} - \dot{Z}\right) < 0$
Shoreline position	$L = L^{old} + \Delta L$	
Alluvial-basement transition position	$U = Z - \gamma\sqrt{\frac{2V}{1-\gamma}}$	$U = \frac{Z-\gamma L}{1-\gamma}$

Table 4-1 Geometric relationships for the base-level rise scenario. The value of Z is obtained from equation (2a).

Shoreline Increment	WHILE $\Delta L = \frac{\sqrt{2V(\beta-\gamma)}}{\beta} + \frac{1}{\beta} - L^{old} \geq 0$	ELSE UNTIL $\Delta L = \frac{\Delta t}{\gamma}\left[\frac{\dot{V}}{L-U} - \frac{\dot{\beta}}{2}(L+U)\right] \geq 0$
Shoreline position	$L = L^{old} + \Delta L$	
Alluvial-basement transition position	$U = \frac{1}{\beta} - \frac{\gamma}{\beta}\sqrt{\frac{2V}{\beta-\gamma}}$	$U = \frac{1-\gamma L}{\beta-\gamma}$

Table 4-2 Geometric relationships for the pivot subsidence scenario. The value of β is obtained from equation (2b).

In Fig. 4 we present the typical model behavior under constant base-level rise (Table1). The base-level rise is $\dot{Z} = 0.8$, the slope ratio is $\gamma = 0.01$, and the net organic production is $P = 0.4$. Initially the total rate of sediment input $\dot{V}$ exceeds the total accommodation rate $\dot{Z}(L-U)$ in the delta plain, and, as depicted in Fig.4, the shoreline trajectory moves seawards $\Delta L > 0$. As time increases the delta length $(L-U)$ increases monotonically and at some point in time cannot be maintained by the sediment input, what leads to shoreline retreat, i.e., $\Delta L < 0$. Rapidly, the shoreline reaches a constant landwards speed $\Delta L / \Delta t = -\dot{Z}$ and the delta length reaches a steady value $(L-U) = 1/((1-\gamma)\dot{Z} - \min(\dot{Z}, P))$.

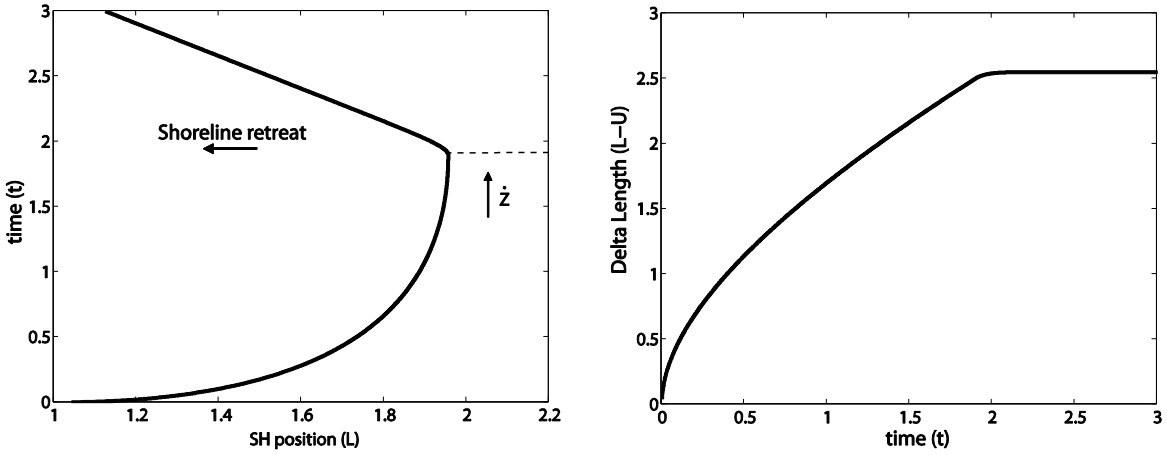

Fig. 4-4 Example model run for the base-level rise scenario.

In Fig. 5 we present the typical model behavior under pivot subsidence (Table 2). We use two subsidence rates: $\dot{\beta} = 2.2$ (black solid lines) and $\dot{\beta} = 2.8$ (red solid lines). The slope ratio is $\gamma = 0.01$, and the net organic production is $P = 0.4$. Initially, similarly to the base-level rise scenario, the total rate of sediment input $\dot{V}$ exceeds the total accommodation rate $\dot{\beta}(L+U)/2$, and, as depicted in Fig.5, the shoreline trajectory moves seawards $\Delta L > 0$. At later stages of delta growth, however, the shoreline can have

two possible behaviors. (1) It can monotonically approach a steady location (black solid line), where the sediment input balances accommodation, and the alluvial-basement transition is fixed at the pivot $U = 0$. And (2), it can overshoot and retreat before reaching the steady location (red solid line).

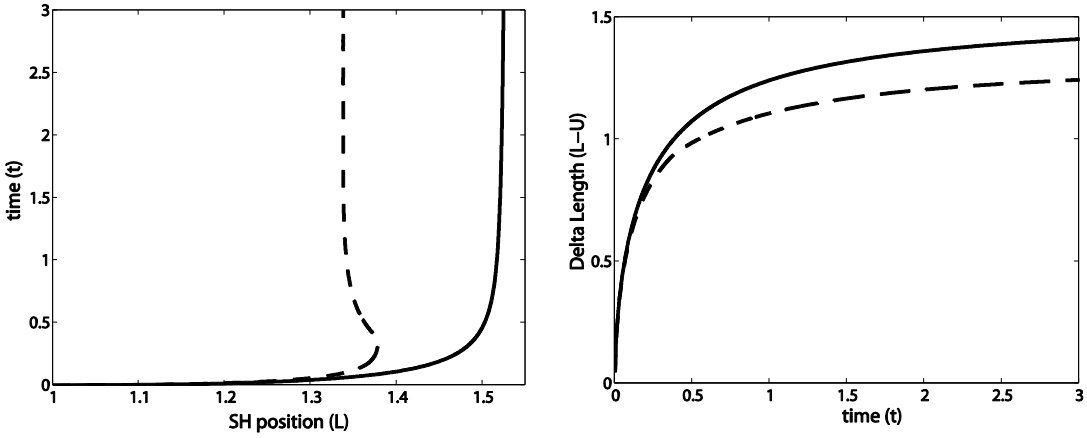

Fig. 4-5 Example model run for the differential subsidence scenario.

6. Calculating Carbon Fraction

A simple and worthwhile extension of the model presented above is to calculate the carbon fraction C_f, defined as the ratio between the organic and total (i.e., organic and inorganic) sediment volume in the sediment column. We define the average carbon fraction in the time interval (t_1, t_2) at a given location x in the delta plain in terms of the organic v_{org} and inorganic v_{in} sedimentation rates as follows

$$C_f(x) = \frac{\sum_{t_1}^{t_2} v_{org}(x)\Delta t}{\sum_{t_1}^{t_2} (v_{org}(x) + v_{in}(x))\Delta t} \tag{11}$$

Organic sedimentation v_{org} is described in equation (4). Inorganic sedimentation v_{in} first fills the fraction of the accommodation A not occupied by organics, and the excess (if any) is distributed between the delta plain and the subaqueous foreset. Since the accommodation rate A is constant in time for the base-level rise $A = \dot{Z}$ and differential subsidence $A = \dot{\beta} x$ scenarios, we can write (11) as follows

$$C_f = \frac{\min(A, P)(t_2 - t_1)}{A(t_2 - t_1) + \sum_{t_1}^{t_2} (v_{in})_{adv} \Delta t} \tag{12a}$$

where $(v_{in})_{adv}$ is the excess of inorganic sediments retained in the delta plain. We exclude the excess that accumulate in the foreset; an approach consistent with how measurements are made in the field, which only consider the carbon rich sections of any given core (Bohacs 1997, Diessel 2000). During shoreline advance $\Delta L > 0$, $(v_{in})_{adv}$ is obtained through geometric construction, and during shoreline retreat $\Delta L \le 0$ the entire inorganic sediment supply is included in the accommodation term A. We can then write it as follows

$$(v_{in})_{adv} = \begin{cases} \gamma \Delta L / \Delta t & \Delta L > 0 \\ 0 & \Delta L \le 0 \end{cases} \tag{12b}$$

7. Comparison with coal and peat data

Coal geologists have observed that the fundamental control of the carbon fraction in the sediment column C_f is the ratio between accommodation A (space created for sediment accumulation) and net peat production rate P (Bohacs and Suter 1997, Diessel et al. 2000).

Under base-level rise the accommodation rate $A = \dot{Z}$ and the carbon fraction are constant along the delta plain. In Fig. 6 we plot the carbon fraction, obtained from (12), as a function of the ratio $\dot{Z} / P$ for the input parameters indicated. The key observation, independent of the parameter values chosen, is the occurrence of a maximum carbon

fraction when the accommodation rate matches the net production, i.e., $\dot{Z}/P = 1$. This result matches the widely made observation in the coal literature of maximum peat fractions in systems where net productivity matches the accommodation rate, i.e., $\dot{Z}/P \sim 1$ (Bohacs and Suter 1997, Diessel et al. 2000).

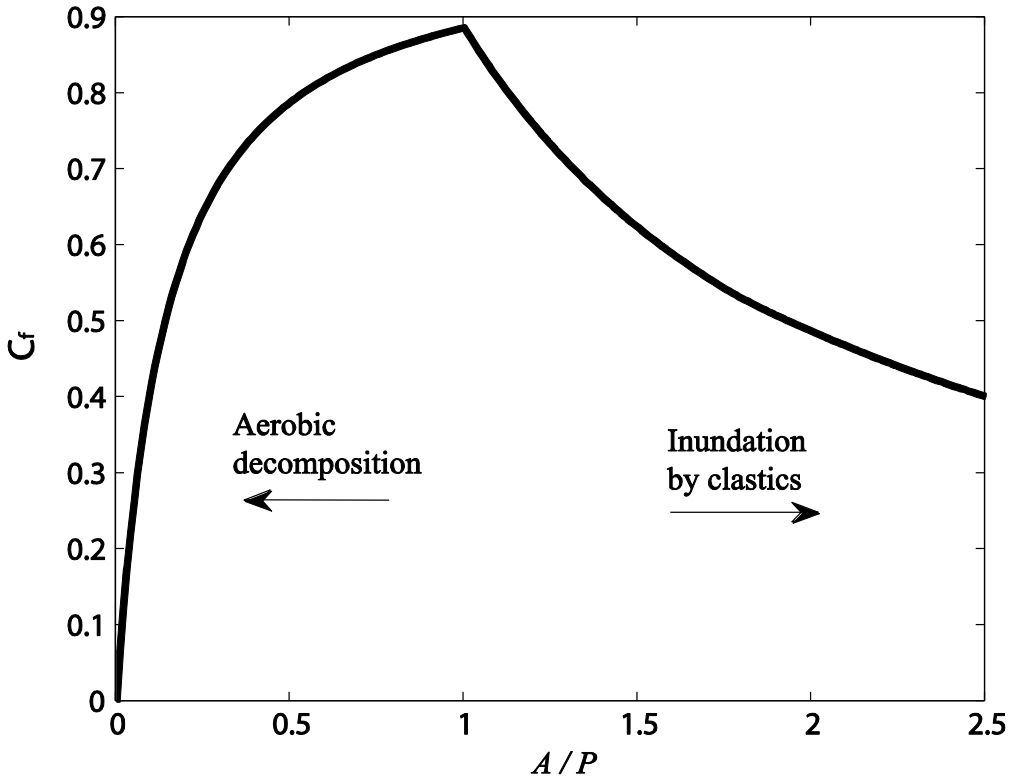

Fig. 4-6 Carbon fraction C_f as a function of the base-level rise to net production ratio $\dot{Z}/P$. The slope ratio is $\gamma = 0.05$, the running time $t = 3$, and the time interval for the carbon fraction calculation is $(t_1, t_2) = (0,3)$.

Under differential subsidence, both the accommodation rate $A = \dot{\beta} x$ and the carbon fraction C_f are functions of the delta plain location x. In Fig.7 and 8 we plot the carbon fraction as a function of $A/P = (\dot{\beta}/P)x$. In Fig.7 we vary the ratio $\dot{\beta}/P$ and fix the location at $x = 1$, whereas in Fig.8 we vary the location x and fix the ratio $\dot{\beta}/P$. Again,

the key observation is the occurrence of the maximum carbon fraction when the accommodation rate matches the net production $A/P=1$ (Bohacs and Suter 1997, Diessel et al. 2000).

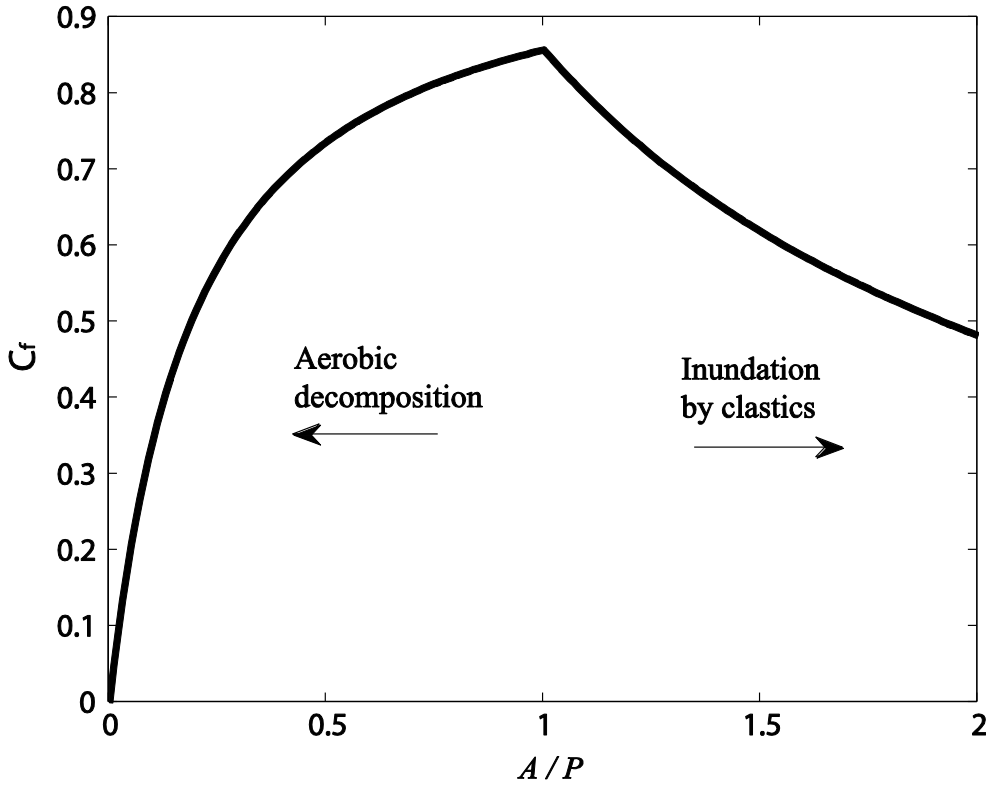

Fig. 4-7 Plot of the carbon fraction C_f as a function of $A/P=(\dot{\beta}/P)x$ at a fixed location $x=1$. We also fix the slope ratio $\gamma=0.1$, the running time $t=3$, and the time interval for the carbon fraction calculation $(t_1,t_2)=(0,3)$.

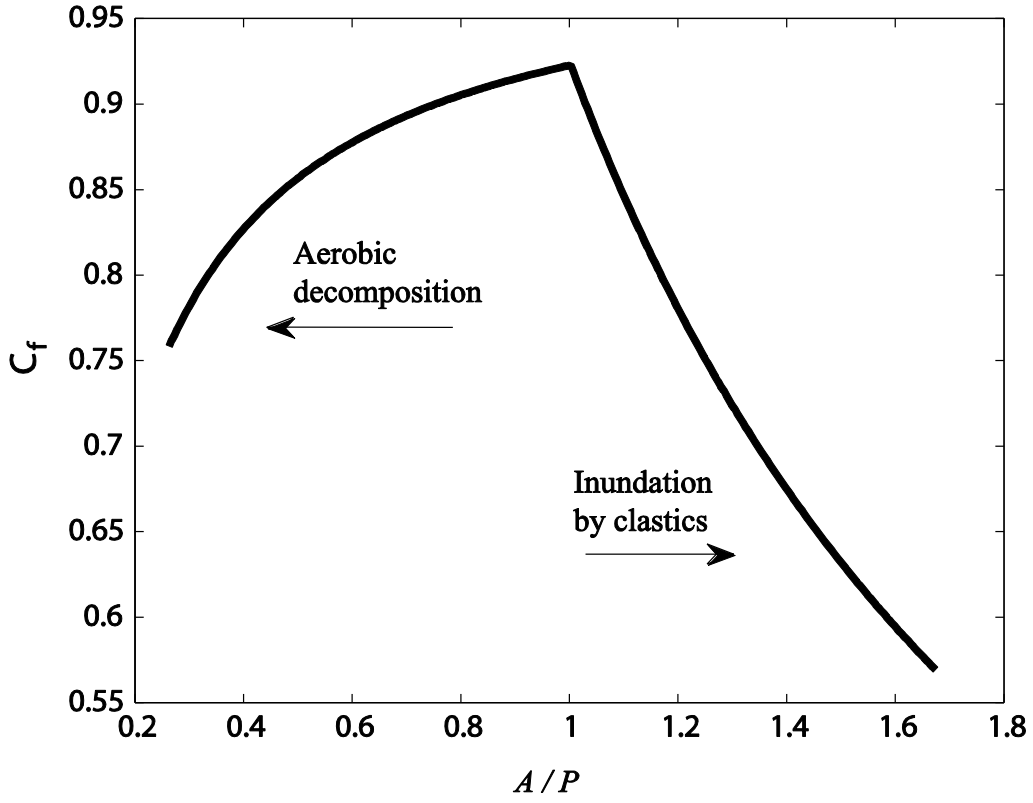

Fig. 4-8 Plot of the carbon fraction C_f as a function of $A/P = (\dot{\beta}/P)x$ for a fixed subsidence rate $\dot{\beta} = 0.2$, and net production $P = 0.4$. We also fix the slope ratio $\gamma = 0.1$, the running time $t = 3$, and the time interval for the carbon fraction calculation $(t_1, t_2) = (1.5, 3)$.

We view these results as a validation of our modeling approach, in particular our assumption of fluvial shape preservation that constrains the organic sedimentation to be the minimum of the net production P and accommodation rate A (eq. (4)).

8. The role of the fresh-salt boundary dynamic in delta evolution

In the initial derivation and application of our model we have assumed a constant value for the net organic production P . We now generalize this assumption by accounting for the potentially important effects of different net production rates between saline and fresh environments (see discussion in section 2). On deltaic coasts, the segmenting of the delta into the fresh and saline regions is largely controlled by the fresh water supply (Ibañez et al. 1997, Sierra et al. 2004). A reduction in the river water supply leads to saltwater intrusion, what accelerates the decomposition of organic soils due to the shift in anaerobic respiration from methanogesis to sulfate reduction (Capone & Kiene 1988, Portnoy and Giblin 1997, Portnoy 1999, Ibañez et al.2010). Changes in water supply on centennial to millennial time scales can be caused naturally by climate change or an abandonment of the river channel. Paleoflood chronologies from the Mississippi river have concluded that minor changes in climate can produce very high changes in water discharge (Knox 1993). Additionally, human activities such as channelization also play a role in controlling the fresh water supply (Day et al. 1997, Williams et al. 1999, Sierra et al. 2004).

To illustrate how our model can be generalized to account for spatial variations in net productivity controlled by changes in fresh-water inputs, we consider a scenario of a delta initially in a purely freshwater environment that at some time t^* converts to a delta that contains both a fresh region of length f and a saline region of length s . This transition is taken to be instantaneous, i.e., short compared to the time scale of delta response. This example does not intend to model any system in particular, but aims to explore the importance of the fresh-salt transition on delta dynamics. If we denote net production in the fresh by P_f and saline regions by P_s a modified form of the governing equation in (7) can be written as

$$\dot{V} = 1 + \int_{U}^{U+f} \min(A, P_f)\,dx + \int_{U+f}^{L} \min(A, P_s)\,dx \qquad (13)$$

which on specification of an appropriate relationship between f , s , L and U can be solved by a simple extension of the approach detailed in Tables 1 and 2. For the case under consideration these relationships are

$$f = \begin{cases} L - U & t < t^* \\ (1-k)(L-U) & t \geq t^* \end{cases} \tag{14a}$$

$$f + s = L - U \tag{14b}$$

where k is the fraction of the delta that is eventually under saline conditions.

Under a steady base-level rise, an early shift of the fresh-salt transition modifies the time and the location at which the shoreline retreat begins (Fig.9a). When the delta is always fresh $(k = 0)$, the shoreline advances further and for a longer time period than a combined fresh/saline delta $(k = 0.5,1)$. In contrast, a shift in a more advanced stage of delta growth leads to an abrupt increase of the shoreline retreat speed (Fig.9b).

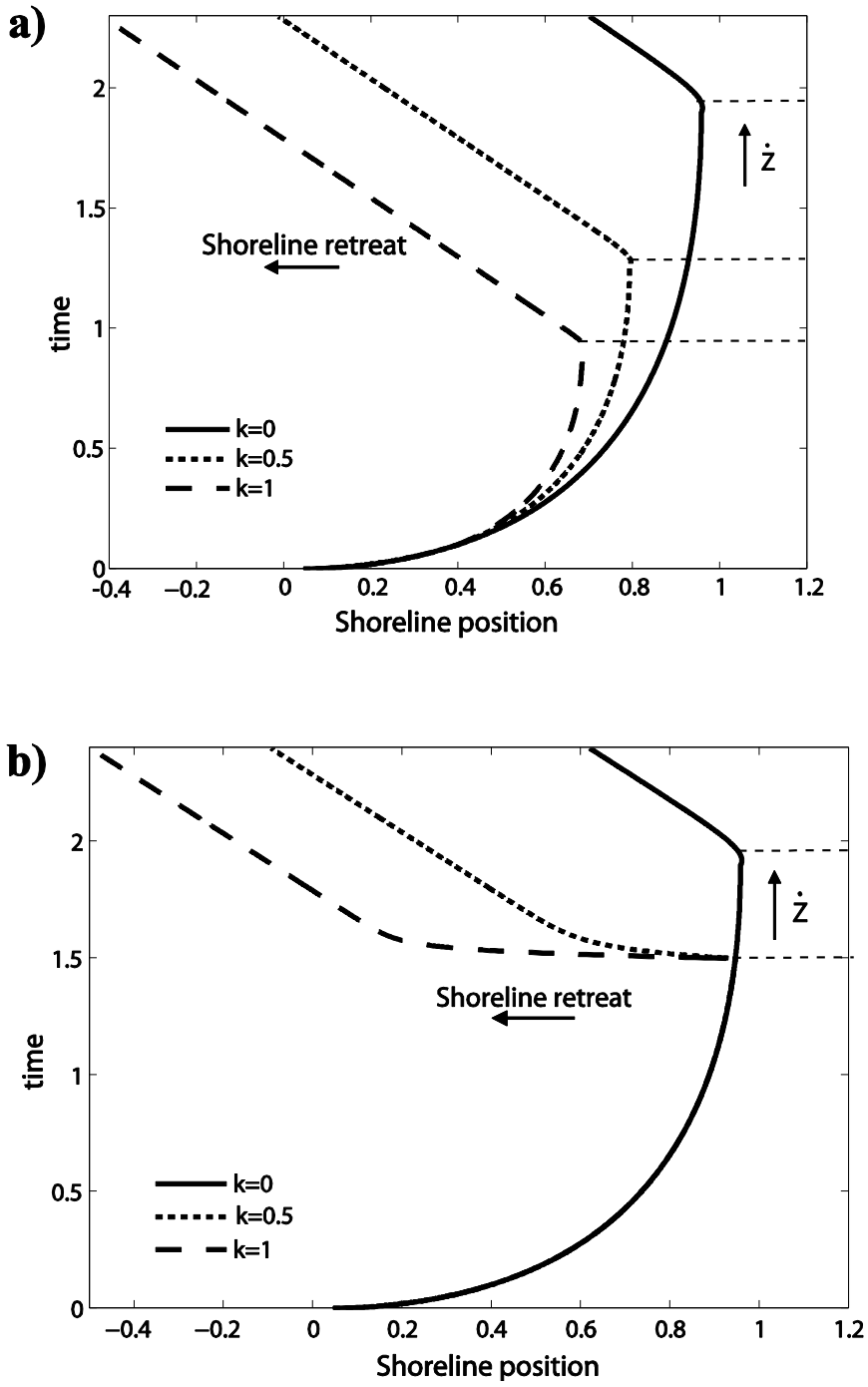

Fig. 4-9 Shoreline response to a landwards shift of the fresh-salt transition at time (a) $t^* = 0.1$, and (b) $t^* = 1.5$, for a steady base-level rise $\dot{Z} = 0.8$. The slope ratio is $\gamma = 0.01$, and the net organic productions are $P_f = 0.4$, and $P_s = 0.1$.

Similarly, under differential subsidence the fresh-salt transition shift can also lead to an abrupt increase of the shoreline retreat speed before reaching a steady location (Fig.10).

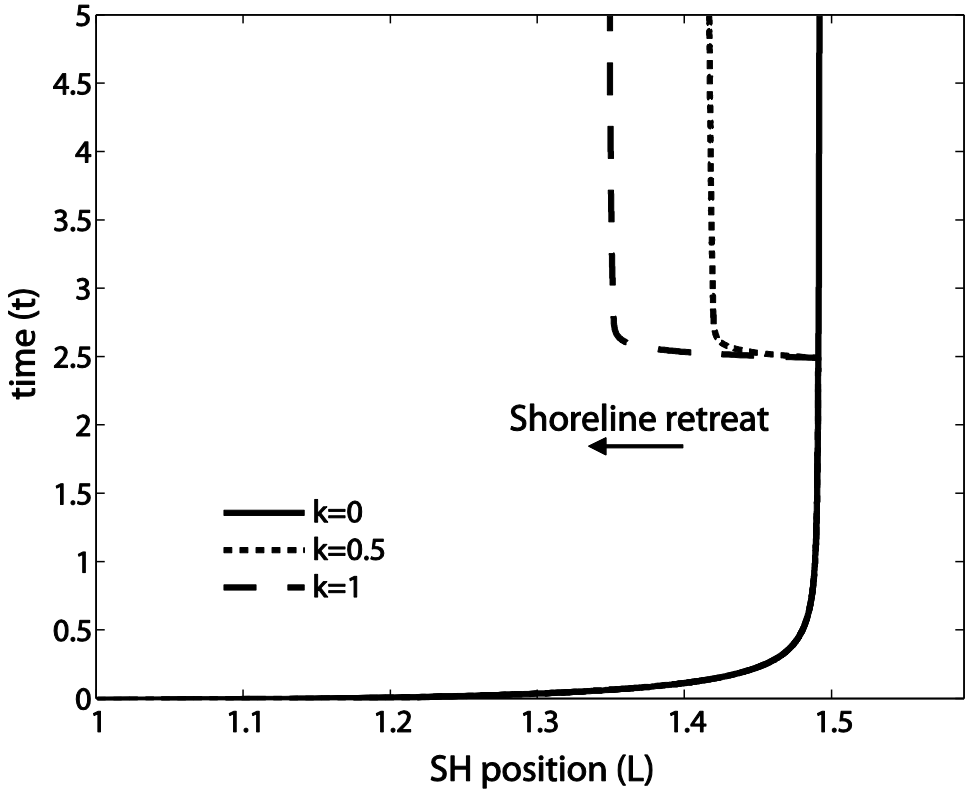

Fig. 4-10 Shoreline response to a landwards shift of the fresh-salt transition at time $t^* = 2.5$, and a subsidence rate $\dot{\beta} = 2.3$. The slope ratio is $\gamma = 0.1$, and the net organic productions are $P_f = 0.4$, and $P_s = 0.1$.

These results (Fig. 9 and 10) highlight the variations in fresh water inputs as a potential candidate to explain the observed punctuated episodes of rapid shoreline retreat in the Gulf of Mexico (J.Anderson 2010).

9. Conclusions

We present a simple geometric model that for the first time captures the basic interplay of organic and clastic deposition in deltas under base-level rise and differential subsidence. The model reproduces without forcing a central observation from coal geology, that

carbon fraction is maximized when the net organic production and accommodation rates are just balanced. Moreover, the model shows that the imbalance in organic sedimentation between fresh and saline environments can significantly alter large-scale delta dynamics. In particular, a landwards shift of the fresh-salt transition caused by a reduction in fresh water inputs can exacerbate shoreline retreat. Using this framework, future work will analyze the role of organic sedimentation on (1) the shoreline response to base-level cycles, and (2) river avulsion and alluvial architecture.

Chapter 5: A geometric model for the dynamics of a fluvially dominated deltaic system under base-level change

J. Lorenzo-Trueba et al. (in press), A geometric model for the dynamics of a fluvially dominated deltaic system under base-level change, *Computer & Geosciences*, Special issue "Modeling for Environmental Change". 10.1016/j.cageo.2012.02.010

We present a geometric model to study the role of base-level change in the dynamics of the alluvial-bedrock transition and shoreline positions in a fluvially dominated deltaic system. The domain of the problem is a sediment wedge in the long-profile cross-section. On assuming that the fluvial surface has a quadratic form, its evolution is determined by imposing an overall volume balance, and conditions for the elevations and slopes at the domain boundaries. This results in a coupled system, involving one ordinary differential equation and one non-linear equation. These equations are solved through an explicit Euler time stepping algorithm to predict the movement of the shoreline and alluvial-bedrock transition boundaries under a wide range of base-level change conditions. The mathematics of the approach are verified by comparing predictions from the geometric model with a closed form solution of a downslope gravity-driven transport model under the specific case of a square-root of time base-level change. Testing with more general base-level change scenarios reveals that this simple geometric mass balance is able to predict system dynamics that are fully consistent with both physical and numerical experiments. Moreover, model predictions under a base-level cycle (fall-rise) suggest a behavior where river incision occurs during the base-level rise stage, a predicted dynamic that has not been previously reported.

1. Introduction

Numerous quantitative tools have been developed during the last decades to gain a better understanding of the coastal response to environmental forcing (e.g., base-level change) (Paola 2000, Fagherazzi and Overeem, 2007). The large range of processes and time scales involved in gaining such understanding requires the use of a variety of modeling approaches, from simple models to highly detailed simulations (Fagherazzi and Overeem, 2007; Blum and Roberts, 2009; Paola et al., 2011). At the simple end of the spectrum, one-dimensional longitudinal profile models have proved to be a useful and physically valid approach in explaining the essential average dynamics of delta evolution in geological time scales (i.e., thousands to millions of years) (Paola, 2000; Swenson et al., 2000; Parker and Muto, 2003; Swenson et al., 2005; Voller et al.,2006; Muto and Swenson, 2005; Swenson and Muto, 2007; Kim and Muto, 2007; Capart et al., 2007; Lai and Capart, 2007; Hoogendoorn et al., 2008; Parker et al., 2008a, 2008b; Lorenzo-Trueba et al., 2009; Lai and Capart, 2009; Lorenzo-Trueba and Voller, 2010; Paola et al., 2011). The key ingredient in models of this nature is the assumption of a one-dimensional domain profile in the form of a sediment wedge depositing onto a bedrock basement in response to a sediment supply q_0 and a base-level change (i.e., the sum of sea-level and basement changes), see Fig. 1. This domain is defined by three vertices, (i) the alluvial-bedrock transition (ABT), the upstream limit of the alluvial-deltaic system, (ii) the shoreline (SH) at the transition between the subaerial to subaqueous regions, and (iii) the submarine toe (TOE) where the submarine sediment wedge re-intersects with the basement. In the evolution of the wedge each of these vertices changes position with time, i.e., they are moving boundaries.

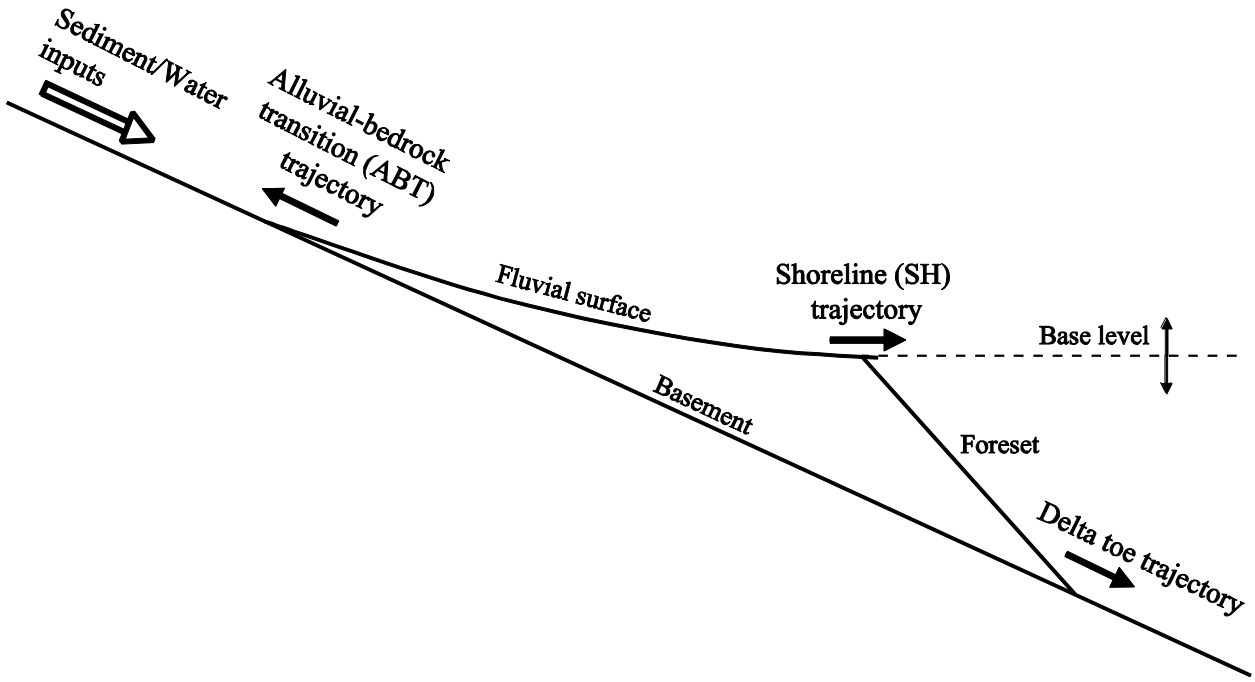

Fig. 5-1 Simplified alluvial deltaic system longitudinal profile.

A breakthrough in developing this one-dimensional cross-shelf models was presented in Swenson et al. (2000), who simplified the configuration by considering only the movements of the SH and the TOE. The key assumption in this model is a subaerial fluvial transport via a linear diffusion model (i.e., the sediment transport rate is proportional to the local bed slope) and a fixed angle of repose for the foreset. The solution of the problem involved the use of a coordinated transformation (i.e., a Landau transformation (Crank, 1984)) that fixes the location of the shoreline. A departure from the basic Swenson et al. (2000) model was due to Parker and Muto (2003) who considered the full domain in Fig.1 and, through a numerical solution, tracked all three of the wedge vertices ABT, SH and TOE. This work and a later effort from Swenson and Muto (2007) also generalized the previous treatment by allowing for the possibility of a non-linear diffusion transport where the sediment flux is set proportional to a power (>1) of the bed slope.

In related analytical work, Voller et al. (2004) presents an analytical similarity solution for tracking the SH under the assumptions of no base-level change and linear diffusion

transport, a solution further developed by Capart et al. (2007) for a variety of alternative geomorphic settings. Analytical solutions for the more general case of tracking both the SH and ABT are presented by Lorenzo-Trueba et al. (2009) and Lai and Capart (2009). With the similarity solution in the former of these works extended by Lorenzo-Trueba and Voller (2010) to consider cases where transport is governed by non-linear diffusion (i.e., a power relationship between the sediment flux and the local slope). In contrast to the diffusion models, Kim and Muto (2007) developed a very simple but effective first order geometric solution for a general base-level curve by assuming a fixed fluvial slope. In relating this effort to the previous diffusion transport models, the analytical work of Lorenzo-Trueba and Voller (2010) shows that the linear geometric model is a limit case of the general non-linear diffusion model. A potential drawback with this simple geometric constant fluvial slope model, however, will occur in attempting to model systems where temporal or spatial changes in the fluvial slope are expected.

In response, we propose a modified geometric model that assumes a quadratic profile shape for the fluvial surface. It will be shown that this model overcomes the restriction of the linear profile model and provides predictions on par with those of the analytical and numerical models noted above.

2. Governing equations

Before we derive the governing equations, we introduce the key geometric variables that define the system in Fig. 2. The origin is chosen at the initial intersection of the base-level with the bedrock, with *x* positive in the seaward direction and *z* positive upwards. We define $h(x,t)$ as the height to the fluvial surface, $Z(t)$ as the base-level, and β as the basement slope. Although the delta front (foreset) generally develops as a function of fluvial input and basin hydrodynamics (Swenson et al., 2005; Lai & Capart 2007), here we focus on systems with weak subaqueous delta development (e.g., Mississippi delta) and, as such, assume a constant foreset slope ψ (Swenson et al., 2000; Parker and Muto, 2003; Muto and Swenson, 2005; Swenson and Muto, 2007; Kim et al., 2006; Lorenzo-Trueba et al., 2009; Lorenzo-Trueba and Voller, 2010). The positions of the ABT, and

SH with time are defined by $r(t)$, and $s(t)$; initially both ABT and SH collapse at the origin, i.e.,

$$r(t=0) = s(t=0) = 0 \tag{1}$$

The main governing equation will take the form of a mass (volume) balance of the sediment in the deltaic wedge of Fig. 2. With a constant input of sediment q_0 (unit flux) into the system the total volume (per unit width) of the wedge at any point in time t is given by $V = q_0 t$. We recognize that this volume can also be defined in terms of the geometry of the wedge, leading to the balance equation

$$V = q_0 t = \int_r^s h dx + \frac{\beta}{2}\left(s^2 - r^2\right) + \frac{(\beta s + Z)^2}{2(\psi - \beta)} \tag{2a}$$

The summation of the first two terms on the right hand side of equation (2a) corresponds to the volume of the wedge between the ABT and the SH (i.e., $r(t) < x < s(t)$), and the last term corresponds to the volume of sediments accumulated beyond the SH (i.e., $s(t) < x < w(t)$). Notice, however, that the volume balance in (2a) may not always hold. In a base-level rise scenario, a point can be reached in which the incoming sediment flux is insufficient to supply the foreset and the fluvial plain abandons the submarine portion, a phenomena that can be referred to as 'autobreak' (Muto, 2001; Parker and Muto, 2003). The wedge configuration shown in Fig.2 is then replaced by the configuration in Fig. 3. In this scenario, all of the incoming sediment q_0 is deposited onto the fluvial surface, and the volume balance in (2a) is supplanted by the differential balance

$$\int_r^s \frac{\partial h}{\partial t} dx = q_0 \tag{2b}$$

where $\partial h / \partial t$ is the rate of sediment accumulation at a given location in the fluvial plain.

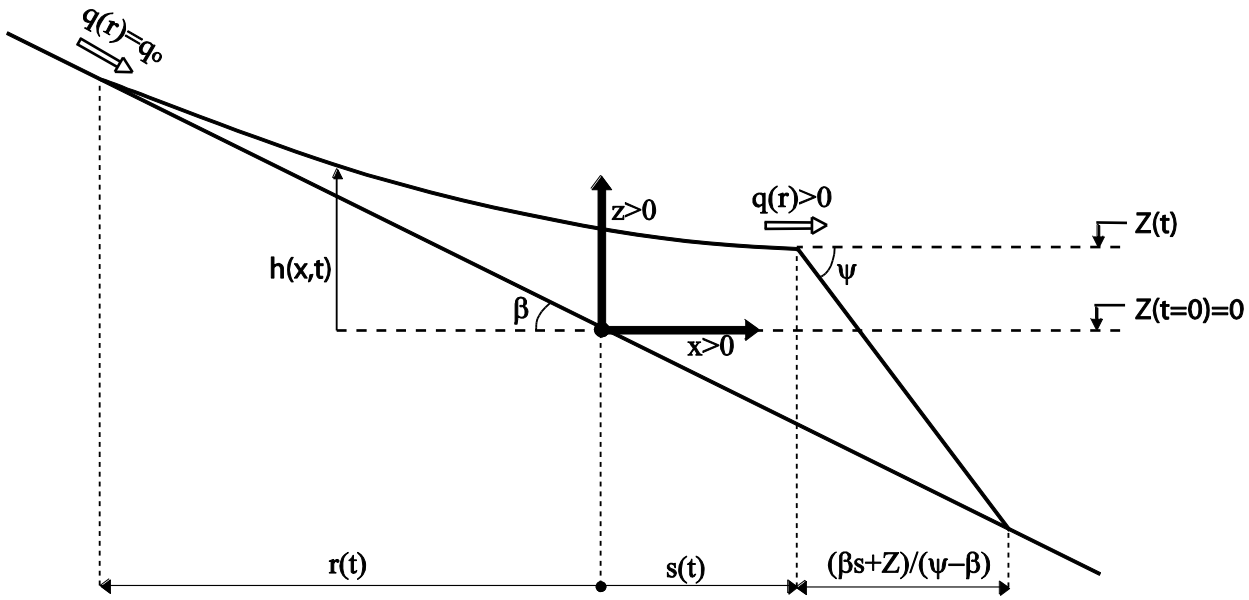

Fig. 5-2 Delta longitudinal profile with the state variables.

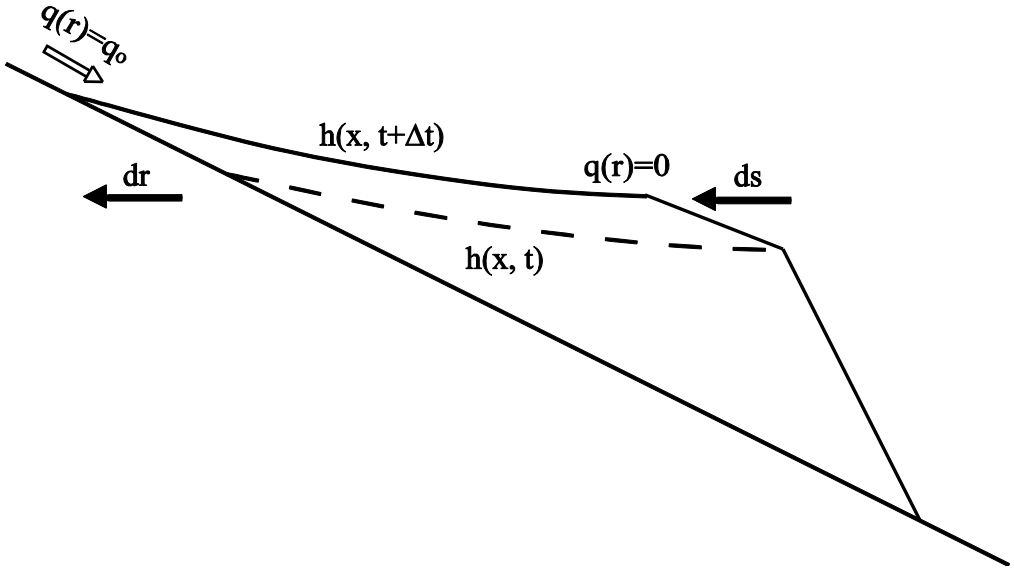

Fig. 5-3 Sketch for autobreak.

In addition to the balance in equation (2) four additional conditions can be identified. The first two conditions are obtained by matching the fluvial surface with the bedrock at the ABT

$$h\big|_{x=r} = -\beta r \tag{3}$$

and with the base-level at the SH

$$h\big|_{x=s} = Z \tag{4}$$

Two additional conditions on the slopes at the ABT and SH domain boundaries can be set by assuming that the sediment flux is a function of the local fluvial slope; an assumption that has been the basis of many previous physically validated modeling studies (Paola, 1992; Paola, 2000; Swenson et al., 2000; Parker and Muto, 2003; Swenson and Muto, 2007; Fagherazzi and Overeem, 2007; Postma et al., 2008; Lorenzo-Trueba and Voller, 2010). The simplest form of this model is to assume that the flux is directly proportional to the fluvial slope, i.e.,

$$q(x) = -\nu \frac{\partial h}{\partial x} \tag{5}$$

where the 'fluvial diffusivity' ν scales with the water discharge and has units of length squared over time. This assumption allows us to impose a condition for the fluvial slope at the ABT of the form,

$$\nu \frac{\partial h}{\partial x}\bigg|_{x=r} = -q_0 \tag{6}$$

At the same time it also allows us to set a condition on the slope at the SH. The exact setting of this last condition, however, depends on the nature of the governing volume balance, equation (2a) or (2b). When the volume balance in equation (2a) is in operation this last condition is

$$\nu \frac{\partial h}{\partial x}\bigg|_{x=s} = -\frac{\psi}{\psi - \beta}\left(s\beta + Z\right)\left(\frac{ds}{dt} + \frac{1}{\psi}\frac{dZ}{dt}\right) \tag{7a}$$

which represents the balance of sediment at the shoreline originally proposed by Swenson et al (2000).

In contrast, when the system reaches autobreak and equation (2b) is the volume balance the appropriate fouth condition is

$$\left.\frac{\partial h}{\partial x}\right|_{x=s} = 0 \tag{7b}$$

Equation (7b) expresses the fact that in autobreak (Fig. 3) all the sediments are accumulated in the subaerial portion of the wedge and the SH flux is identically zero.

Equations (1-7) are sufficient to describe the fluvial elevation and the movements of the ABT and SH during base-level fall or base-level rise. The model can therefore account for regression (e.g., a seawards migration of the SH), transgression (e.g., a landwards migration of the SH), as well as cases where regression is followed by transgression.

3. A dimensionless form

In order to have a better understanding of the dynamic behavior of the system it is worthwhile to rewrite the governing equations (1-7) in dimensionless form. Toward this end the following scaling is introduced

$$x^d = \frac{x}{\ell}, \quad t^d = \frac{t}{\tau}, \quad s^d = \frac{s}{\ell}, \quad r^d = \frac{r}{\ell}, \quad Z^d = \frac{Z}{\ell\beta}, \quad h^d = \frac{h}{\ell\beta}, \quad V^d = \frac{V}{\ell^2\beta} \tag{8}$$

where ℓ is a length (e.g., a characteristic basin length), $\ell\beta$ is an elevation scale, and $\tau = \ell^2 / \nu$ is the 'basin equilibrium timescale' defined by Paola et al. (1992). The scaling in (8) leads to two dimensionless groups: the ratio of the fluvial to the bedrock slope at the ABT

$$R_{ab} = -\left.\frac{\partial h}{\partial x}\right|_{x=r} = \frac{q_0}{\beta\nu} \tag{9}$$

and the slope ratio at the shoreline SH

$$R_{sh} = \frac{\psi}{\psi - \beta} \tag{10}$$

In equation (10) we note that since the foreset slope ψ is typically orders of magnitude larger than the basement slope β it is reasonable to set $R_{sh} \sim 1$ (Swenson and Muto, 2007; Lorenzo-Trueba et al., 2009; Lorenzo-Trueba and Voller, 2010; Paola et al., 2011) and thus assume that autobreak (i.e., the abandonment of the subaqueous foreset) and the shift from regression to transgression occur simultaneously. This allows us to separate our model into a regressive component, in which the SH always progrades seawards, and the transgressive component, when 'autobreak' is reached. In this way, dropping the *d* superscript for convenience of notation, the dimensionless volume balance governing equation becomes:

$$R_{ab} = \begin{cases} \dfrac{1}{t}\left[\displaystyle\int_r^s h\,dx + \frac{1}{2}(s^2 - r^2)\right], & \text{regression} \qquad (11a) \\ \displaystyle\int_r^s \frac{\partial h}{\partial t}\,dx, & \text{transgression} \qquad (11b) \end{cases}$$

with conditions

$$h\big|_{x=s} = Z \qquad (12a)$$

$$h\big|_{x=r} = -r \qquad (12b)$$

$$\left.\frac{\partial h}{\partial x}\right|_{x=r} = -R_{ab} \qquad (12c)$$

$$\left.\frac{\partial h}{\partial x}\right|_{x=s} = \begin{cases} -(s+Z)\dfrac{ds}{dt}, & \text{regression} \\ 0, & \text{transgression} \end{cases} \qquad (12d)$$

The initial conditions are (see equation (1))

$$s(t=0) = r(t=0) = 0 \qquad (13)$$

4. The Fluvial Profile Model

4.1 Regressive model

For a given base-level curve, $Z(t)$, and the ratio of the fluvial to the bedrock slope at the ABT, R_{ab}, the key to solving equation (11a) subject to the conditions (12) and (13) for tracking the movements of the ABT, $r(t)$, and SH, $s(t)$, rests in evaluating the integral in the first term on the right hand side. To achieve these we assume that the surface elevation of the subaerial fluvial profile at any point in time $h(x,t)$ can be approximated by a quadratic, formed to satisfy the conditions (12a) through (12c), i.e.,

$$h = \left[\frac{Z+r}{s-r} + R_{ab}\right]\frac{(x-s)^2}{s-r} + \left[2\frac{Z+r}{s-r} + R_{ab}\right](x-s) + Z \tag{14}$$

With this, the target integral in equation (11a) can be evaluated as

$$\int_r^s h dx = -\frac{(s-r)^2}{3}\left(2\frac{Z+r}{s-r} + \frac{R_{ab}}{2}\right) + Z(s-r) \tag{15}$$

which on substitution into equation (11a) gives the following algebraic mass balance equation

$$6R_{ab}t = 2(Z+s)(s-r) + (1-R_{ab})(s-r)^2 \tag{16}$$

The additional equation that fully specifies the problem is formed by using the approximation in equation (14) in the trangressive element of the SH condition of equation (12d) to arrive at the ODE

$$\frac{ds}{dt} = \frac{-1}{(s+Z)}\left[\frac{2(Z+r)}{s-r} + R_{ab}\right] \tag{17}$$

So our contention is that for a given $Z(t)$ and R_{ab}, the movements of SH and ABT can be determined by a coupled solution of the non-linear algebraic equation (16) and the nonlinear ODE in (17). A range of possible solvers can be used for these equations but the work here shows that an effective solution can be obtained using a simple Euler

scheme for equation (17). Thus, leading to the following explicit time stepping scheme for calculating the movement of the ABT, $r(t)$, and the SH, $s(t)$

$$s(t+\Delta t) = s(t) - \frac{\Delta t}{s(t)+Z(t)}\left[2\frac{Z(t)+r(t)}{s(t)-r(t)} + R_{ab}\right] \tag{18a}$$

$$r = s - \frac{\sqrt{(Z+s)^2 + (1-R_{ab})6R_{ab}t} - (Z+s)}{1-R_{ab}} \tag{18b}$$

where Δt is the time step. With this simple explicit solver we need to impose initial values at the time $t = t_0 > 0$ for the positions $s(t_0)$ and $r(t_0)$; specific values depend on the problem under investigation. In general, however, the solution is relatively insensitive to the initial guess, it is only during base-level fall scenarios in which the ABT initially migrates seawards (incises) that the solution becomes sensitive to the initial guess. In addition to the requirement of initial values for solving (18) it is also noted that stability requires a small time step, typically in the range $10^{-4} \geq \Delta t \geq 10^{-7}$. Such values, however, have no meaningful effect on computation times; the maximum run time on a very basic PC for the calculations made here is never more than 20 seconds and in many cases significantly less.

4.2. Transgressive model

The regressive model described above works as long as a finite amount of sediment reaches the SH, e.g.,

$$\left.\frac{\partial h}{\partial x}\right|_{x=s} \geq 0 \tag{19a}$$

Or by differentiating (14) while

$$2\frac{Z+r}{s-r} + R_{ab} \geq 0 \tag{19b}$$

As we discussed above equation (19) is not always satisfied under base-level rise and we need to define a different system of equations to define the problem. Similarly to the regressive model we approximate the fluvial profile with a quadratic

$$h = \frac{R_{ab}}{2}\frac{(x-s)^2}{s-r} + Z \tag{20}$$

satisfying in this case the conditions (12a), (12c), and the transgressive component in the SH condition of (12d). On substitution of (20) into the condition on the surface elevation at the ABT (12b), the following relationship between the ABT and SH positions is obtained

$$r = -\frac{2Z + R_{ab}s}{2 - R_{ab}} \tag{21}$$

At the same time the profile in (20) can be used in the trangressive volume balance in equation (11) giving

$$(s-r)\left[\frac{R_{ab}}{6}\left(2\frac{ds}{dt} + \frac{dr}{dt}\right) + \frac{dZ}{dt}\right] = R_{ab} \tag{22}$$

Taking the derivative of (21) and substituting into (22) we obtain the following ODE in terms of the SH location

$$\frac{ds}{dt} = \frac{2}{4 - 3R_{ab}}\left[\frac{3(2-R_{ab})}{s-r} - 2\left(\frac{3-2R_{ab}}{R_{ab}}\right)\frac{dZ}{dt}\right] \tag{23}$$

In this way the ABT and SH trajectories are fully defined with linear equations (21) and ODE in (23). Similarly to the regressive model we can use a simple forward Euler scheme for equation (23), leading to the following explicit time stepping operations for calculating the ABT and SH trajectories,

$$s(t+\Delta t) = s(t) + \frac{2\Delta t}{4 - 3R_{ab}}\left[\frac{3(2-R_{ab})}{s(t)-r(t)} - 2\left(\frac{3-2R_{ab}}{R_{ab}}\right)\frac{dZ(t)}{dt}\right] \tag{25a}$$

$$r = -\frac{2Z + R_{ab}s}{2 - R_{ab}} \tag{25b}$$

The initial conditions are in general provided from the regressive model (18) at the point in time when condition (19) is first met. There are some cases, however, in which the system initially transgresses and we need again an artificial initial condition for the ABT, $r(t_0)$, and SH locations, $s(t_0)$.

5. Verification of the geometric assumption

The quadratic model is presented as a geometric model, but it can also be seen as an integral profile approximation of the Exner equation (Paola and Voller 2005) combined with a sediment transport relationships such that the sediment flux is a function of local slope (Paola et al., 1992; Paola, 2000; Swenson et al., 2000; Marr et al., 2000; Capart et al., 2007; Lai and Capart, 2007; Lorenzo-Trueba et al., 2009; Lai and Capart, 2009). In this context, we can take advantage of analytical solutions previously derived for the same set of conditions (equations 3-7) to verify the accuracy of the quadratic profile assumption. Under the condition of no base-level change, i.e., $Z = 0$, Lorenzo-Trueba et al. (2009) developed an analytical similarity solution for the regressive problem defined by (11-13). In this solution the movements of the ABT and SH are given by equations of the form

$$r = -2\lambda_{ab}\sqrt{t} \tag{26a}$$

$$s = 2\lambda_{sh}\sqrt{t} \tag{26b}$$

where λ_{ab} and λ_{sh} are constants determined through the solution of two algebraic equations. Following from an idea by Capart et al. (2007) this solution can be extended to a base-level change case, provided that the base level change is proportional to the a square root of time dependence i.e., $Z = 2\lambda_z\sqrt{t}$, and the value of the parameter λ_z is not too large. The key ingredients of this solution are given in the appendix and more details can be found in Lorenzo-Trueba et al. (2009). This solution provides a powerful verification benchmark for our proposed model, in particular the validity of approximating the fluvial surface with a quadratic profile.

In benchmarking, first the similarity solution is used to predict values of λ_{ab} and λ_{sh} across the entire feasible range of the alluvial-bedrock slope ratio $0 < R_{ab} < 1$; with in each case the value of λ_z set proportional to λ_{sh}. We then extract the values of λ_{ab} and λ_{sh} at specific values of $R_{ab}[0.05:0.05:0.95]$ through fitting the forms in (26) to the

predicted trajectories r and s given by the time-stepping solution in (18). Benchmarks are made for both a base-level rise (e.g., $\lambda_z = 0.5\lambda_{sh}$) and a base-level fall (e.g., $\lambda_z = -0.5\lambda_{sh}$). In Fig.4 we present a comparison of the analytical values of the moving boundary parameters (solid-line) with those predicted by the time stepping algorithm (18) (points). We clearly see that across a wide range of conditions the time stepping solution closely matches the similarity (non-approximate) solution. It is only at large value of $R_{ab} > 0.8$, beyond the upper limit of field observations (Lorenzo-Trueba et al., 2009; Lorenzo-Trueba and Voller, 2010) that a deviation in the results is observed.

In closing this verification section, we note that in all cases tested, and all the results presented below, predictions form the simple Euler-based time stepping algorithm have been checked against high-order schemes for solving (16) and (17) or (21) and (23). We did not find significant differences between methods.

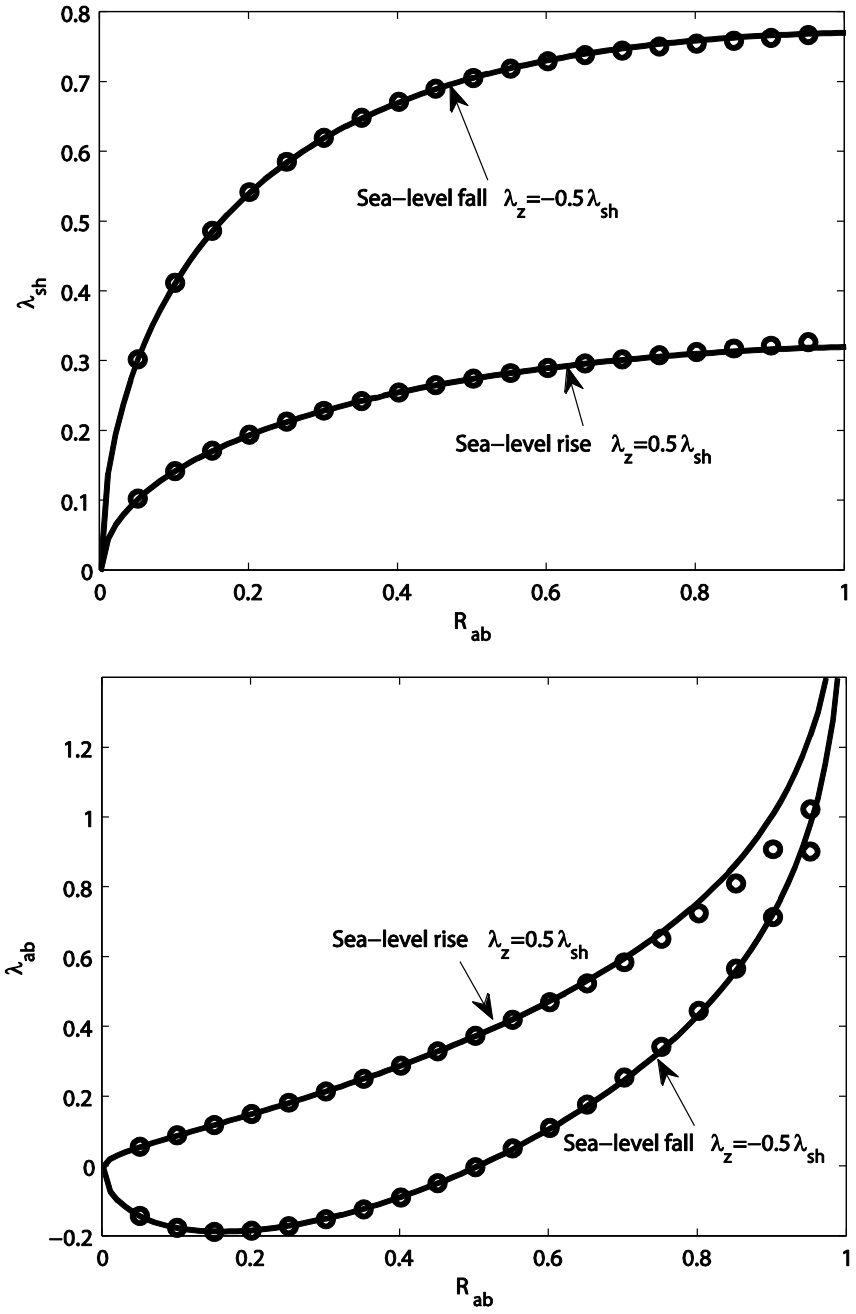

Fig. 5-4 Comparison between analytical and time stepping predictions of the moving boundary parameters λ_{sh} and λ_{ab} for a sea-level fall and a sea-level rise scenarios. The solid is the analytical solution given by equations (A9) and the symbols is the quadratic approximation given by (18). In these efforts we use a time step $\Delta t = 2 \cdot 10^{-7}$ and an initial time $t_0 = 10^{-4}$. During the base-level fall scenario, at low values of $R_{ab} < 0.5$, the ABT initially migrates seaward and a

solution of (18) requires the initial settings $s(t_0) = 100t_0$ and $r(t_0) = t_0$. For all other cases (base-level rise and $R_{ab} > 0.5$) the initial settings $s(t_0) = t_0$ and $r(t_0) = -t_0$ is appropriate.

6. Predictions under base-level change scenarios

To demonstrate how the proposed geometric model (the regressive form (18) and the transgressive form (25)) can be used to understand delta dynamics under base-level change conditions, we consider more general cases than those investigated in the benchmarking. In particular we investigate the dynamics of the delta boundaries (SH and ABT) in three situations (i) a monotonic base-level fall, (ii) a monotonic base-level rise, and (iii) a base-level cycle of a fall followed by a rise.

6.1 Base-level fall

We model base-level fall with the general form

$$Z = -at^b; \quad a, b \geq 0 \tag{27}$$

Since with a base-level fall the SH always migrates seawards, the interesting dynamic with this scenario is the movement of the ABT, which can be studied with the regressive form of the model in (18). In using (27), we would like to explore the role of the exponent b in controlling the movement of the ABT. In previous theoretical work, Muto and Swenson (2005) show that $b = 0.5$ represents a critical value. In particular they show, and experimentally confirm, that a square root base-level fall with a particular choice of $a = a^*$ (see A(10) in the appendix)) is the only possible way to obtain a 'graded profile' in which the ABT remains fixed in time. This led to the hypothesis that for values of $b > 0.5$, the ABT would have an initial landward movement followed by a seaward movement, i.e., a fall in base-level is not a sufficient condition for river incision. This hypothesis has been confirmed with physical and numerical experiments for the case of constant base-level fall $b = 1 > 0.5$ (Muto and Swenson, 2005; Swenson and Muto, 2007). In Fig.5 we show two predictions using (27) in the regressive model (18) for two choices of b, above ($b = 2$) and below ($b = 0.35$) the critical value. These results further confirm the ABT dynamic for the case of $b > 0.5$ (left plot), and not surprisingly reveal

that the opposite behavior occurs below the critical value $b < 0.5$ (right plot); i.e., an initial seawards advance followed by a landward movement.

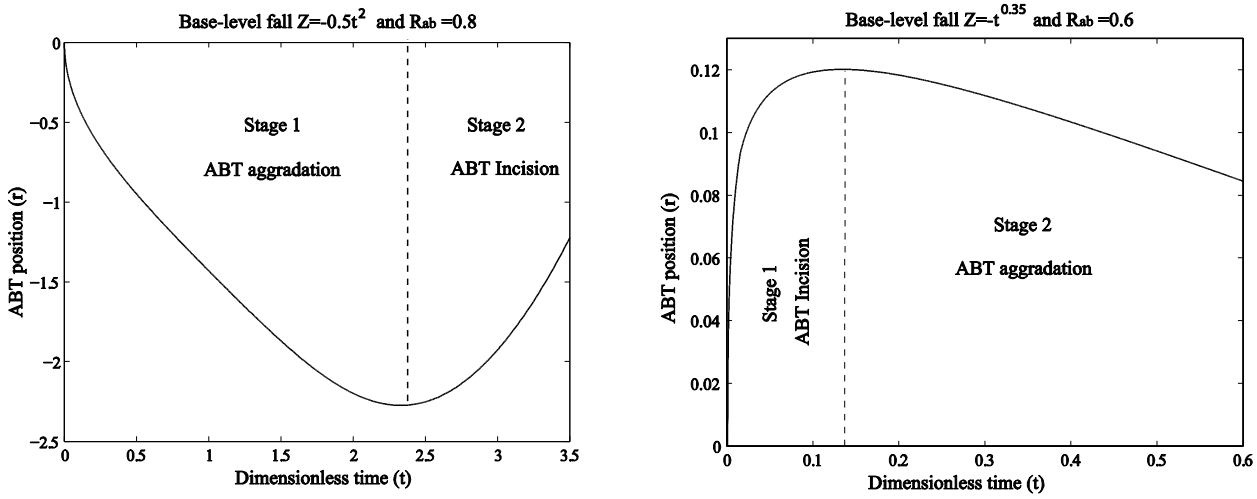

Fig. 5-5 ABT movements under two base-level fall scenarios with their 'b' exponents (see (17)) above and below the critical value '0.5'. Predictions on the left were obtained using a time step $\Delta t = 10^{-4}$, an initial time of $t_0 = 10^{-4}$, and initial guesses for the ABT and SH locations of $s(t_0) = t_0$ and $r(t_0) = -t_0$. On the right we use $\Delta t = 2 \cdot 10^{-7}$, $t_0 = 10^{-3}$, $s(t_0) = 100 t_0$ and $r(t_0) = t_0$.

To help to visualize the dynamics of the fluvial plain, in Fig.6 we include the profile evolution of the case presented in the left plot of Fig.5 ($b > 0.5$). In the first stage the delta plain undergoes degradation in the seaward portion and aggradation in the landward portion. In stage two the situation reverses, and the delta plain undergoes mostly degradation in the landward portion. Note the significant change in slope of the fluvial surface during this process; an alternative linear profile assumption, although simpler to implement, would be restricted to a constant slope and would not be able to capture this dynamic of the fluvial surface.

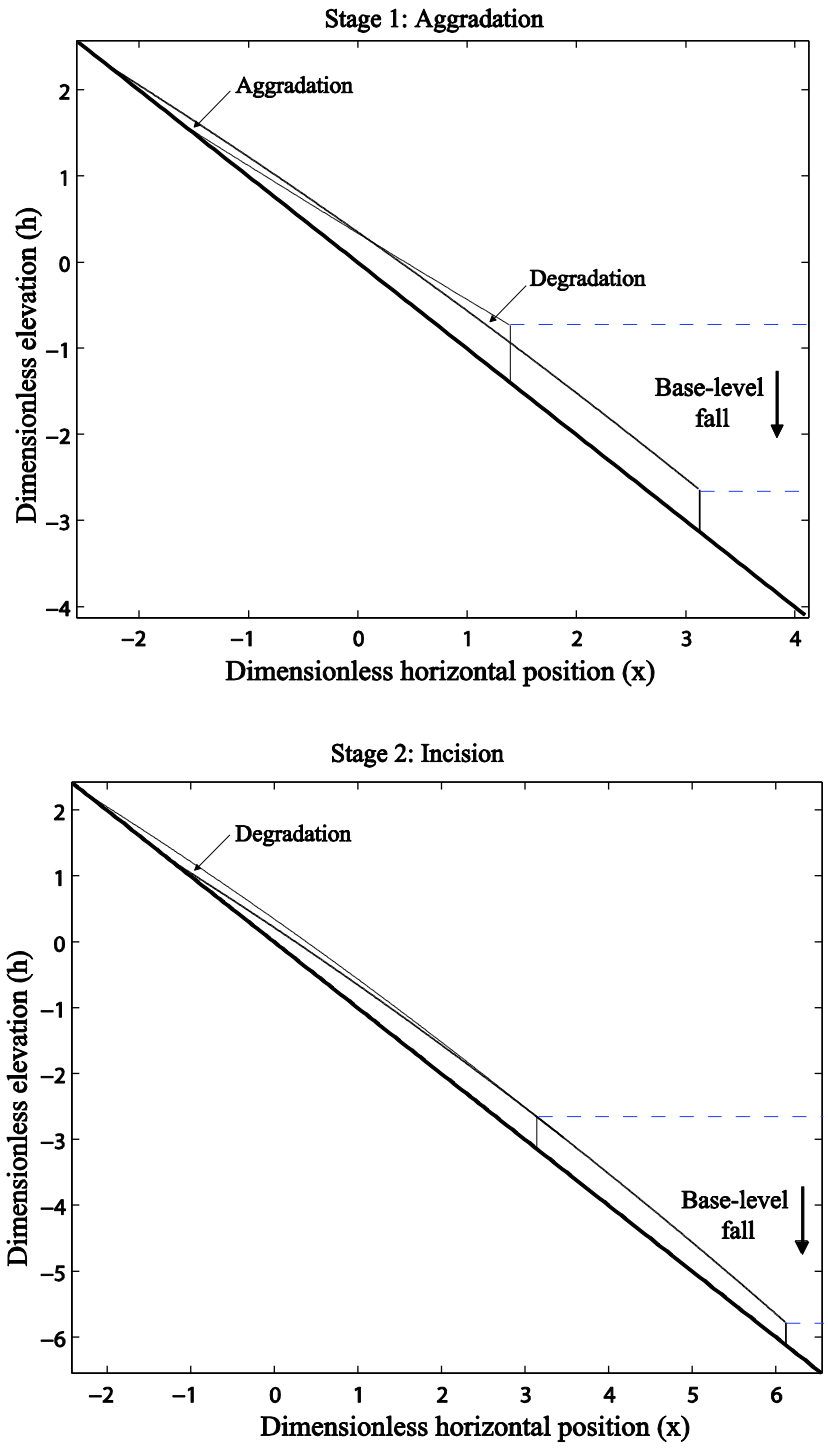

Fig. 5-6 Profile evolution predicted by the model given by $R_{ab} = 0.8$ and base-level curve $a = -0.5$, $b = 2$, corresponding to the evolution in the left plot of Fig. 5. Note that on stage 1 there is aggradation in the landward portion and degradation in the seaward portion of the delta plain. In stage 2 there is mostly landwards degradation.

6.2 Base-level rise

Under a base-level rise scenario

$$Z = a t^b; \quad a, b \geq 0 \tag{28}$$

we need to use both the regressive (18) and transgressive (24) models. In this case the interesting dynamic is the movement of the SH, which once again is largely controlled by the exponent b in (28). Also, as before, the only possible scenario in which the SH remains fixed is under a square root $(b = 0.5)$ base-level rise—a solution that can be obtained from the analytical solution in appendix 2 (9) by setting the SH movement parameter to $\lambda_{sh} = 0$.

In Fig.7 we predict the SH trajectory when the base-level curve exponent is above and below this critical value. When $b > 0.5$ the SH initially regresses followed by a later transgression. A situation experimentally and numerically (a full solution of the governing PDE's) confirmed in the works of Muto (2001) and Parker and Muto (2003). Further, in the situation where $b < 0.5$ the SH initially transgresses and then regresses. Note that, in this last case, current models (including this work) here are not able to model this regression—this would require a careful bookkeeping of the submarine deposits as the SH retreats during the transgressive phase.

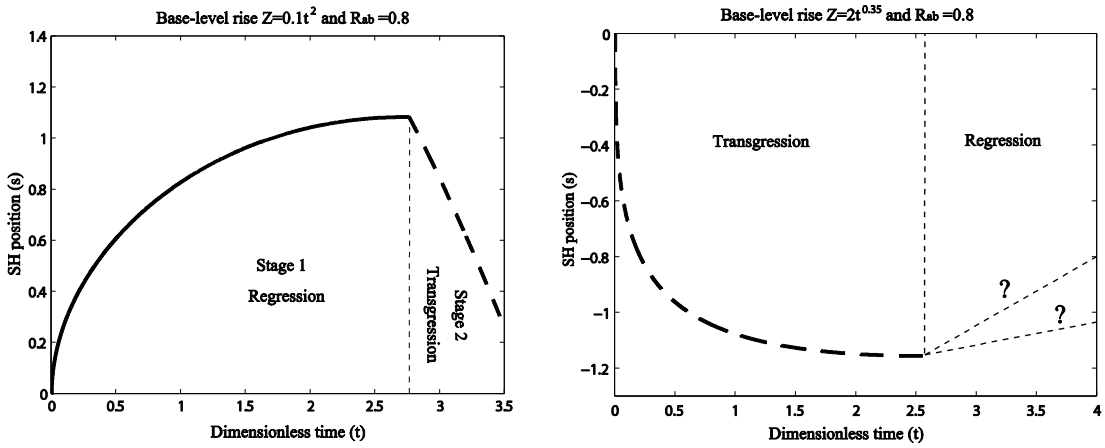

Fig. 5-7 ABT movements under two base-level fall scenarios with their 'b' exponents (see (17)) above and below the critical value '0.5'. The black solid line is calculated using the regressive model (18), the red line is calculated using the transgressive model given by (24), and the dashed black line on the right plot is a hypothetical trajectory for the regression. Predictions on the left were obtained using a time step $\Delta t = 10^{-4}$, an initial time of $t_0 = 10^{-4}$, and initial guesses for the ABT and SH locations of $s(t_0) = t_0$ and $r(t_0) = -t_0$. On the right we use $\Delta t = 10^{-6}$, $t_0 = 10^{-4}$, $s(t_0) = -t_0$ and $r(t_0) = -100t_0$.

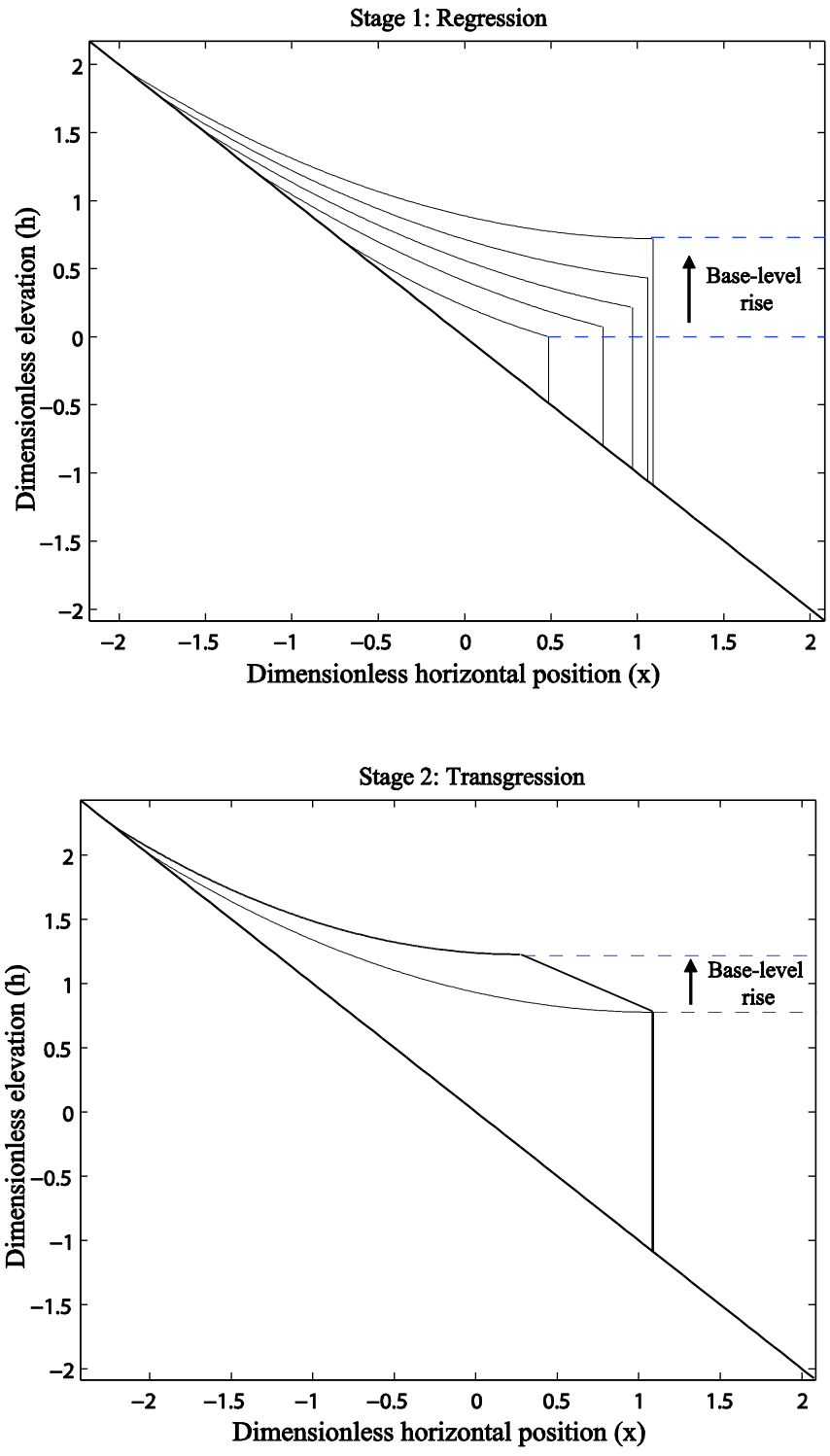

Fig. 5-8 Profile evolution predicted by the model given by $R_{ab} = 0.8$ and base-level curve $a = 0.1$, $b = 2$, corresponding to the evolution shown in the left plot of Fig.7.

6.3 Base-level cycle

In addition to a monotonic rise or fall we can also study a base-level cycle with the proposed model, provided it is in the order of a fall followed by a rise.

In Fig.9 we indicate a base-level cycle given

$$Z = \begin{cases} 0 & t < 2 \\ \dfrac{\cos(t-2)-1}{2} & t \geq 2 \end{cases} \tag{29}$$

and the resulting ABT response predicted with the regressive model (18)—note with (29) the SH always migrates seawards.

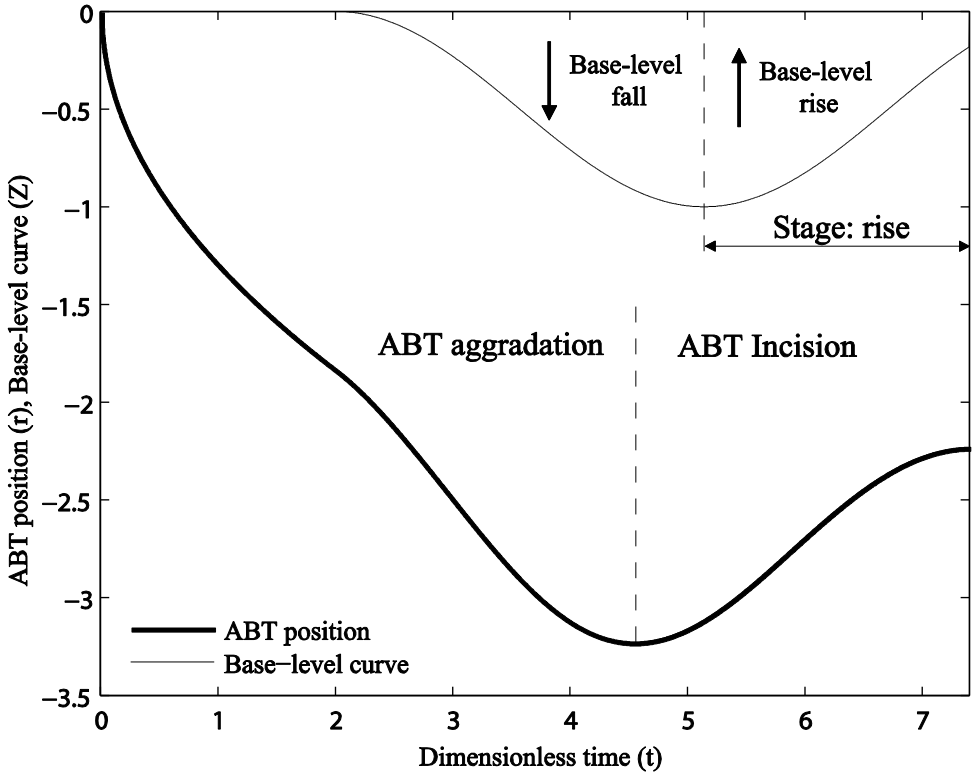

Fig. 5-9 ABT movement predicted by the model given by $R_{ab} = 0.8$ and a base-level fall-rise cycle (also included in the top plot). In the calculations we use a time step $\Delta t = 10^{-4}$, an initial time of $t_0 = 10^{-4}$, and initial guesses for the ABT and SH locations of $s(t_0) = t_0$ and $r(t_0) = -t_0$.

The striking feature in the ABT predictions is that it exhibits a continuous seawards movement during the entire period of base-level rise; this indicates the possibility that river incision can occur under base-level rise. This is well illustrated in Fig.10, which shows two delta plain profiles during the base-level rise stage in (29). In these plots, we observe that as the profile evolves over time a significant sediment volume from the landwards region is eroded downstream to fill the space created in the near shore region. Long-standing conceptual models for stratigraphic correlation between valley formation and sea-level, however, associate river incision with a fall in sea-level (Haq and Schutter 2008). Note that this behavior arises in the current model due to the ability of the quadratic profile to account for spatial changes in the fluvial slope.

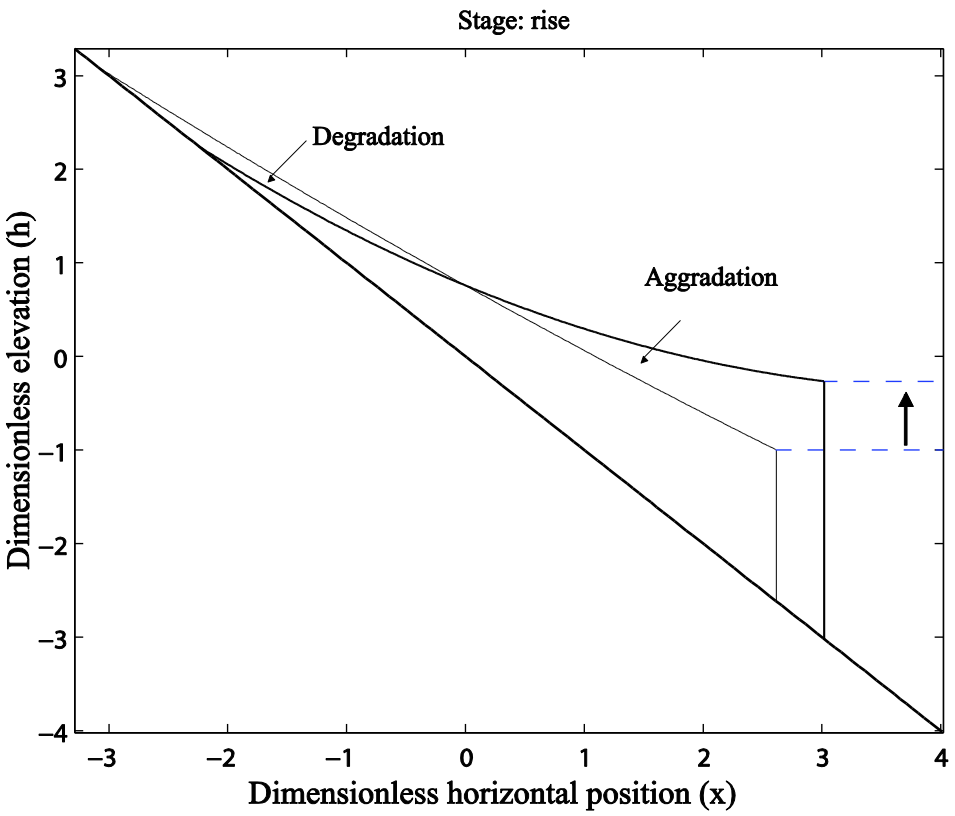

Fig. 5-10 Profile evolution during the base-level rise stage, corresponding to the evolution in Fig.4-9. Note that for these parameter values the system undergoes significant river incision during base-level rise.

7. Conclusion

One-dimensional longitudinal profile models have proved to be an effective means toward gaining an understanding of delta dynamics. Apart from a minority of special cases where similarity solutions can be obtained, the majority of previous models rely on numerical solutions of partial differential equations that require the tracking or (through transformation) the fixing of the moving domain boundaries at the ABT and SH. Although such treatments are successful they can involve coding complexity that makes their wide spread use as general analysis tools problematic. An obvious alternative is to employ a geometric model based on assuming a given shape for the sediment wedge. A

previous model assuming a fixed linear slope for the fluvial surface (Kim and Muto, 2007) is very successful in treating delta building dynamics under base level change, but by its nature may not be able to capture the appropriate physics in cases where the fluvial slope undergoes spatial or temporal changes. Here an alternative geometric solution approach is proposed based on assuming a quadratic shape for the fluvial surface. The problem reduces, in its most general form, to solving a coupled non-linear algebraic equation with a non-linear ODE. We have shown that this solution can be achieved by using a simple explicit Euler based time stepping algorithm. Despite its simplicity, the quadratic model captures an interesting phenomenon of river incision during base-level rise that, to the authors' knowledge, is the first time to be reported. Future work will (1) study in detail what conditions and sea-level history would make such behavior likely, and (2) carry out simple laboratory-scale experiments to validate the model results.

In closing, it is important to point out that, although the model presented here has focus on the dynamic delta responses at large time-scale (thousands to millions of years), it may, in keeping with similar delta models (Capart 2007, Lai and Capart 2007, Lai and Capart 2009), also find application at human time-scales; in particular for problems related to costal management and protection (Paola et al. 2011).

Chapter 6: Conclusions and Future work

In summary, we recognize that the power of a model's application in the management and assessment of environmental systems is not fully determined by its complexity. **Chapters 2, 3, and 5** of the thesis provide sufficient evidence that, under a wide set of clearly defined conditions, simple models—including those based on purely geometric constructs—can account for key sediment transport processes in ocean delta dynamics. This allows us, for the first time, to develop a delta building model that takes account of organic sediment and ecosystem dynamics (**chapter 4**). We believe this model can contribute to quantitative predictions of delta evolution that can then be used to establish baselines for coastal management and protection.

A number of modifications will significantly improve the utility of our model. In particular we plan to include a more complete mechanistic description of the movement of the fresh-salt boundary, which is currently assumed to be an input of the model. Additionally, we need to incorporate field and experimental data to constrain the model parameters of organic net production. Several groups are currently collecting data that could potentially be useful in this regard. For instance, Elizabeth Williams and Brad E. Rosenheim, at Tulane University, are studying the chemistry of decomposition of fresh and saline wetlands. Among other things, they are planning to carry laboratory experiments to analyze the differences in decomposition rate between both fresh and saline environments. These experiments can potentially help us to constrain the net production in our model. Additionally, Torbjörn E. Törnqvist's group at Tulane University has developed a database with numerous borehole locations at the Mississippi River Delta Plain. This database includes information about the organic content that can be used to compare with the pattern of organic matter accumulation produced by the model.

The above improvements will lead to a consistent mathematical model for the characterization of the creation/consumption of organic soil in deltas. A tool that can be used to advance existing modeling efforts pertaining to land building in the Mississippi River Delta (Kim et al. 2009). This in turn will allow us to address current concerns related to the increase of nutrient supply into the wetland ecosystems of the Mississippi River Delta (Perez et al. 2011). Among other important effects, an increase in nutrient concentration in river water can enhance above-ground versus below-ground productivity. This can result in an increase in vulnerability of wetland vegetation, and thus, a decrease in long-term plant matter accumulation in the sediment column. We intend to use future versions of the model to quantify these effects. Complementarily, we will support our model analysis with field campaigns to the Wax Lake Delta Observatory with David Mohrig, at UT Austin, and Robert Twilley, at Louisiana State University.

In this thesis work we have also shown that relatively simple modeling tools can produce counterintuitive behaviors and open new scientific questions. Some of these questions are beyond the scope of this thesis, and below we briefly discuss how we plan to tackle them in the near future.

In **chapter 4** we find that organic sediment dynamics can have an important effect on the long-term shoreline evolution. This result leads to the following question: how do shoreline variations induced by organic sediment dynamics compare to those caused by external forces? Preliminary results show that the long-term shoreline response to variations of the fresh-salt boundary, which plays an important role on preservation of organic sediments in the delta plain, and the sediment input are of similar order of magnitude. This result could have important implications for paleoshoreline reconstruction and the interpretation of past changes in sea-level and climate from the stratigraphic record.

A recent study by Davies and Giblind (2011) highlights the importance of organic sediment dynamics on river avulsion (i.e., an abrupt change in the river channel path). Inspired by this work we are working on a framework capable of quantifying the linkages between organic sedimentation and the spatial distribution of channel deposits in the rock record. We recognize that in this case one-dimensional approaches are not suitable since lateral processes are predominant; we expand to a two-dimensional framework. Preliminary analysis suggests that the organic sedimentation pattern, which is mainly controlled by biogeochemical processes, is a primary control of the channel stacking pattern in organic-rich systems.

In **chapter 5** we present an interesting phenomenon of river incision during base-level rise. Well-known conceptual models, however, always associate valley incision with a fall in sea-level (Vail et al. 1977, Muto and Swenson 2005, Haq and Schutter 2008). We plan to use the theoretical model developed in **chapter 5** to offer suggestions of what conditions (and sea-level history) would make such behavior likely, and test it with simple flume experiments.

References

Anderson, J.B., Rodriguez, A., Abdulah, K.C., Fillon, R.H., Banfield, L.A., McKeown, H.A. and Wellner, J.S. (2004) 'Late Quaternary Stratigraphic Evolution of the Northern Gulf of Mexico Margin: a synthesis', in Anderson, J.B. and Fillon, R.H. (ed.) *Late Quaternary Stratigraphic Evolution of the Northern Gulf of Mexico Margin*, Society for Sedimentary Geology (SEPM).

Anderson, J.B., Rodriguez, A.B., Milliken, K.T., Simms, A. and Wallace, D. (2010) 'Coastal Impact Underestimated From Rapid Sea Level Rise', *Eos Trans. AGU*, vol. 91, no. 23, pp. 205-206.

Barry, S.I. and Caunce, J. (2008) 'Exact and numerical solutions to a Stefan problem with two moving boundaries', *Applied Mathematical Modelling*, vol. 32, no. 1, pp. 83-98, Available: ISSN: 0307-904X DOI: 10.1016/j.apm.2006.11.004.

Blum, M.D. (2009) *Continental Shelves as the Lowstand Fluvial Longitudinal Profile: Possible Implications for Icehouse vs. Greenhouse Stratigraphic Records*, Available: http://www.searchanddiscovery.com/documents/2009/50154blum/ndx_blum.pdf.

Blum, M.D. and Roberts, H.H. (2009) 'Drowning of the Mississippi Delta due to insufficient sediment supply and global sea-level rise', *Nature geoscience*, vol. 2, no. 7, Jul, pp. 488-491, Available: ISSN: 1752-0894 DOI: 10.1038/ngeo553.

Bohacs, K. and Suter, J. (1997) 'Sequence stratigraphic distribution of coaly rocks: Fundamental controls and paralic examples', *AAPG Bulletin-American Association of Petroleum Geologists*, vol. 81, no. 10, OCT, pp. 1612-1639, Available: ISSN: 0149-1423.

Capart, H., Bellal, M. and Young, D.-L. (2007) 'Self-similar evolution of semi-infinite alluvial channels with moving boundaries', *Journal of Sedimentary Research*, vol. 77, no.

Capone, D.G. and Kiene, R.P. (1988) 'Comparison of microbial dynamics in marine and freshwater sediments: Contrasts in anaerobic carbon catabolism', *Limnology and Oceanography*, vol. 33, no. 4, Part 2, JUL, pp. 725-749, Available: ISSN: 0024-3590.

Cherniha, R. and Kovalenko, S. (2009) 'Exact solutions of nonlinear boundary value problems of the Stefan type', *Journal of Physics A: Mathematical and Theoretical*, vol. 42, no. 35, pp. 355202 doi:10.1088/1751-8113/42/35/355202.

Craft, C.B. (2001) 'Wetland soils: genesis, hydrology, landscapes, and classification' CRC Press LLC.

Crank, J. (1984) *Free and Moving Boundary Problems*, Clarendon Press.

Crowell, J.C. (2003) *Evolution of Ridge Basin, Southern California: An Interplay of Sedimentation and Tectonics*, Geological Society of America.

Dade, W. and Friend, P. (1998) 'Grain-size, sediment-transport regime, and channel slope in alluvial rivers', *Journal of Geology*, vol. 106, no.

Davies, N.S. and Gibling, M.R. (2011) 'Evolution of fixed-channel alluvial plains in response to Carboniferous vegetation', *Nature Geoscience*, vol. 4, p. 629–633.

Day, J.W., Boesch, D.F., Clairain, E.J., Kemp, G.P., Laska, S.B., Mitsch, W.J., Orth, K., Mashriqui, H., Reed, D.J., Shabman, L., Simenstad, C.A., Streever, B.J., Twilley, R.R., Watson, C.C., Wells, J.T. and Whigham, D.F. (2007) 'Restoration of the Mississippi Delta: Lessons from Hurricanes Katrina and Rita', *Science*, vol. 315, no. 5819, pp. 1679-1684.

Diessel, C., Boyd, R., Wadsworth, J., Leckie, D. and Chalmers, G. (2000) 'On balanced and unbalanced accommodation/peat accumulation ratios in the Cretaceous coals from Gates Formation, Western Canada, and their sequence-stratigraphic significance', *International Journal of Coal Geology*, vol. 43, no. 1–4, pp. 143-186, Available: ISSN: 0166-5162 DOI: 10.1016/S0166-5162(99)00058-0.

Fagherazzi, S. and Overeem, I. (2007) 'Models of deltaic and inner continental shelf landform evolution', *Annual review of aerth and planetary sciences*, vol. 35, pp. 685-715, Available: ISBN: 978-0-8243-2035-5 ISSN: 0084-6597 DOI: 10.1146/annurev.earth.35.031306.140128.

Gambolati, G., Putti, M., Teatini, P. and Stori, G.G. (2006) 'Subsidence due to peat oxidation and impact on drainage infrastructures in a farmland catchment south of the Venice Lagoon', *Environmental Geology*, vol. 49, pp. 814-820, Available: ISSN: 0943-0105.

Haq, B.U. and Schutter, S.R. (2008) 'A Chronology of Paleozoic Sea-Level Changes', *Science*, vol. 322, no. 5898, pp. 64-68, Available: DOI: 10.1126/science.1161648.

Hoogendoorn, R.M., Overeem, I. and Storms, J.E.A. (2008) 'Process-response modelling of fluvio-deltaic stratigraphy', *Computers and Geosciences*, vol. 34, no. 10, pp. 1394-1416, Available: ISSN: 0098-3004 DOI: 10.1016/j.cageo.2008.02.006.

Howarth, R.W. and Hobbie, J.E. (1982) 'Estuarine comparisons' Academic Press.

Ibañez, C., Pont, D. and Prat, N. (1997) 'Characterization of the Ebre and Rhone estuaries: A basis for defining and classifying salt-wedge estuaries', *Limnology and Oceanography*, vol. 42, no. 1, JAN, pp. 89-101, Available: ISSN: 0024-3590.

Ibañez, C., Sharpe, P.J., Day, J.W., Day, J.N. and Prat, N. (2010) 'Vertical Accretion and Relative Sea Level Rise in the Ebro Delta Wetlands (Catalonia, Spain)', *Wetlands*, vol. 30, no. 5, OCT, pp. 979-988, Available: ISSN: 0277-5212 DOI: 10.1007/s13157-010-0092-0.

Kierzenka, J. and Shampine, L.F. (2001) 'A BVP solver based on residual control and the Maltab PSE', *ACM Trans. Math. Softw.*, vol. 27, September, pp. 299-316, Available: ISSN: 0098-3500.

Kim, W., Mohrig, D., Twilley, R., Paola, C. and Parker, G. (2009) 'Is It Feasible to Build New Land in the Mississippi River Delta?', *Eos Trans. AGU*, vol. 90, pp. 373-374.

Kim, W. and Muto, T. (2007) 'Autogenic response of alluvial-bedrock transition to base-level variation: Experiment and theory', *Journal of Geophysical Research*, vol. 112, no.

F3, JUL 14, pp. F03S14, doi: 10.1029/2006JF000561, Available: ISSN: 0148-0227 DOI: 10.1029/2006JF000561.

Kim, W., Paola, C., Voller, V. and Swenson, J. (2006) 'Experimental measurement of the relative importance of controls on shoreline migration', *Journal of Sedimentary Research*, vol. 76, no. 1-2, JAN-FEB, pp. 270-283, Available: ISSN: 1527-1404 DOI: 10.2110/jsr.2006.019.

Kirwan, M.L. and Murray, A.B. (2007) 'A coupled geomorphic and ecological model of tidal marsh evolution', *Proceedings of the national academy of sciences of the United States of America*, vol. 104, no. 15, APR 10, pp. 6118-6122, Available: ISSN: 0027-8424 DOI: 10.1073/pnas.0700958104.

Knox, J.C. (1993) 'Large increases in flood magnitude in response to modest changes in climate', *Nature*, vol. 361, pp. 430-432.

Kosters, EC, Chmura, GL & Bailey, A 1987, 'Sedimentary and botanical factors influencing peat accumulation in the Mississippi Delta', *Journal of the Geological Society*, vol 144, pp. 423-434.

Kosters, E.C. and Suter, J.R. (1993) 'Facies relationship and system tracts in the late Holocene Mississippi delta plain', *Journal of Sedimentary Petrology*, vol. 63, no. 4, Jul, pp. 727-733, Available: ISSN: 0022-4472.

Lai , S.Y.J. and Capart, H. (2007) 'Two-diffusion description of hyperpycnal deltas', *Journal of Geophysical Research*, vol. 112, pp. F03005, doi:10.1029/2006JF000617.

Lai, S.Y.J and Capart, H. (2009) 'Reservoir infill by hyperpycnal deltas over bedrock', *Geophysical Research Letters*, vol. 36, pp. L08402, doi:10.1029/2008GL037139.

Long, A.J., Waller, M.P. and Stupples, P. (2006) 'Driving mechanisms of coastal change: Peat compaction and the destruction of late Holocene coastal wetlands', *Marine Geology*, vol. 225, no. 1–4, pp. 63-84, Available: ISSN: 0025-3227 DOI: 10.1016/j.margeo.2005.09.004.

Lorenzo-Trueba, J. and Voller, V.R. (2010) 'Analytical and numerical solution of a generalized Stefan problem exhibiting two moving boundaries with application to ocean delta formation', *Journal of Mathematical Analysis and Applications*, vol. 366, no. 2, pp. 538-549, Available: ISSN: 0022-247X DOI: 10.1016/j.jmaa.2010.01.008.

Lorenzo-Trueba, J., Voller, V.R., Muto, T., Kim, W., Paola, C. and Swenson, J.B. (2009) 'A similarity solution for a dual moving boundary problem associated with a coastal-plain depositional system', *Journal of Fluid Mechanics*, vol. 628,

Marr, J.G., Swenson, J.B., Paola, C. and Voller, V.R. (2000) 'A two-diffusion model of fluvial stratigraphy in closed depositional basins', *Basin Research*, vol. 12, pp. 381-398.

Meckel, T.A., Ten, U.S. and Williams, S.J. (2007) 'Sediment compaction rates and subsidence in deltaic plains: numerical constraints and stratigraphic influences', *Basin Research*, vol. 19, no. 1, pp. 19-31, Available: ISSN: 1365-2117 DOI: 10.1111/j.1365-2117.2006.00310.x.

Meyer-Peter, E. and Muller, R. (1948) 'Formulas for bed-load transport', in *2nd Meeting, International Association for Hydraulic Structures Research, Stockholm, Sweden*, IAHR,

Available: http://repository.tudelft.nl/view/hydro/uuid:4fda9b61-be28-4703-ab06-43cdc2a21bd7/.

Monaghan, J.J., Huppert, H.E. and Worster, M.G. (2005) 'Solidification using smoothed particle hydrodynamics', *J. Computat. Phys.*, vol. 206, pp. 684-705.

Moore, P.D. (1989) 'The ecology of peat-forming processes: a review', *International Journal of Coal Geology*, vol. 12, no. 1–4, pp. 89-103, Available: ISSN: 0166-5162 DOI: 10.1016/0166-5162(89)90048-7.

Murray, A.B. (2007) 'Reducing model complexity for explanation and prediction', *Geomorphology*, vol. 90, no. 3–4, pp. 178-191, Available: ISSN: 0169-555X DOI: 10.1016/j.geomorph.2006.10.020.

Muto, T. (2001) 'Shoreline autoretreat substantiated in flume experiments', *Journal of sedimentary research*, vol. 71, no. 2, MAR, pp. 246-254.

Muto, T. and Swenson, J. (2005) 'Large-scale fluvial grade as a nonequilibrium state in linked depositional systems: Theory and experiment', *Journal of Geophysical Research*, vol. 110, no. F3, JUL 22, pp. F03002, doi:10.1029/2005JF000284, Available: ISSN: 0148-0227.

Muto, T. and Swenson, J. (2006) 'Autogenic attainment of large-scale alluvial grade with steady sea-level fall: An analog tank-flume experiment', *Geology*, vol. 34, no. ,

Paola, C. (2000) 'Quantitative models of sedimentary basin filling', *Sedimentology*, vol. 47, pp. 121-178, Available: ISSN: 1365-3091 DOI: 10.1046/j.1365-3091.2000.00006.x.

Paola, C., Heller, P.L. and Angevine, C.L. (1992) 'The large-scale dynamics of grain-size variation in alluvial basins, 1: Theory', *Basin Research*, vol. 4, no. 2, pp. 73-90, Available: ISSN: 1365-2117 DOI: 10.1111/j.1365-2117.1992.tb00145.x.

Paola, C., Twilley, R.R., Edmonds, D.A., Kim, W., Mohrig, D., Parker, G., Viparelli, E. and Voller, V.R. (2011) 'Natural Processes in Delta Restoration: Application to the Mississippi Delta', in Carlson, C. and Giovannoni, S. (ed.) *Annual Review of Marine Science*, Annual Reviews.

Paola, C. and Voller, V.R. (2005) 'A generalized Exner equation for sediment mass balance', *Journal of Geophysical Research*, vol. 110, pp. F04014, doi:10.1029/2004JF000274.

Parker, G. (1978) 'Self-formed straight rivers with equilibrium banks and mobile bed. Part 2. The gravel river', *Journal of Fluid Mechanics*, vol. 89, pp. 127-146.

Parker, G. and Muto, T. (2003) 'One-dimensional numerical model of delta response to rising sea-level', IAHR, Barcelona, 558–570.

Parker, G., Muto, T., Akamatsu, Y., Dietrich, W.E. and Lauer, J.W. (2008) 'Unravelling the conundrum of river response to rising sea-level from laboratory to field. Part I: Laboratory experiments', *Sedimentology*, vol. 55, no. 6, pp. 1643-1655, Available: ISSN: 1365-3091 DOI: 10.1111/j.1365-3091.2008.00961.x.

Parker, G., Muto, T., Akamatsu, Y., Dietrich, W.E. and Lauer, J.W. (2008) 'Unravelling the conundrum of river response to rising sea-level from laboratory to field. Part II. The

Fly-Strickland River system, Papua New Guinea', *Sedimentology*, vol. 55, no. 6, pp. 1657-1686, Available: ISSN: 1365-3091 DOI: 10.1111/j.1365-3091.2008.00962.x.

Parker, G., Paola, C., Whipple, K.X. and Mohrig, D.C. (1998) ' Alluvial fans formed by channelized fluvial and sheet flow. I: theory ', *Journal of Hydraulic Engineering*, vol. 124, pp. 985-995.

Parker, G., Wilcock, P.R., Paola, C., Dietrich, W.E. and Pitlick, J. (2007) 'Physical basis for quasi-universal relations describing bankfull hydraulic geometry of single-thread gravel bed rivers', *Journal of Geophysical Research*, vol. 112, pp. F04005, doi:10.1029/2006JF000549.

Ponce, V.M. (1989) 'Online resource: Initiation of motion', in *Engineering Hydology, Principles and Practices*, Prentice Hall, Available: http://onlinecalc.sdsu.edu/onlineshields.php.

Portnoy, J.W. (1999) 'Salt Marsh Diking and Restoration: Biogeochemical Implications of Altered Wetland Hydrology', *Environmental Management*, vol. 24, pp. 111-120, Available: ISSN: 0364-152X.

Portnoy, J.W. and Giblin, A.E. (1997) 'Biogeochemical effects of seawater restoration to diked salt marshes', *Ecological applications*, vol. 7, no. 3, AUG, pp. 1054-1063, Available: ISSN: 1051-0761 DOI: 10.2307/2269455.

Posamentier, H.W., Allen, H.W., James, D.P. and Tesson, M. (1992) 'Forced regressions in a sequence stratigraphic framework: Concepts, examples, and sequence stratigraphic significance', *AAPG Bull.* , vol. 76, pp. 1687-1709.

Postma, G., Kleinhans, M.G., Meijer, P.T. and Eggenhuisen, J.T. (2008) 'Sediment transport in analogue flume models compared with real-world sedimentary systems: a new look at scaling evolution of sedimentary systems in a flume', *Sedimentology*, vol. 55, no. 6, pp. 1541-1557, Available: ISSN: 1365-3091 DOI: 10.1111/j.1365-3091.2008.00956.x.

Reddy, R. and DeLaune, R.D. (2008) *Biogeochemistry of wetlands: science and applications*, Boca Ratón, Florida: CRC Press.

Reed, D.J. and Wilson, L. (2004) 'Coast 2050: A New Approach to Restoration of Louisiana Coastal Wetlands', *Physical geography*, vol. 25, pp. 4-21.

Sierra, J.P., Sánchez-Arcilla, A., Figueras, P.A., Del, J.G., Rassmussen, E.K. and Mösso, C. (2004) 'Effects of discharge reductions on salt wedge dynamics of the Ebro River', *River Research and Applications*, vol. 20, no. 1, pp. 61-77, Available: ISSN: 1535-1467 DOI: 10.1002/rra.721.

Sommerfield, C.K., Ogston, A.S., Mullenbach, B.L., Drake, D.E., Alexander, C.R., Nittrouer, C.A., Borgeld, J.C., Wheatcroft, R.A. and Leithold, E.L. (2007) 'Oceanic dispersal and accumulation of river sediment', in Field, M.E. (ed.) *Continental Margin Sedimentation: From Sediment Transport to Sequence Stratigraphy*, Wiley-Blackwell.

Staub, J.R. and Esterle, J.S. (1994) 'Peat-accumulating depositional systems of Sarawak, East Malaysia', *Sedimentary Geology*, vol. 89, no. 1–2, pp. 91-106, Available: ISSN: 0037-0738 DOI: 10.1016/0037-0738(94)90085-X.

Stern, N.H. (2007) *The economics of climate change : the Stern review*, Cambridge Univ. Press.

Swenson, J.B. and Muto, T. (2007) 'Response of coastal plain rivers to falling relative sea-level: allogenic controls on the aggradational phase', *Sedimentology*, vol. 54, no. 1, FEB, pp. 207-221, Available: ISSN: 0037-0746.

Swenson, J.B., Voller, V.R., Paola, C., Parker, G. and Marr, J.G. (2000) 'Fluvio-deltaic sedimentation: A generalized Stefan problem', *European Journal of Applied Mathematics*, vol. 11, pp. 433-452.

Syvitski, J.P.M., Kettner, A.J., Overeem, I., Hutton, E.W.H., Hannon, M.T., Brakenridge, G.R., Day, J., Vorosmarty, C., Saito, Y., Giosan, L. and Nicholls, R.J. (2009) 'Sinking deltas due to human activities', *Nature Geoscience*, vol. 2, no. 10, OCT, pp. 681-686, Available: ISSN: 1752-0894 DOI: 10.1038/NGEO629.

Tornqvist, T.E., Wallace, D.J., Storms, J.E.A., Wallinga, J., Dam, R.L.V., Blaauw, M., Derksen, M.S., Klerks, C.J.W., Meijneken, C. and Snijders, E.M.A. (2008) 'Mississippi Delta subsidence primarily caused by compaction of Holocene strata', *Nature Geoscience*, vol. 1, no. 3, MAR, pp. 173-176, Available: ISSN: 1752-0894 DOI: 10.1038/ngeo129.

Tritscher, P. and Broadbridge, P. (1994) 'A similarity solution of a multiphase Stefan problem incorporating general non-linear heat conduction', *International Journal of Heat and Mass Transfer*, vol. 37, no. 14, pp. 2113-2121, Available: ISSN: 0017-9310 DOI: 10.1016/0017-9310(94)90312-3.

Vail, P.R., R.M., M. and Thompson, S. (1977) 'Seismic Stratigraphy and Global Changes of Sea Level, Part 3: Relative Changes of Sea Level from Coastal Onlap', *Am. Assoc. Pet. Geol. Mem.*, vol. 26, pp. 63-81.

Van Asselen, S., Stouthamer, E. and Van Asch, T.W.J. (2009) 'Effects of peat compaction on delta evolution: A review on processes, responses, measuring and modeling', *Earth-Science Reviews*, vol. 92, no. 1–2, pp. 35-51, Available: ISSN: 0012-8252 DOI: 10.1016/j.earscirev.2008.11.001.

Van Asselen, S. (2010) 'The contribution of peat compaction to total basin subsidence: implications for the provision of accommodation space in organic-rich deltas', *Basin Research*, vol. 23, no. 2, pp. 239-255, Available: ISSN: 1365-2117 DOI: 10.1111/j.1365-2117.2010.00482.x.

Voller, V.R. (1997) 'A similarity solution for the solidification of a multicomponent alloy', *International Journal of Heat and Mass Transfer*, vol. 40, no. 12, pp. 2869-2877, Available: ISSN: 0017-9310 DOI: 10.1016/S0017-9310(96)00330-4.

Voller, V.R. (2010) 'A model of sedimentary delta growth: a novel application of numerical heat transfer methods', *International Journal of Numerical Methods for Heat and Fluid Flow*, vol. 20, no. 5, pp. 570-586, DOI:10.1108/09615531011048259.

Voller, V.R., Swenson, J.B. and Paola, C. (2004) ' An analytical solution for a Stefan problem with variable latent heat', *Int. J. Heat Mass Transfer*, vol. 47, pp. 5387-5390.

Voller, V.R., Swenson, J.B., W.Kim and Paola, C. (2006) 'An enthalpy method for moving boundary problems on the earths surface', *Int. J. Heat and Fluid Flow*, vol. 16, pp. 641-654.

Williams, K., Z.S. Pinzon, R.P. Stumpf, and E.A. Raabe (1999) 'Sea-level Rise and Coastal Forests on the Gulf of Mexico', *U.S. Geological Survey Open File Report* 99-441. Available: http://coastal.er.usgs.gov/wetlands/ofr99-441/OFR99-441.pdf

Worster, M.G. (1986) 'Solidification of an alloy from a cooled boundary', *Journal of Fluid Mechanics*, vol. 167, pp. 481-501, DOI: 10.1017/S0022112086002938.

Appendix

1. Argument for assuming a linear diffusion representation for the sediment flux

A key assumption in the diffusion model of sediment bed-load transport is that the line flux of sediment, q_s , at any location on the fluvial surface, is proportional to the local slope $S=\partial h/\partial x$ of the sediment–water interface, i.e. $q_s = -\nu \partial h/\partial x$, where ν is termed the 'fluvial diffusivity' (Paola et al. 1992). For completness, it is worthwhile to summarize the assumptions embodied in this relationship; Paola et al. (1992) provide a rigorous derivation of these 'diffusive' fluvial morphodynamics. We consider length scales $l > L_{bw}$, where $L_{bw}=h/S$ is the backwater length scale and *h* the average flow depth. In this case, the momentum balance reduces to the familiar depth-slope product, $\tau = ghS$, where τ is the kinematic bed shear stress (dimensions of $[L^2/T^2]$). Equivalently, the shear stress can be related to the average flow velocity U through a typical quadratic drag relationship, $\tau = C_f U^2$, where C_f is a friction coefficient. Combining these two relationships and allowing for the fact that in general only a fraction β ($0<\beta<1$) of the fluvial surface is covered with flowing water, i.e. channelized, we arrive at

$$\tau^{3/2} = \beta^{-1} g q_w \sqrt{C_f}\, S \qquad (1)$$

where $q_w = Uh$ is the depth-integrated water flux. Note in a laboratory flume the water discharge q_w is a constant. A constant value for q_w can also be assumed for field settings, provided tributary input is minimal, a common feature in depositional systems.

In fully turbulent field settings, the friction coefficient C_f (1) is a weak (logarithmic) function of relative roughness and for present purposes can be taken to be approximately constant. In contrast, in small-scale laboratory flume settings the flow is often laminar to transitional, and so the friction coefficient is a function of the flow conditions. In particular, for a slot-like flume of constant width w, with a fully wetted surface ($\beta = 1$) and shallow flow depth h_w, the friction coefficient is a function of the grain diameter d and Reynolds number $Re=\rho q_w/\mu$, i.e. $C_f = f(Re, d)$.

There are two ways to progress from (1). First, consider a bed-load relation, such as the well-known Meyer-Peter & Muller (1948) formula, that can be written in the form

$$q_s^* = K(\tau_* - \tau_{*c})^{3/2} \qquad (2)$$

where $q_s^* = q_s / d\sqrt{g(s_g - 1)d}$ is dimensionless sediment flux; K is a constant (typically~8); s_g is the specific gravity ($s_g = \rho_s/\rho \sim 2.65$); $\tau* = \tau/g(s_g - 1)d$ is the dimensionless bed shear stress (the Shields number); and τ_{*c} is the dimensionless critical shear stress at which bed-load transport is initiated. Two limiting cases are of interest here. For bed-load-dominated rivers with weak banks, which in the field generally means gravel-bed rivers, the channel typically self-adjusts by widening to keep the bed shear stress slightly above critical, i.e. $\tau_* = (1 + \varepsilon)\tau_{*c}$. The mechanistic justification for this is presented in Parker (1978), and further analysis and field evidence are presented in Parker et al. (2007). In this case (2) becomes $q_s^* = K(\varepsilon/(1+\varepsilon)\tau^*)^{3/2}$. Alternatively, as discussed in Dade & Friend (1998) and Parker et al. (1998), for most sand-bed and finer grained rivers the bed shear stress substantially exceeds the critical value, i.e. $\tau_* >>> \tau_{*c}$. In that case, (2) is modified to $q_s^* = K\tau_*^{3/2}$. Similarly, at the laboratory scale, where bed slopes are relatively large, e.g. S ~0.1–0.2, the bed shear stress is significantly larger than the critical shear stress. Consider, for example, the following representative values taken from the experiments reported in this work: sand particle diameter d_s =0.2 mm, fluvial slope in the range $0.065<S<0.211$ and flow depth h=1.5 mm. In this scenario the critical stress for motion is 7 to 21 times smaller than the stress applied on the bed surface (Ponce 1989, pp. 549–552). Hence in each of the above noted field and experimental settings the critical shear stress in (2) can be absorbed as a constant in the flux relationship or ignored altogether to arrive at, on combining (1) and (2), a linear relationship between the sediment flux and the local slope. More generally, we note that for any case in which a channel self-adjusts (e.g. via bank erosion) or is otherwise constrained to maintain a constant value of dimensionless shear stress τ_*, any sediment-flux relation of the form gives, with (2), a linear relationship between sediment flux and slope. For the specific

scenarios above, the fluvial diffusivity ν has the form

$$\nu = \begin{cases} \dfrac{K\sqrt{C_f}}{\beta(s_g - 1)} q_w, & \text{field - scale, sand or finer} \\ \dfrac{K\sqrt{C_f}}{\beta(s_g - 1)} \left(\dfrac{\varepsilon}{1+\varepsilon} \right)^{3/2} q_w, & \text{field - scale, gravel} \\ \dfrac{K}{(s_g - 1)} (f(\mathrm{Re}, d))^{1/2} q_w, & \text{slot – flume} \end{cases}$$

Fluvial diffusivity is most sensitive to the water supply (q_w) in the system. Typically, q_w is assumed constant in field settings; i.e. tributary input is neglected; in experimental systems, q_w is a constant (upstream) input. The key point is that the sediment flux varies linearly with bed slope in both field- and laboratory-scale systems.

2. Similarity solution

In dimensionless form, the governing equations for the diffusive transport model of the regressive system in Fig. 2a (Lorenzo-Trueba et al., 2009) is (assuming a filed scenario $R_{sh} = 1$)

$$\frac{\partial h}{\partial t} = \frac{\partial^2 h}{\partial x^2}, \qquad r(t) \le x \le s(t) \tag{1}$$

with boundary conditions

$$h\big|_{x=r} = -r \tag{2a}$$

$$h\big|_{x=s} = Z \tag{2b}$$

$$\left.\frac{\partial h}{\partial x}\right|_{x=s} = -R_{ab} \tag{2c}$$

$$\left.\frac{\partial h}{\partial x}\right|_{x=s} = -(s+Z)\frac{ds}{dt} \tag{2d}$$

We set the movement of the ABT and the SH to be respectively

$$r = -2\lambda_{ab}\sqrt{t} \tag{1}$$

$$s = 2\lambda_{sh}\sqrt{t} \tag{2}$$

and base-level

$$Z = 2\lambda_{z}\sqrt{t} \tag{7}$$

In addition, following the same steps of Lorenzo-Trueba et al. (2009), we introduce the similarity variable

$$\xi = \frac{x}{2\sqrt{t}} \tag{3}$$

and scaling the sediment height by

$$\eta = \frac{h}{2\sqrt{t}} \tag{4}$$

to obtain the following analytical solution for the fluvial profile

$$\eta(\xi) = R_0\left[\left(\lambda_{sh} + \frac{\lambda_z}{R_{ab}}\right)\left(\frac{e^{-\xi^2} + \pi^{\frac{1}{2}}\xi\left(erf(\xi) + erf(\lambda_{ab})\right)}{e^{-\lambda_{sh}^2} + \pi^{\frac{1}{2}}\lambda_{sh}\left(erf(\lambda_{ab}) + erf(\lambda_{sh})\right)}\right) - \xi\right] \tag{8}$$

which satisfies (2b) and (2c). We use the remaining two boundary conditions (2a) and (2d) to obtain the moving boundary constants λ_{ab} and λ_{sh}

$$\frac{R_{ab}e^{-\lambda_{sh}^2} - \lambda_z\pi^{\frac{1}{2}}\left(erf(\lambda_{ab}) + erf(\lambda_{sh})\right)}{e^{-\lambda_{sh}^2} + \pi^{\frac{1}{2}}\lambda_{sh}\left(erf(\lambda_{ab}) + erf(\lambda_{sh})\right)} = 2\left(\lambda_{sh} + \lambda_z\right)\lambda_{sh} \tag{9a}$$

$$\frac{\left(\lambda_{sh}R_{ab} + \lambda_z\right)e^{-\lambda_{ab}^2}}{e^{-\lambda_{sh}^2} + \pi^{\frac{1}{2}}\lambda_{sh}\left(erf(\lambda_{ab}) + erf(\lambda_{sh})\right)} = \lambda_{ab}\left(1 - R_{ab}\right) \tag{9b}$$

Given the base-level constant, λ_z, we solve the system of equations (9) to track both the SH and the ABT simultaneously over time. For the particular case $\lambda_{ab} = 0$ we reach the following expression

$$a^* = 2\lambda_z = \sqrt{\frac{2R_{ab}^3}{1 - R_{ab}}} \tag{10}$$

which matches with equation (16) in Muto and Swenson (2005) under the assumption that the foreset slope, ψ, is much larger than the basement slope, β (i.e., $\beta/\psi << 1$).